2008-01-01

A Second Generation Ex-Vivo Accommodation Simulator: Design and Calibration

Derek Nankivil
University of Miami, derek.nankivil@gmail.com

UNIVERSITY OF MIAMI

A SECOND GENERATION EX-VIVO ACCOMMODATION SIMULATOR:
DESIGN AND CALIBRATION

By

Derek Nankivil

A THESIS

Submitted to the Faculty
of the University of Miami
in partial fulfillment of the requirements for
the degree of Master of Science

Coral Gables, Florida

December 2008

UNIVERSITY OF MIAMI

A thesis submitted in partial fulfillment of
the requirements for the degree of
Master of Science

A SECOND GENERATION EX-VIVO ACCOMMODATION SIMULATOR:
DESIGN AND CALIBRATION

Derek Nankivil

Approved:

_____   _____
Fabrice Manns, Ph.D.   Terri A. Scandura, Ph.D.
Associate Professor of Biomedical Engineering   Dean of the Graduate School
And Ophthalmology

_____   _____
Jean-Marie Parel, Ph.D.   Klaus Ehrmann, Ph.D.
Henri and Flore Lesieur Chair in Ophthalmology   Research Manager in
Research Associate Professor of Ophthalmology   Technology, Project Director
And Biomedical Engineering

NANKIVIL, DEREK D.   (M.S., Biomedical Engineering)

A Second Generation Ex-Vivo Accommodation   (December 2008)
Simulator: Design and Calibration

Abstract of a thesis at the University of Miami.

Thesis supervised by Professors Jean-Marie Parel and Fabrice Manns.
No. of pages in text. (118)

Presbyopia is the progressive decrease in accommodative ability with age, and it implies a major loss of visual function. Presbyopia is the only condition of the eye which affects everyone who lives beyond 50 years of age. As part of a joint effort, the Ophthalmic Biophysics Center at the Bascom Palmer Eye Institute and the Vision Cooperative Research Centre at the University of New South Wales, developed two different ex-vivo accommodation simulators (EVAS) to examine the mechanisms of accommodation and presbyopia, and to test and validate new ophthalmic surgical procedures such as lens refilling. The purpose of this thesis is to mechanically and optically calibrate the second generation instrument (EVASII), and to compare it to the first generation design (EVASI). To validate the optical measurements of EVASII, an optical calibration has been performed, yielding a lens power measurement system with a mean accuracy of ±0.56D. To enhance the optical capabilities and tissue dissection options, the mechanics of mounting the tissue has been improved by using magnetic mounts, and the mechanical calibration of EVASII, yielded a force measurement system with a mean uncertainty of ±0.81g   Also, a comparison of EVASII and EVASI has been performed, showing that the results of the two systems are significantly different; however, both systems successfully simulate accommodation. Thus, general trends

concerning efficacy and optimization of surgical procedures as well as age related accommodative changes can be compared for each individual system.

DEDICATION

To my mother and father, Judy and Dennis Nankivil, for their unending support of my educational pursuits. My mother's strength, determination, and perseverance carried me through the toughest times, and my father's encouragement and optimism gave me the confidence to accomplish even the most monumental tasks.

To my wife, Matilde Nankivil, for her endless love and caring nature. She was there for every moment of success and failure, and her daily sacrifice has given me the stability and balance in life needed to accomplish this endeavor.

ACKNOWLEDGEMENTS

TABLE OF CONTENTS

LIST OF FIGURES

LIST OF TABLES

LIST OF ABBREVIATIONS

BFL   Back Focal Length

BSS   Balanced Salt Solution

CAD   Computer Aided Design

CCD   Charge-Coupled Device

CVI   C (language) Virtual Instrumentation

EVAS   Ex-Vivo Accommodation Simulator

EVASI   First Generation Ex-Vivo Accommodation Simulator

EVASII   Second Generation Ex-Vivo Accommodation Simulator

FDA   Food and Drug Administration

IOL   Intraocular Lens

OBC   Ophthalmic Biophysics Center

OCT   Optical Coherence Tomography

OSLO   Optical Software for Layout and Optimization

PDMS   Polydimethylsiloxane

PCX   Plano-Convex

PMMA   Poly(methyl methacrylate)

PMT   Post-Mortem Time

Chapter 1: Aims

Presbyopia is the progressive decrease in accommodative ability with age (Weale 1989, Kaufman 1992, Gilmartin, 1995, Werner et al. 2002). It implies a major loss of visual function, and the estimated economic impact of this is staggering, since people with presbyopia are likely to lose productivity due to this impairment. Presbyopia is the only condition of the eye which affects everyone who lives beyond 50 years of age (Kaufman 1992, Pandey et al. 2002). Presbyopia can potentially be cured by lens refilling (Kessler 1964, Parel et al. 1986, Nishi 2003, Norrby et al. 2006, Menapace 2007, Glasser 2008), and this hope provides a driving force behind understanding accommodation.

As part of a joint effort, the Ophthalmic Biophysics Center (OBC) at the Bascom Palmer Eye Institute and the Vision Cooperative Research Centre at the University of New South Wales, developed two different ex-vivo accommodation simulators (EVAS), a first generation (EVASI) and a second generation (EVASII) instrument. Using cadaver tissue, these instruments provide the opportunity to examine the mechanisms of accommodation and presbyopia, and to test and validate new ophthalmic surgical procedures such as lens refilling.

The goal of this project is to design, fabricate, and validate a mechanical mounting system for post-mortem human and higher-primate tissue for use in EVASII experiments, to characterize and calibrate both the optical and mechanical measurement systems of EVASII, and to compare the results of EVASII to that of EVASI.

Chapter 2: Background and Significance

2.1 Accommodation

Accommodation is a process which relies on the change in curvature of the crystalline lens to maintain focus on objects at the near (Young 1793, Cramer 1853, Helmholtz 1855, Koretz et al. 1984, Koretz et al. 1987). According to the Helmholtz theory of accommodation (Helmholtz 1855), these changes in curvature are induced as the zonules apply a load to the lens equator (Fincham 1937, Glasser & Kaufman 1999, Ludwig et al. 1999, Croft et al., 2006). When the ciliary muscle is relaxed, the zonules are taught, imparting a load on the lens capsule, causing it to flatten. This reduced curvature lowers the optical power of the eye, allowing the observer to focus on distant objects. When the ciliary body is constricted, the zonules are slack, reducing the load on the lens capsule, allowing it to assume a relaxed and more curved form. This increase in curvature increases the optical power of the eye, allowing the observer to focus on objects at the near.
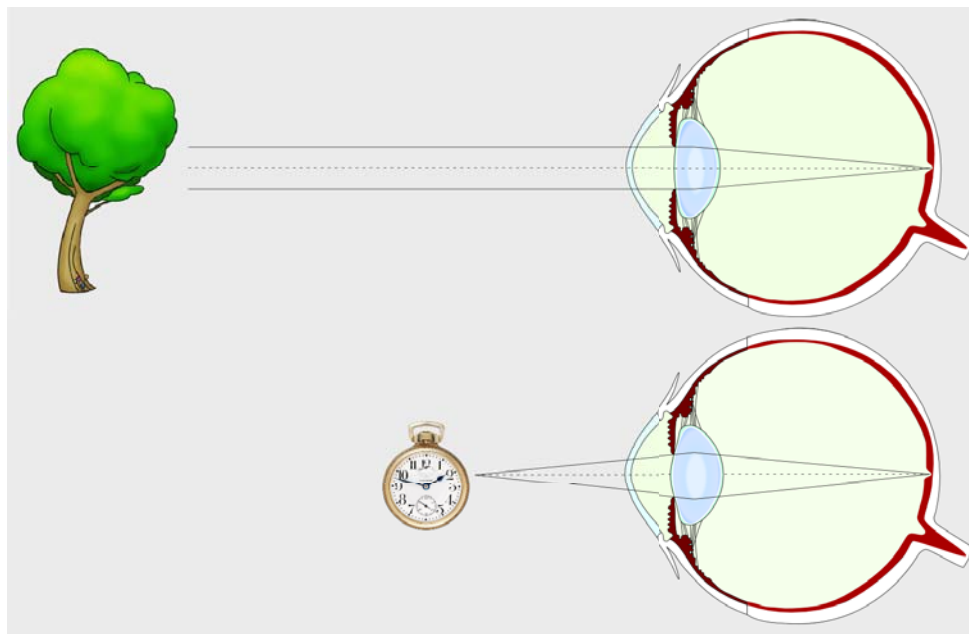
Figure 2.1: Principle of accommodation. (Modified from an original by David Borja).

www.manaraa.com

2.2 Presbyopia

Presbyopia is the progressive decrease in accommodative ability with age, (Weale 1989, Kaufman 1992, Gilmartin, 1995, Werner et al. 2002) which is primarily due to age related changes in the optical and mechanical properties of the lens (Fisher 1973, Pau & Kranz 1991, Glasser & Campbell 1998). It is a symptom of the natural course of aging, and is usually first noticed between the ages of 40 and 50. Presbyopia implies a major loss of visual function, and its estimated economic impact of is staggering, as people with presbyopia are likely to lose productivity due to this impairment. The study of accommodation and presbyopia is very important, since presbyopia is the only condition of the eye which affects everyone who lives beyond 50 years of age (Donders 1864, Duane 1912, Kaufman 1992, Pandey et al. 2002).
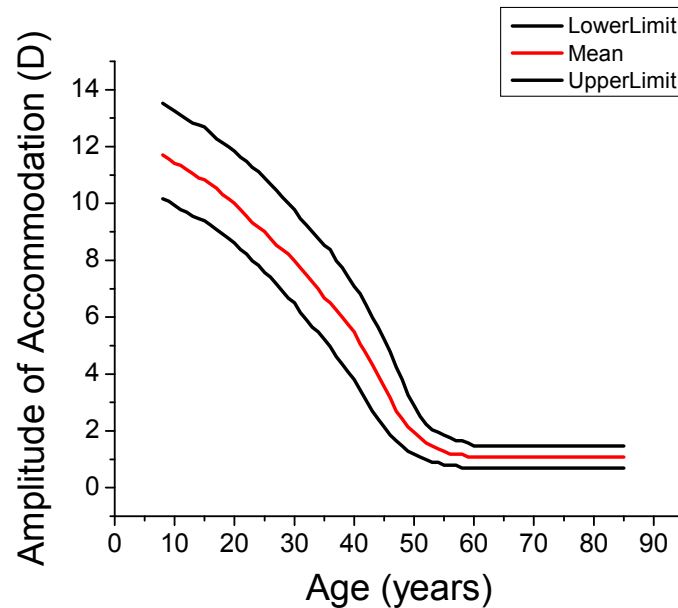
Figure 2.2: Amplitude of accommodation as a function of age (Duane 1912).

2.3 Presbyopia Correction

Scientists and engineers have been working together to develop new potential treatments for presbyopia (Menapace 2007, Glasser 2008). There are several different treatment modalities presently in research and development which rely on the finding that the extra lenticular components of the accommodative mechanism remain functional beyond the onset of presbyopia (Fisher 1977, Strenk et al. 1999, Pardue & Sivak 2000). The only technique accepted by the Food and Drug Administration (FDA) utilizes an accommodating intraocular lens (IOL). In this procedure, the lens contents are removed and the IOL, which is typically a silicon or acrylic lens, is implanted in the remaining lens capsule. The accommodating IOL utilizes haptics, or arms, that act as force distributors to translate and/or change the shape of the lens. In principle, changes in the ciliary body diameter alter the stress state of the lens capsule. The forces acting on the capsule are then distributed to the haptics of the IOL, and these natural forces of accommodation, induce translation and/or changes in shape of the IOL.

Another potential method of restoring accommodation is lens refilling. In this procedure the lens contents are removed, and a polymer is injected into the lens capsule (Kessler 1964, Parel et al. 1986, Nishi 2003, Norrby et al. 2006, Menapace 2007, Glasser 2008). This polymer has similar optical and mechanical characteristics to a young lens, thereby allowing the eye to change shape upon activation of the ciliary muscle.
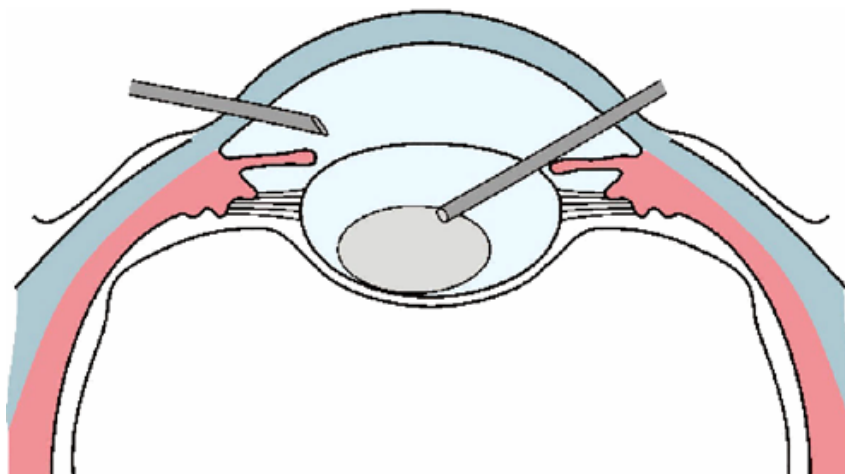
Figure 2.3: Lens refilling schematic (Menapace 2007).

Both of these approaches have shown great promise as a potential method of presbyopia correction, but there is still a great deal of work to be done. This hope has given rise to a collaborative effort between the Ophthalmic Biophysics Center at the Bascom Palmer Eye Institute in the University of Miami, and the Dynamic Vision Project at the Vision Cooperative Research Centre in the University of New South Wales. This joint effort has the goal of developing a flexible polymer gel which can be used to replace the presbyopic lens, as well as surgical procedures and instruments to evaluate, deliver, and crosslink the gel in situ.

2.4 EVASI

Ex-vivo accommodation simulation, allows for the testing of potential techniques of presbyopia correction and exploration of the process of accommodation. Humans and monkeys are good models to test these procedures. In addition, the forces exerted by the zonules cannot be measured in-vivo. Due to these difficulties, there is a strong need for an ex-vivo model.
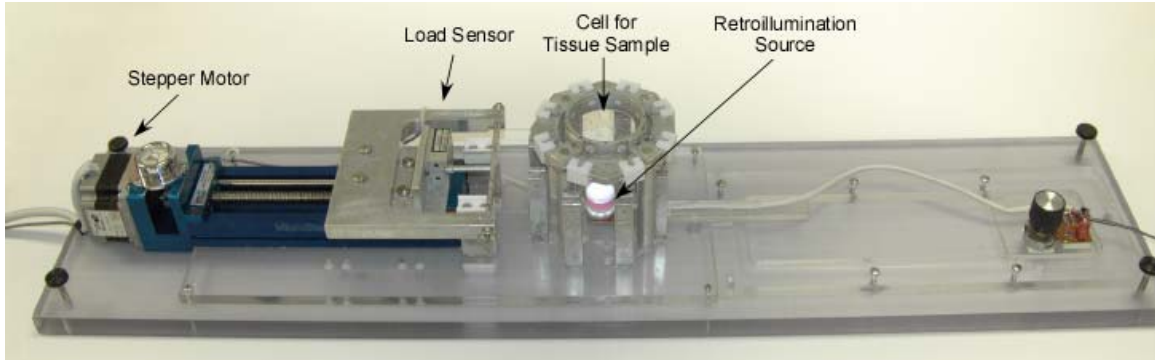
Figure 2.4: Lens stretching system - EVASI. (Designed and built by Jean-Marie Parel and David Denham at the OBC).

EVASI is a lens stretching system that simulates accommodation by stretching radially on 8 segments of tissue preparation consisting of the lens, zonules, ciliary body, hyaloid membrane, anterior vitreous and the sclera. The system uses an assembly of strings and pulleys to simultaneously actuate each individual segment through the use of a motorized translation stage (MS33-LXB-L200; Servo-Systems Co., Montville, NJ), which is linked via a T-bar to the string and pulley system. A load cell with a range of 100g and resolution of 0.01g (GSO-100; Transducer Techniques, Temecula, CA) is mounted on the T-bar to record the total load during the experiment.

Post-mortem eyes from cynomolgus monkeys (*Macaca fascicularis*) are obtained from the University of Miami, Division of Veterinary Resources after euthanasia following institutional animal care guidelines through an approved tissue-sharing protocol. All experiments adhere to the tenets of the Declaration of Helsinki, and to the Association for Research in Vision and Ophthalmology statement for the use of animals in ophthalmic and vision research. Eyes are obtained after euthanasia for experiments unrelated to this study. Post-mortem human eyes are obtained from the Florida Lions Eye Bank (Miami, FL). After enucleation, the eyes are placed in sealed containers with gauze soaked in a Balanced Salt Solution (BSS, Alcon, Fort Worth TX) to prevent

dehydration of the globe. All eyes are stored at 5ºC and returned to room temperature before they are dissected. Experiments are performed no more than 3 days post-mortem. The posterior pole, cornea, and iris are removed, leaving intact the lens, zonules, ciliary body, hyaloid membrane, anterior vitreous and a scleral rim, which is bonded to eight custom-made scleral shoes, each with a curvature sized to match the globe. Next, the tissue is then mounted into the chamber of EVASI. Then, while being very careful not to sever the ciliary body, the scleral rim is sectioned radially between the shoes to eliminate interference during stretching, and the tissue is ready for the experiment.

During the stretching experiment, using a retro-illumination system and an industrial color CCD camera (GP-KR222, Panasonic, Secaucus NJ), a top view of the lens and ciliary body is captured, and the lens and inner ciliary ring diameter are measured in the horizontal and vertical directions.
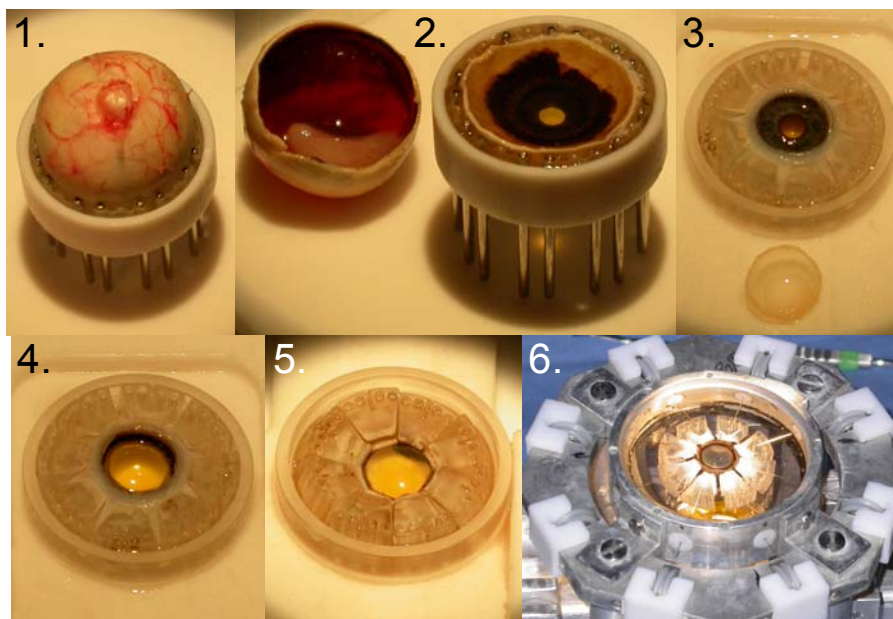
Figure 2.5: EVASI tissue preparation. (1) The intact globe is bonded to 8 independent scleral shoes. The posterior hemisphere (2) and the cornea (3) are removed. The iris is removed (4), and then, segments of sclera are excised between adjacent shoes (5). Finally, the tissue preparation is mounted in the EVASI chamber (6). (Images courtesy: Noel Ziebarth, Dissection courtesy: Esdras Arrieta).
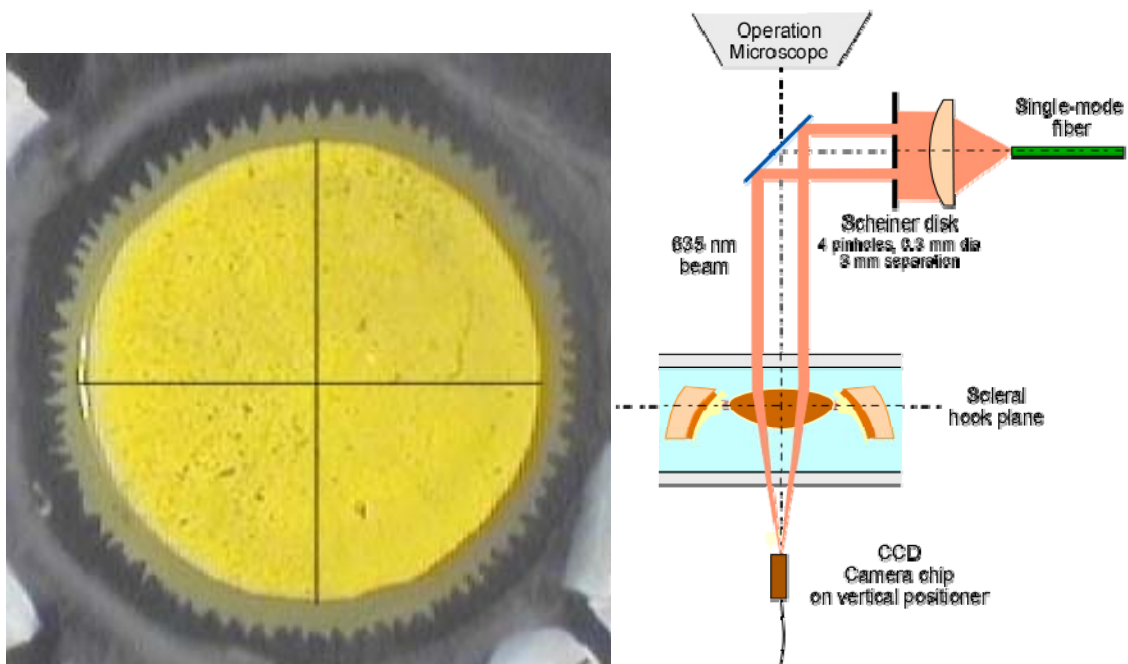
Figure 2.6: Top view of the lens and ciliary body in EVAS (left). Scheiner system schematic (right) (Manns et al. 2007).

The lens power is measured with a Scheiner system that uses 4 parallel beams aimed onto the lens, which are then focused and detected by a miniature board level CCD camera (510x492 pixels, 15-BB13, Jameco Electronics, Belmont, CA) whose position is accurately measured with a height gauge (±0.01mm resolution, 570-227, Mitutoyo, Aurora IL), so that via an optical model, the focal length, and therefore refractive power of the lens can be determined.

Typical measurements include load, lens diameter, and ciliary body diameter vs. scleral stretch, load vs. lens diameter and ciliary body diameter, and power vs. load. The load vs. lens diameter, the load vs. ciliary body diameter, and the power vs. load trends are fit with a line using a least squares linear regression.
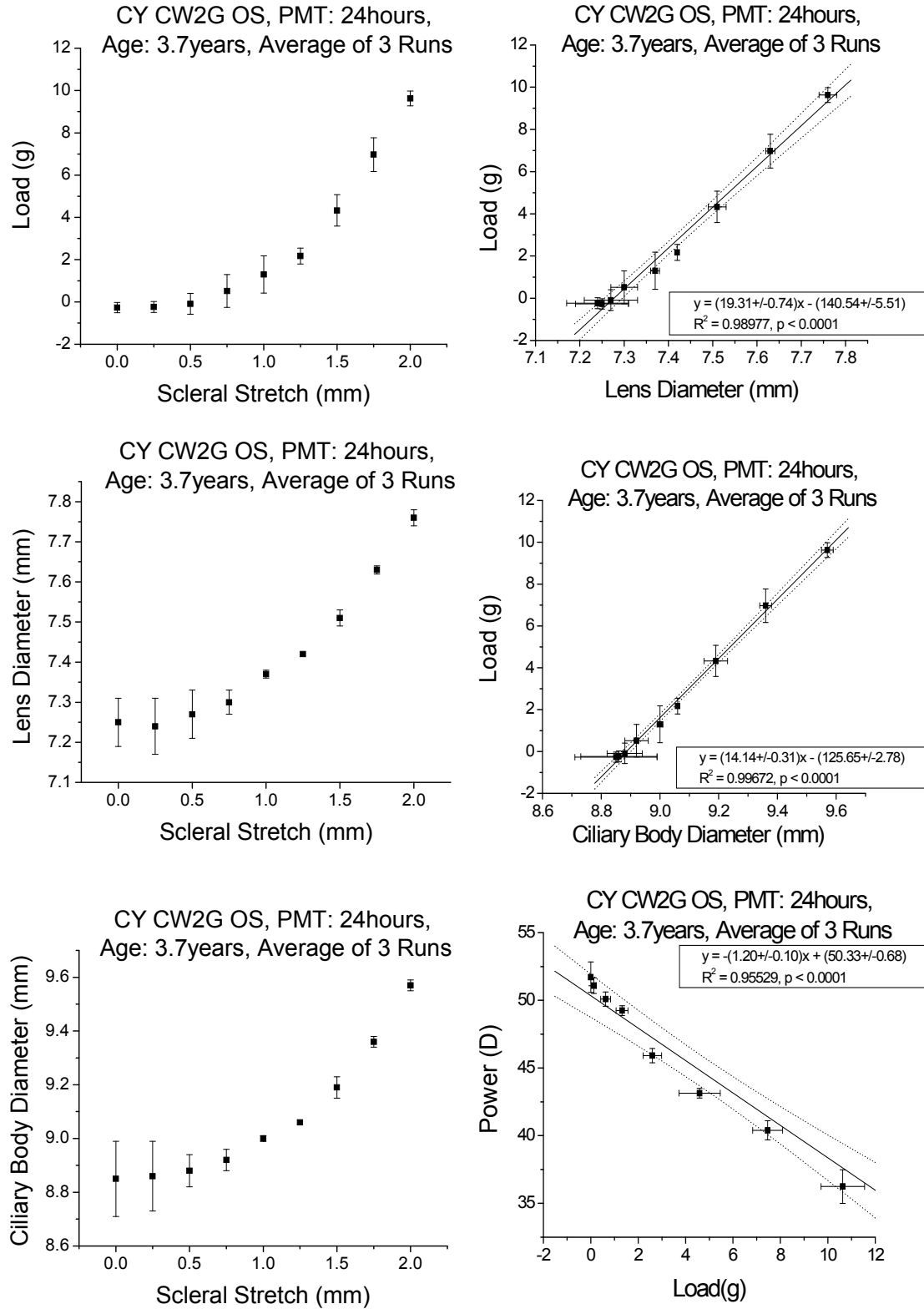
Figure 2.7: Representative EVASI data set for a cynomolgus monkey. Linear fits are shown as a solid line, error bars represent the standard deviation, and the 95% confidence intervals of the linear fits are shown as a dashed line.

It is important to note that the conditions in EVAS are not identical to in-vivo conditions. First, the entire posterior portion of the globe is removed, and although the anterior vitreous and hyaloid membrane remain intact, the potential affect that vitreous pressure (Coleman 1986, Coleman & Fish 2001) may have on the accommodative process is altered. In addition, the positioning of the lens in EVAS is such that the gravitational loading vector corresponds to a supine position. Researchers have shown that the gravitational load has a measurable effect on the lens position during maximum accommodation (Glasser & Kaufman 1999, Glasser et al. 2001) although others have shown that gravity has no effect on the amplitude of accommodation (Schachar & Cudmore 1994).

Furthermore, in EVASI, the globe is bonded to polymethylmethacrylate (PMMA) segments (shoes) that fit the scleral curvature (Denham et al. 2002), and each individual segment of the sclera is sectioned. These shoes are pulled on by hooks through a system of pulleys and strings that are connected to the load cell; thus, measurements of load in EVASI include components not present in the eye in-vivo. However, previous studies have shown that the lens performance in EVASI is similar to other in-vivo measurements, which indicates that the zonular loading (although not directly measured) is comparable to physiological conditions (Manns et al. 2007). EVASI uses 8 individual segments to radially stretch 8 discrete sections of tissue, but in the living eye, changes in the ciliary body diameter are elicited circumferentially, without segmentation. Also, the use of a single stepper motor does not give information about the uniformity of the position of each individual segment, which is compromised by differences in the length of the string attachment. This can be further exacerbated by differences in string length, diameter and

strain, and by differences in the amount of friction in each pulley. Further, the use of a single transducer does not provide information about the individual load applied to each segment, and these limitations served as the motivation for the design of EVASII.

2.5 EVASII

EVASII (Ehrmann et al. 2008) is a lens stretching system that simulates accommodation by stretching on 8 segments of tissue preparation much like the original EVASI. Instead of using a system of strings and pulleys, EVASII has 8 linear actuators (M-110.1DG, Physik Instrumente, GmbH & Co., Karlsruhe Germany) to control the position of each individual segment. EVASII is also equipped with 8 load transducers (FORT-100, World Precision Instruments, Sarasota FL) for measuring the load on each individual segment.
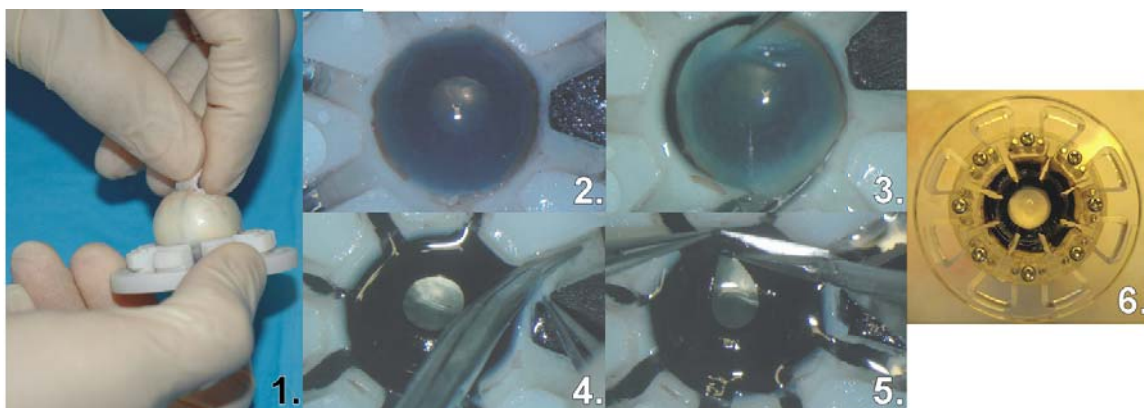
Figure 2.8: EVASII tissue preparation. (1) The intact globe is bonded to 8 independent scleral shoes. The posterior hemisphere (2) and cornea (3) are removed. Segments of sclera are excised between adjacent shoes (4). Finally, the iris is removed (5), and the tissue preparation is ready to be mounted into EVASII (6). (Images courtesy: David Borja, Dissection courtesy: Esdras Arrieta).
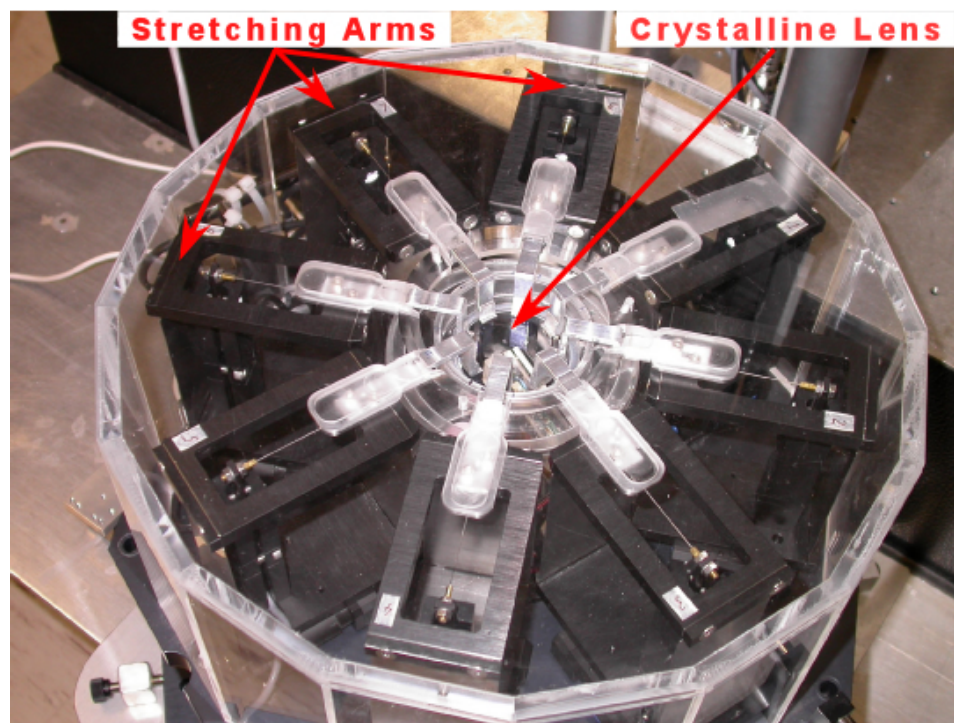
Figure 2.9: Lens stretching system - EVASII. (Design and manufacture courtesy: Klaus Ehrmann and Darrin Falk).

During the stretching experiment, using a retro-illumination system, a zoom lens system (1-60123D & 1-60110, Navitar, Rochester, NY), and a Firewire CCD camera (U58-301, Basler IEEE-1394, Edmund Optics, Barrington, NJ) a top view of the lens and ciliary body is captured, and the lens and inner ciliary ring diameter are measured in the horizontal and vertical directions in a semi-automated fashion using custom built software written in C (Language) for Virtual Instrumentation (CVI). The EVASII graphical user interface allows for control of all motion and image capture parameters, and automatically generates a data file for analysis. Once all of the experimental parameters are set, and the optical system is properly focused, a scale image is captured for converting pixels in the plane of the image into actual distances. After the calibration is complete, the diameters are measured manually, and can be controlled by as small an increment as a single pixel.
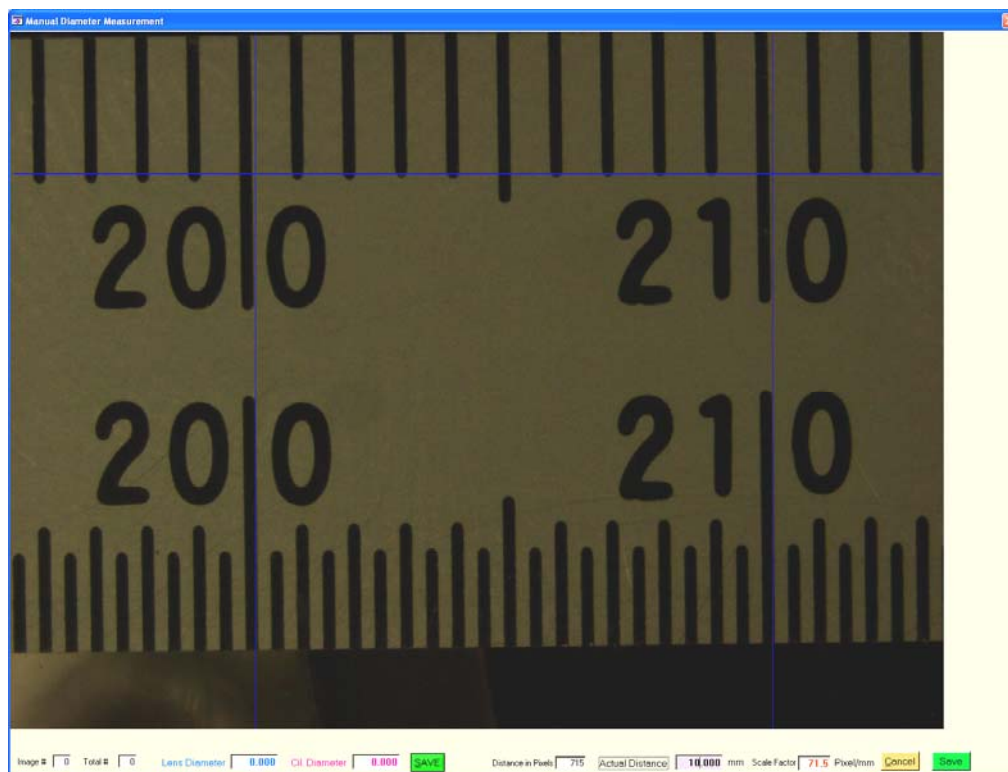
Figure 2.10: Scale image for diameter measurements.   (Software courtesy: Klaus Ehrmann).
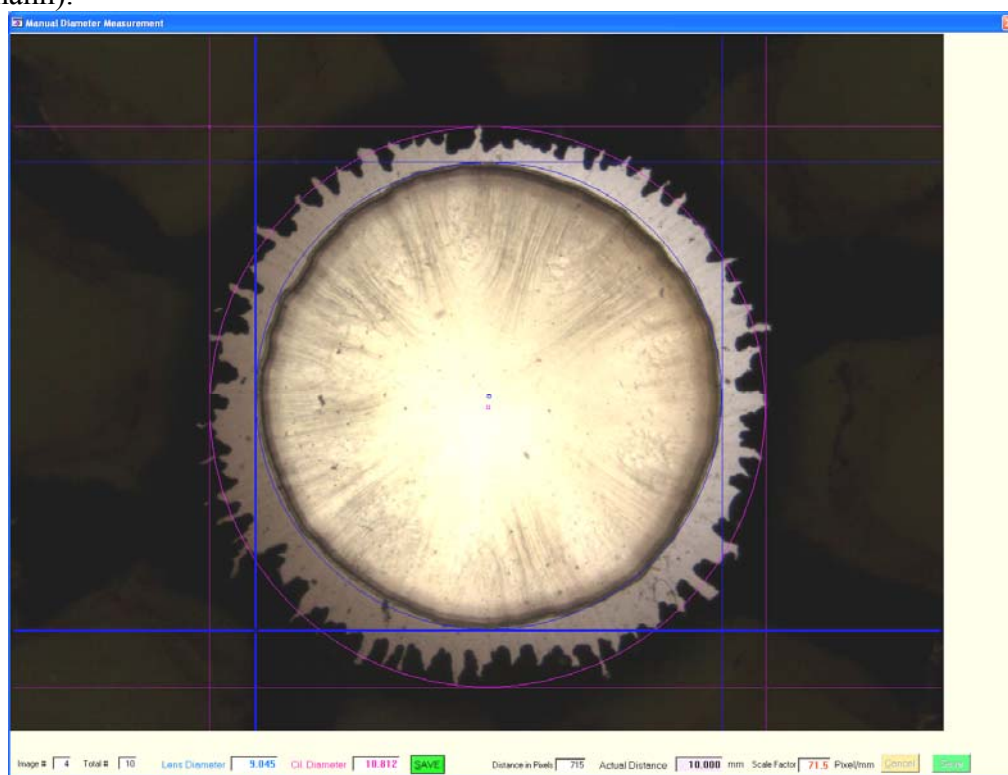
Figure 2.11: Sample diameter measurement. (Software courtesy: Klaus Ehrmann).

Further, EVASII has a Scheiner optical system incorporated, which allows for measurement of optical power before and during stretching. Just as in the original EVAS, this system uses a camera (GP-CX261V, NTSC, Panasonic, Secaucus, NJ) whose position is accurately measured, so that via an optical model, the focal length, and therefore refractive power of the lens can be determined. The Scheiner system used in EVASII is slightly different from that used in EVASI, as a series of spots are scanned parallel to the optical axis of the crystalline lens using a set of x-y galvanometers to form a circular pattern in the image plane in EVASII, as opposed to 4 spots used in the EVASI system. Also, the EVASII Scheiner system uses a linear actuator to control the position of the CCD, as opposed to a manual adjustment in EVASI.

EVASII has a custom built Optical Coherence Tomography (OCT) system. This system has a long scan depth, allowing for images of the entire lens cross section to be obtained during stretching. The system has a 10mm axial scan depth, 825nm central wavelength, and a 20nm bandwidth, giving an image resolution of 12μm. The laser gives 6mW of output power, and the system is capable of scanning at 20A-lines/sec.
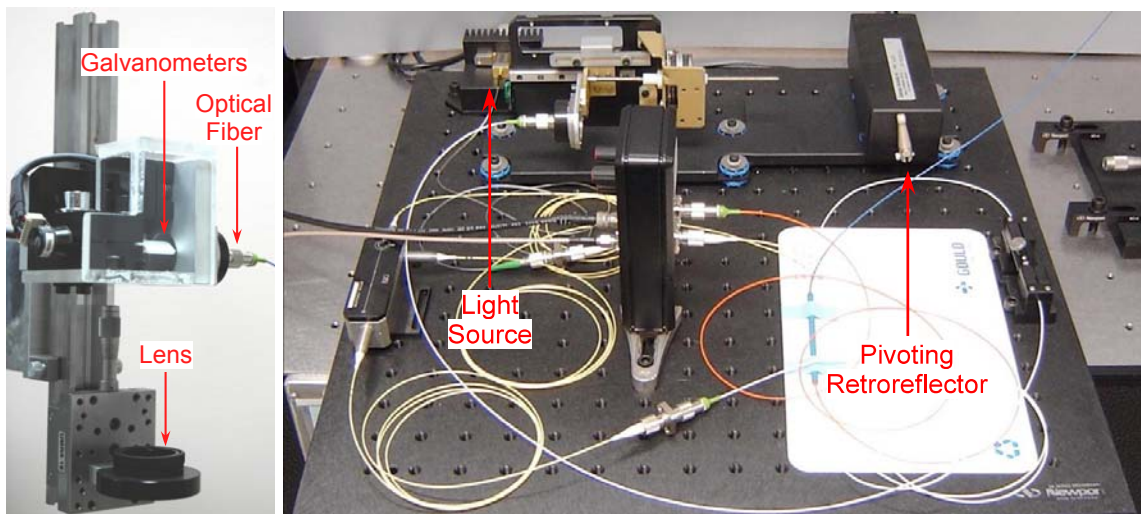
Figure 2.12: OCT beam delivery system (left). OCT interferometer (right). (OCT system courtesy: Stephen Uhlhorn).
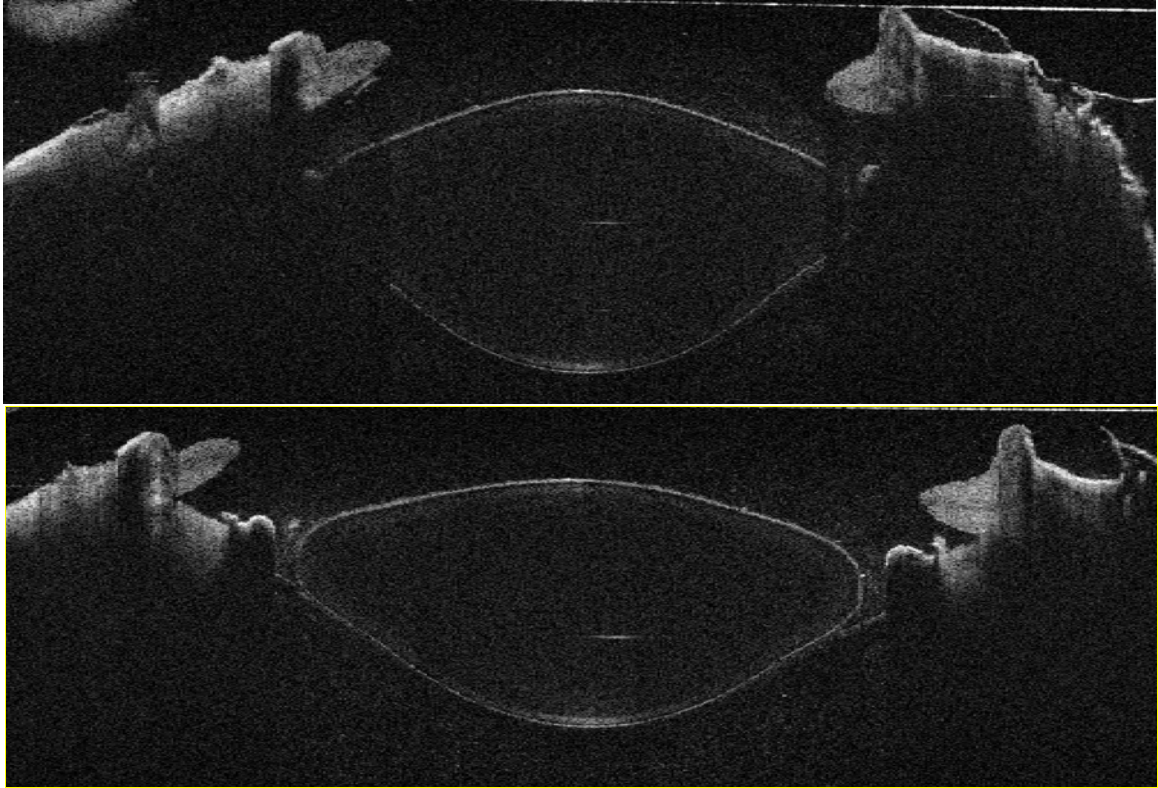
Figure 2.13: Representative OCT images of a cynomolgus monkey eye during stretching, unstretched or accommodated (top) and stretched or unaccommodated (bottom). (Images courtesy: Stephen Uhlhorn and David Borja).

The original design of the EVASII system had one significant limitation; surgery was not possible in EVASII. The EVASII tissue chamber was recessed significantly, making it difficult for a surgeon to insert instruments within the lens. Also, the solid arms of EVASII blocked access all the way around the tissue. Despite efforts to shield the electronic components from the tissue chamber, the possibility of fluid infiltrating these components during surgery is a risk not worth taking. Thus, with this limitation in mind, a mechanism to transfer the tissue from EVASII to the operating microscope was designed and manufactured, and this design is discussed in the next chapter.

Chapter 3: EVASII Opto-Mechanical Tissue Transfer System

3.1 Purpose

The purpose of this chapter is to design and manufacture an EVASII compatible mounting system capable of holding human and monkey lenses of various sizes. In addition, this mounting system will also allow for transfer of EVASII tissue preparations so that surgical procedures can be performed on the tissue, which can then be returned to the EVASII testing chamber for analysis.

3.2 Design of Shoes and Shoe Mounts

In order to mount the tissue preparation in EVASII so that it is transferable for surgical operations, a number of custom built components were designed and manufactured. The tissue preparation procedure in EVASII is identical to that of EVASI, except the shoes are designed differently to fit the EVASII system. The mounting mechanism consists of a set of shoes that are cut with a spherical revolution to fit the size of the globe. A number of different sizes were manufactured to properly fit any size eye. The shoes have a set of grooves, to provide for centration and symmetrical alignment. Each shoe is aligned with an annular base plate via these groves and a corresponding groove in the base plate.

16
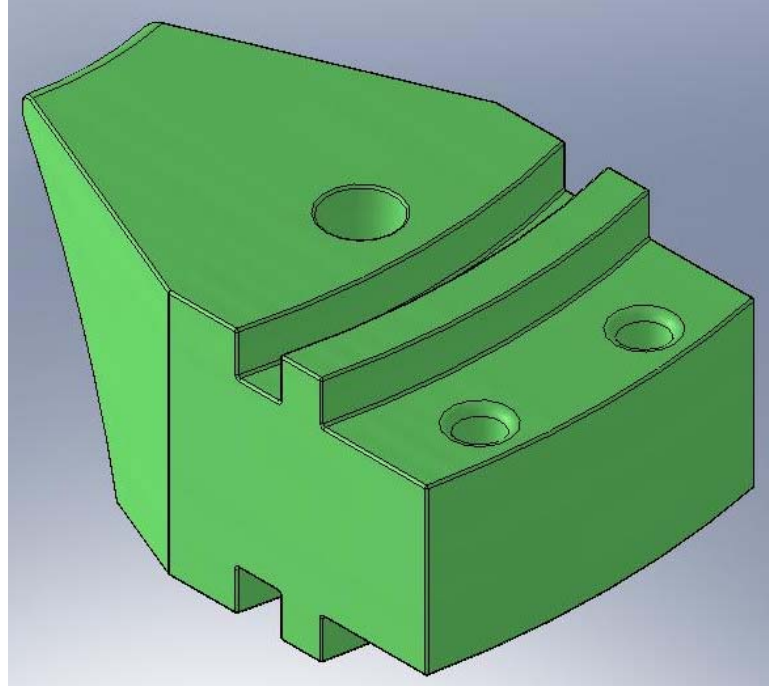
Figure 3.1: EVASII shoe - isometric view.
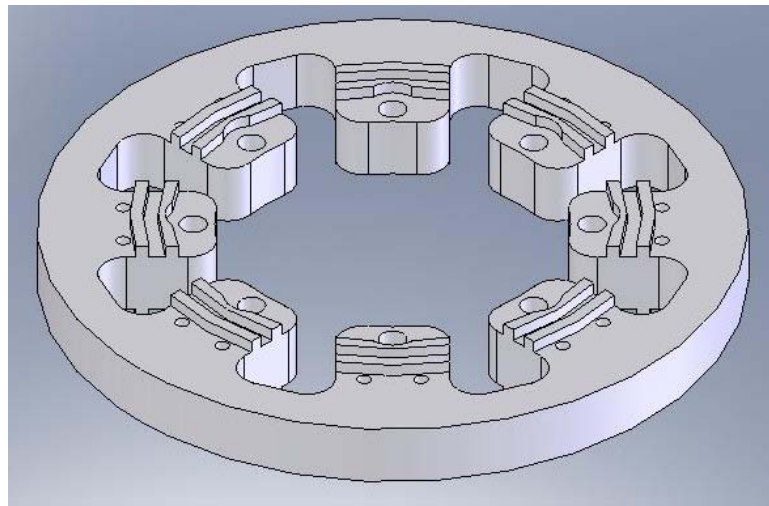
Figure 3.2: EVASII shoe alignment mount, base plate - isometric view.

3.3 Shoe Sizes

Based on data acquired over a 5 year period from a total of 532 eyes from both monkey and human donors, the exact dimensions of each shoe were determined to provide the necessary aperture to clear space for the cornea. In order to maximize the contact area on each shoe, a theoretical model was developed to determine the design parameters (Courtesy: Andres Bernal). Based on a spherical approximation of the globe, a relationship for the location of the center of rotation for the revolve cut used for computer aided design (CAD) of EVASII shoes intended for various globe diameters was determined, in terms of the shoe thickness and aperture and the diameter of the globe.
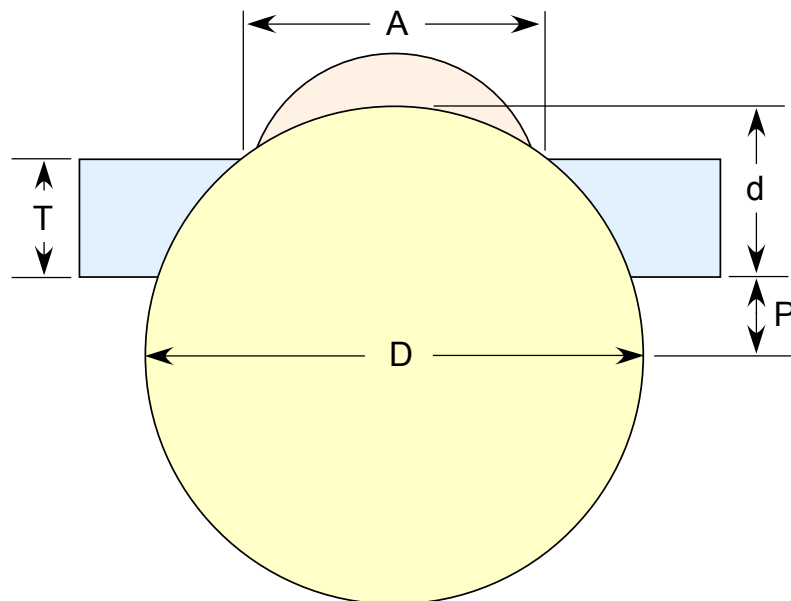
Figure 3.3: Model to determine EVASII shoe design parameters. (Following the model of Andres Bernal)

Using the model of Figure 3.5, the parameters are all related by the following equations:

$$P = -T + \frac{1}{2}\sqrt{D^2 - A^2} \quad ; \quad d = D - P$$

Where

A = aperture for removal of the cornea,

D = equatorial globe diameter,

d = depth or distance from the posterior surface of the shoe to the anterior pole of the spherical approximation of the globe = depth of the cut by the size D ball end mill = ball depth

T = thickness of the shoe,

P = distance from the posterior surface of the shoe to the centroid of the spherical approximation of the globe = the location of the center of rotation for the revolve cut used for CAD of EVASII shoes = plane depth

Since the equatorial globe diameter, D, varies among individuals, a number of different size shoes designs were made. A histogram was performed on globe diameter measurements, categorizing each bin by 1mm increments to determine which values of D are most needed. Then, the recommended aperture of removal of the cornea, A, was determined for each globe size, and using the relationship from the model, the exact parameters of each design were obtained.
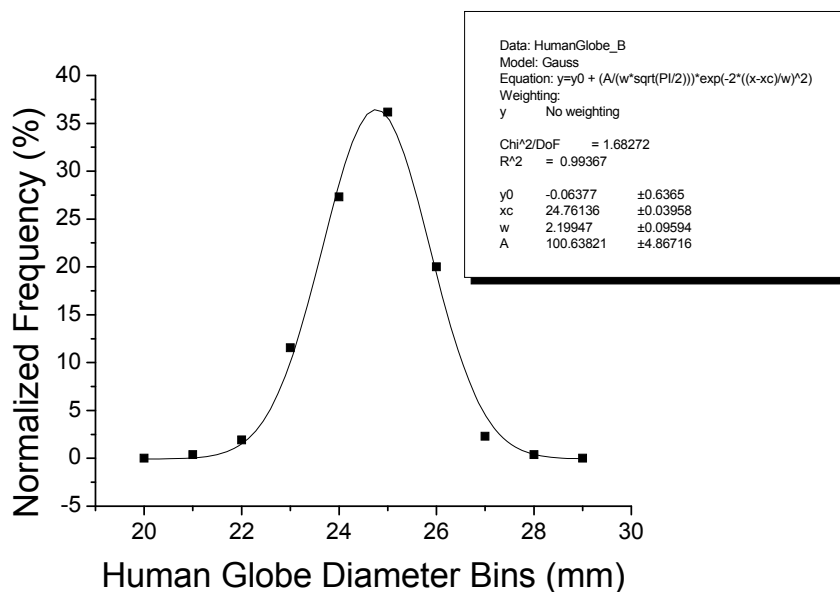
Figure 3.4: Human globe diameter histogram, with best fit Gaussian (solid black line). The best fit equation is shown in the legend (upper right).
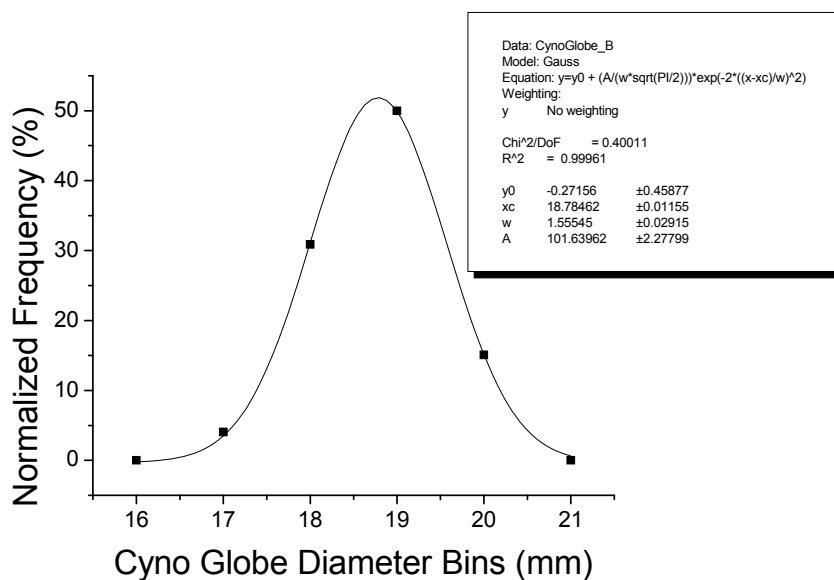
Figure 3.5: Cynomolgus monkey globe diameter histogram, with best fit Gaussian (solid black line). The best fit equation is shown in the legend (upper right).
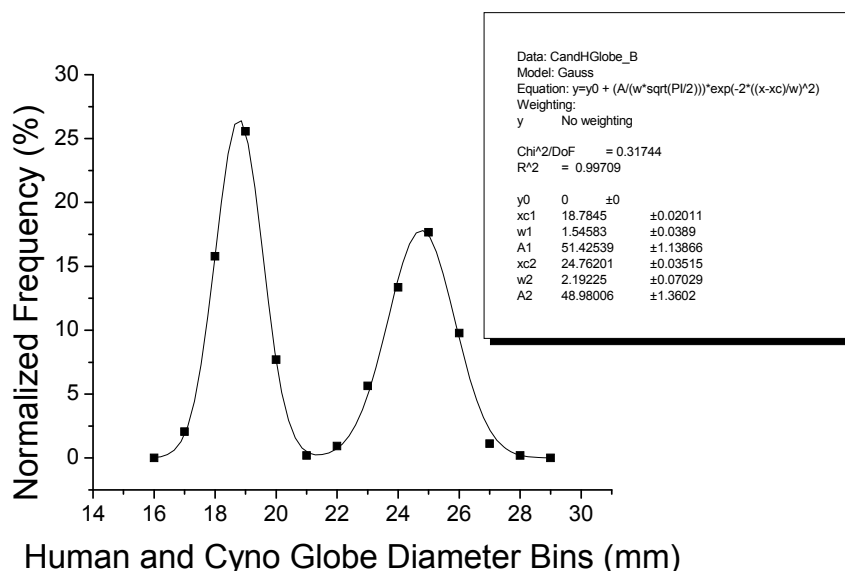
Figure 3.6: Human and cynomolgus monkey globe diameter histogram, with best fit 2-peak Gaussian (solid black line). The best fit equation is shown in the legend (upper right).

	Equatorial Diameter, D (mm)	Max Corneal Diameter (mm)	Recommended Aperture, A (mm)	Shoe Thickness, T (mm)	Ball Depth, d (mm)	Plane Depth, P (mm)
Monkey	16	9.97	10.1	6	7.795	0.205
	17	10.95	11.1	6	8.062	0.438
	18	11.25	11.4	6	8.035	0.965
	19	11.25	11.4	6	7.9	1.6
	20	10.35	11.4	6	7.784	2.216
Human	22	11.91	12.1	6	7.813	3.187
	23	11.98	12.1	6	7.72	3.78
	24	12.66	12.8	6	7.849	4.151
	25	12.75	12.9	6	7.793	4.707
	26	12.97	13.1	6	7.771	5.229
	27	11.77	13.1	6	7.695	5.805

Table 3.1: Maximum corneal diameter, recommended aperture for corneal clearances, shoe thickness, ball depth, and plane depth as a function of incremental equatorial diameter. Shoe sizes made for EVASII experiments.

3.4 Portable Dissection Stage

The shoes also have an M2 tapped hole that aligns with a through hole on the base plate. Once the shoes are aligned with the base plate, the screws are inserted, and the position of each shoe is constrained. The outer diameter of the base plate was designed to fit snuggly inside a custom built portable dissection stage, which is used for tissue preparation and other surgeries such as lens refilling.

Figure 3.7: Shoes mounted on annular base plate (left), shoes constrained onto annular base plate using M2 screws (right).
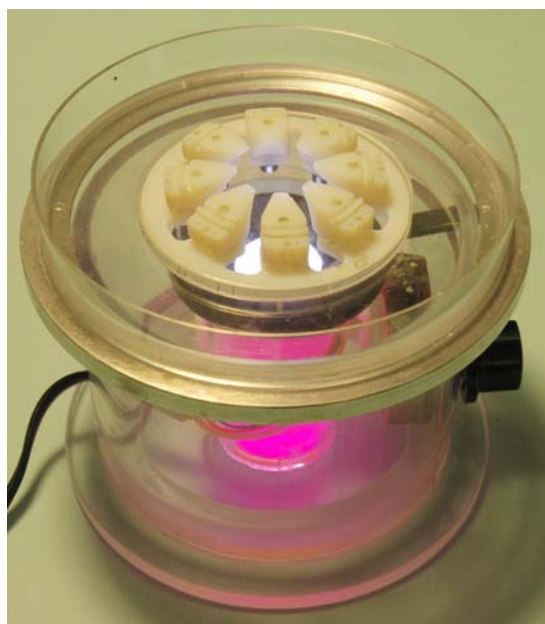
Figure 3.8: Shoes on annular base plate inside dissection stage. (Dissection stage courtesy: Jean-Marie Parel, Billy Lee and Izuru Nose).

3.5 Tissue Transfer

Once the tissue is prepared by the surgeon, just as described for EVASI, except for the use of the custom EVASII shoes, an annular retaining ring is mounted to the top side of the shoes. This ring has 8 through holes and a single groove for maintaining the orientation and position of each shoe. Once this ring is mounted, and the screws are inserted, the base plate is removed.

A custom built tool was designed to transfer the tissue from the dissection stage into EVASII. This tool has two stainless steel pegs, each with a socket and bulb at the tip. The distance between the pegs can be reduced by squeezing the tool, which is made of poly(methyl methacrylate) (PMMA). There is a small relief removed from the center of the tool, so that when pressure is applied, the PMMA tool bends, and the distance between the two pegs is reduced. When this distance is reduced, the tool fits precisely inside two holes located at opposite sides of the annular ring. This hole has a counter bore of a larger diameter, so that when the pressure is removed from the tool and the distance between each peg is increased, the bulbs of the peg serve to grab the annular ring.
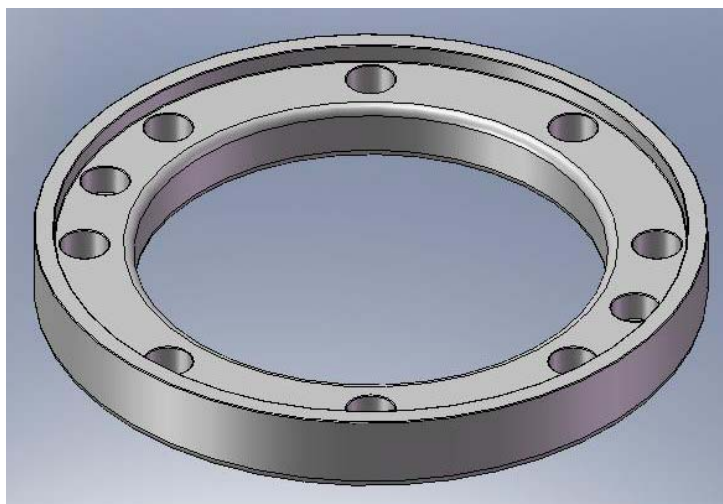
Figure 3.9: Annular retaining ring - isometric view (courtesy: Klaus Ehrmann).
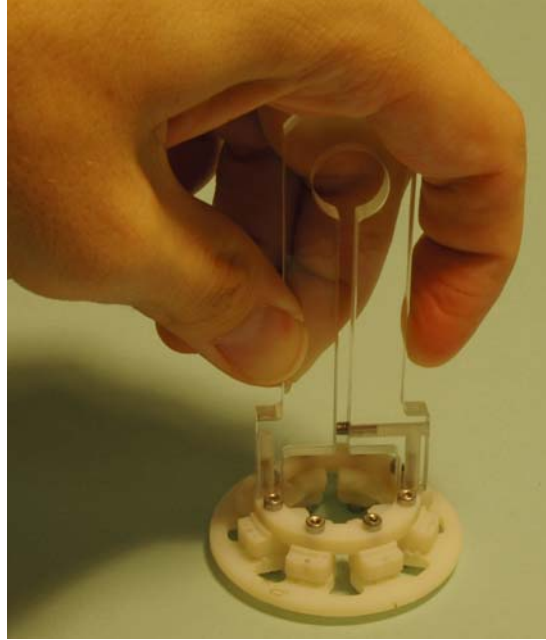
Figure 3.10: Device for transferring the tissue into EVASII. (Device courtesy: Klaus Ehrmann).

With this, the tissue preparation is ready for transfer into EVASII. The shoes are constrained in EVASII magnetically. Each shoe mounts to an arm of EVASII, which has a disk magnet imbedded at the height of the location of the shoe. A small shelf was built in on each arm, which has two holes in it, and each shoe also has two corresponding holes in it. A two pronged U-shaped steel pin (Ø = 0.83mm) is inserted into each shoe and down into the shelf of each arm. Also, the curvature of the arm was built to match that of the shoe, and with this geometry and the magnetic mount, the shoe is constrained. Once the tissue preparation is affixed magnetically, the screws and the annular ring are removed, and the system is ready for experiment.
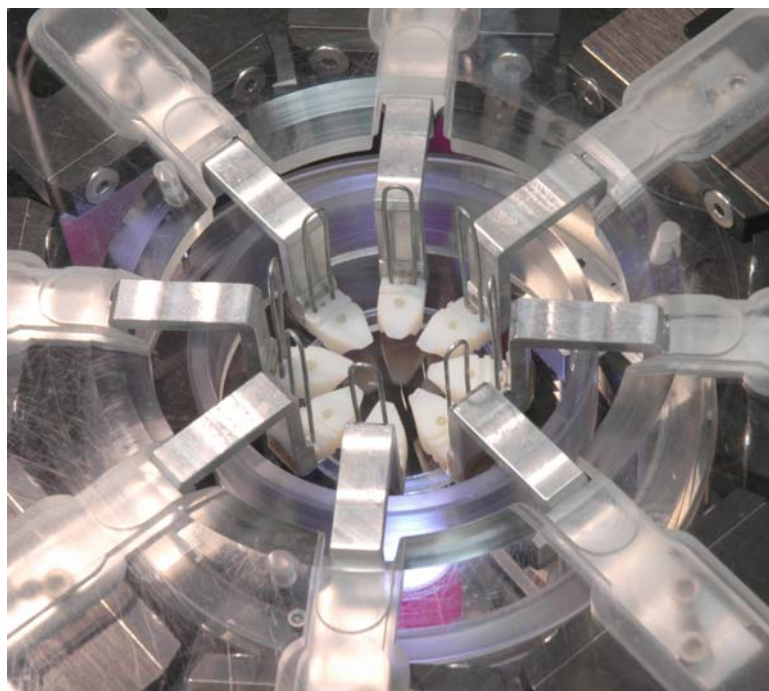
Figure 3.11: Shoes inside of EVASII mounted via U-shaped steel pins (Ø = 0.83mm) and a magnetic disk (rare earth magnet, Ø = 6mm) imbedded into each arm.

3.6 Calibration Ring

A calibration ring was designed and manufactured to access the reproducibility of the EVASII force measurement system. The calibration ring is a small Polydimethylsiloxane (PDMS, n = 1.41) annular ring (PDMS sheets, BioPlexus Corporation, Los Angeles CA). The outer and inner diameters of the PDMS calibration ring were made using a custom manufactured punch, and each individual mounting hole was made by hand using a small knife (Courtesy: Billy Lee). The thickness of the ring was measured using OCT, and it was found to be 61.55±5.05μm. Since PDMS acts as an elastic solid at room temperature (such as rubber), so long as no plastic deformation of the ring occurs during stretching, the load-stretch profile using this ring should be very repeatable. Thus, the calibration ring will provide an opportunity to access the precision of the EVASII force measurement system.
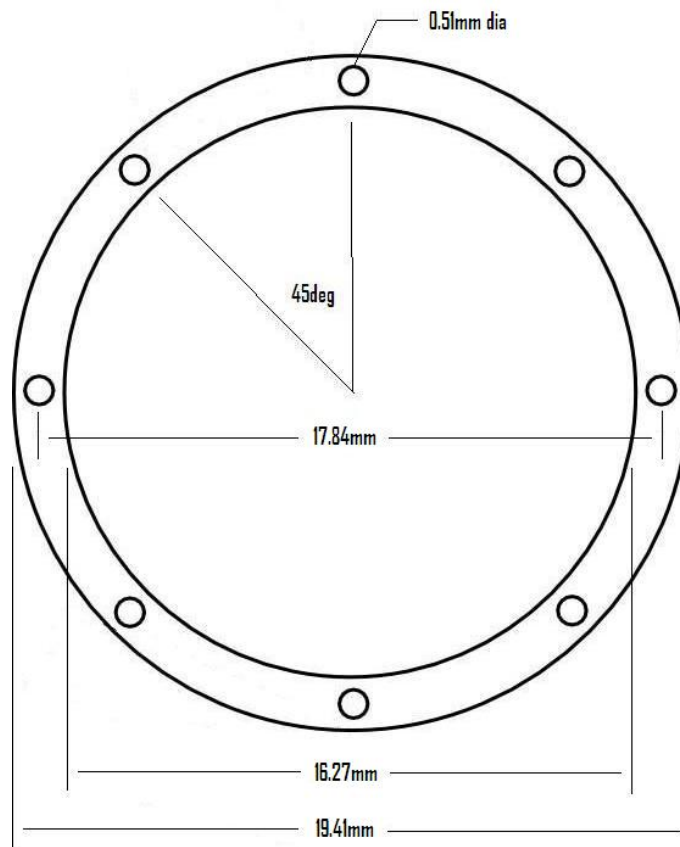
Figure 3.12: Dimensions of the calibration ring (approximate tolerances ±0.1mm).
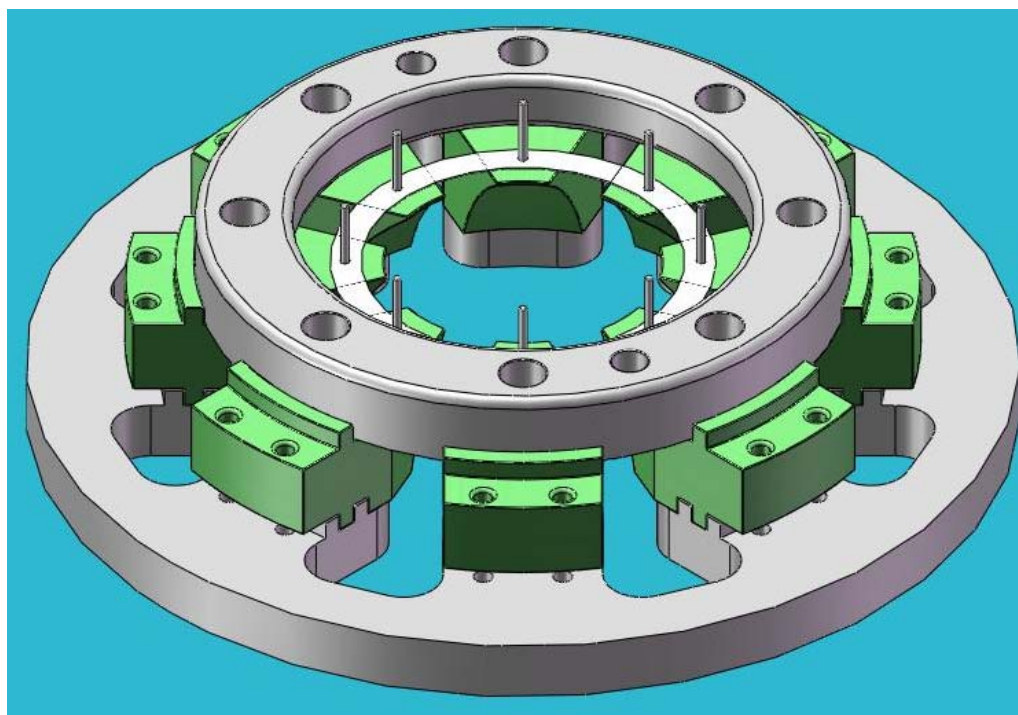
Figure 3.13: EVASII calibration ring assembly.

A mounting mechanism for the calibration ring was designed and manufactured. This mounting mechanism utilized the design discussed in Chapter 3, with one significant difference; each shoe was given a non-magnetic stainless steel peg (Ø = 0.406mm) extruding orthogonally from the upper surface of the shoe. Each peg was positioned so that the ring could be mounted in EVASII with no initial stress.

3.7 Conclusions

The tissue transfer design accomplishes the goal of providing a means to transfer the tissue from EVASII to the operating microscope and back again; however, this accomplishment is accompanied by a complication. The addition of the magnetic mounting mechanism causes magnetic coupling between neighboring arms. Thus, when the arms are translated, as is done during an experiment, the load measured by each arm changes. This magnetic interference introduces a significant position dependent offset in the experiment, with an amplitude about 5 times that of the signal (i.e. tissue load). However, since the ferromagnets used are permanent magnets, the magnetic load as a function of position is quite reproducible, thereby suggesting the possibility of cancellation during post processing. Thus, a method to cancel this artifact was established, and this is discussed in the next chapter.

In addition, a calibration ring and a calibration ring mounting mechanism has been designed. The calibration ring load-stretch profile will provide a repeatable standard which will be used to access the repeatability of the EVASII force measurement system.

Chapter 4: EVASII Load Analysis and Magnetic Load Offset

4.1 Background

A mechanism for mounting tissue in EVASII was developed. This mechanism employs magnets to hold the shoes in place. Initial experiments showed that increasing the distance between the magnets causes the measured sum load to increase, even with no tissue, no shoes, and no pins mounted in the system. This increase was qualitatively repeatable, suggesting the possibility of cancellation. The purpose of the experiments described in this chapter is to identify a method to cancel this artifact and to assess the effect of this added computation.
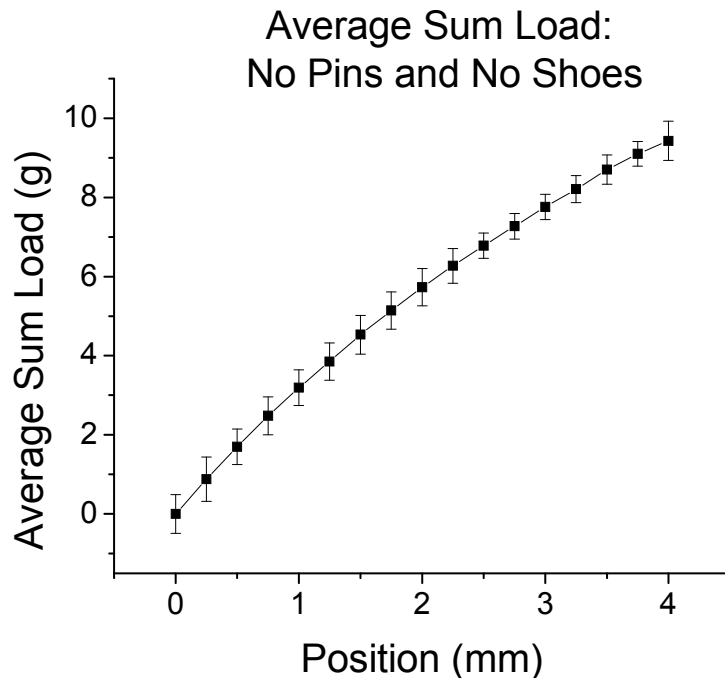
Figure 4.1: Average sum load (for 10 experiments, with no pins and no shoes) as a function of position, where the error bars give the 95% confidence interval derived through a standard first order error propagation analysis.

Furthermore, questions about the effect of the pins used to mount the shoes have arisen concerning the repeatability of the magnetic load offset. The malleable pins used to secure the shoes magnetically are not all exactly identical. In total, 20 pins were made by hand, and of these, 11 provided a proper fit. The weights of these 11 pins were measured with a balance with a resolution of 1mg (Mettler PM400, Satorius, Goettingen Germany), and the mean weight was 0.303±0.003g, with the heaviest pin weighing 0.308g and the lightest pin weighing 0.299g. Since the pin weights and shape are different, it is likely that orientation of the pins will affect the magnetic coupling measured in EVASII. Thus, the purpose of these experiments are to characterize the new magnetic load offset, to identify a method to cancel the magnetic load artifact, to access the effect of this added computation, to determine the effect of the mounting pins, and to measure the repeatability of the load vs. position profile of the calibration ring.

4.2 Correction and Characterization of the Magnetic Load

4.2.1 No Tissue, No Pins, No Shoes

4.2.1.1 Purpose

To characterize the magnetic load as a function of displacement with no tissue, no pins, and no shoes, only the magnetic arms.

4.2.1.2 Methods

With no tissue, no pins and no shoes, the system was taken through a stretch cycle, stretching radially from 0 to 4mm in intervals of 0.25mm, with a 10s hold (position hold) at each position. For the purposes of analysis, the load during each position hold was averaged to obtain the position-load behavior of the magnetic system.
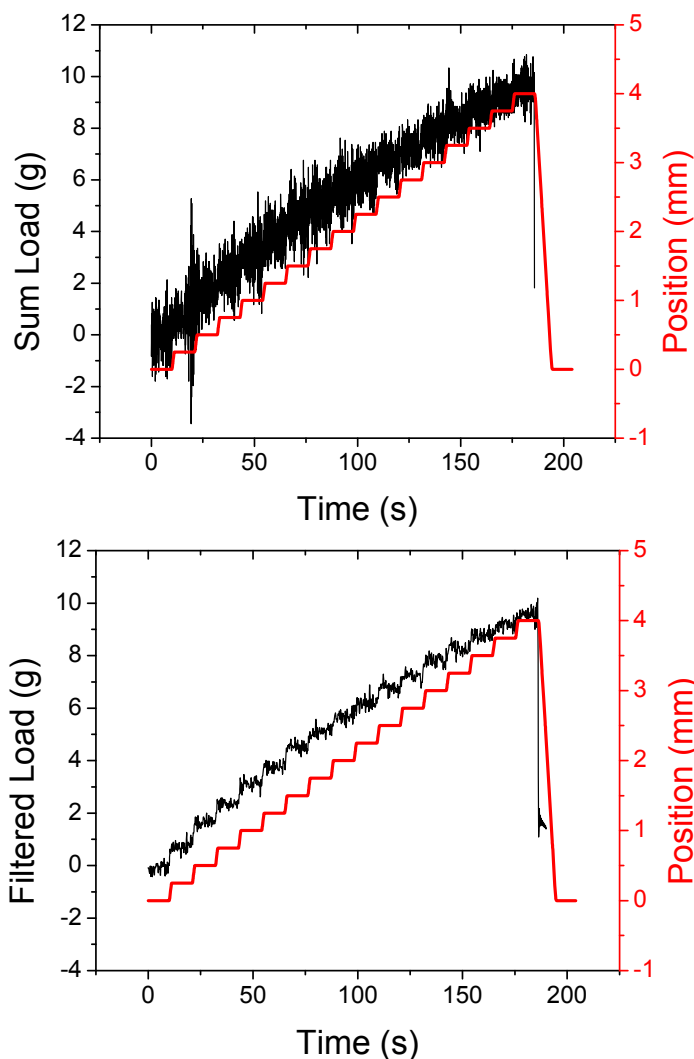
Figure 4.2: Sum load and position vs. time, with no tissue, no shoes, and no pins, raw data (top) and filtered data (bottom). The average and standard deviation of the load is determined for each position hold, where a position hold refers to the plateaus in the position-time profile. This method of analysis eliminates the effect of motion of the arms, and considers only the equilibrium behavior of the system.

After reaching the 4mm plateau, the position returned to 0mm in a single step. In between each experiment, the motors were homed and the load was zeroed. This process was repeated until 10 measurements were complete. The load data was extracted and analyzed using a Matlab program (Appendix 1).

4.2.1.3 Results

The average and standard deviation of the sum load during each position hold for all of the 10 runs has been tabulated. However, use of the average, standard deviation, and standard error all depend on the assumption that the data follows a normal probability distribution. To test for normality, the Shapiro-Wilk normality test was used on all data in this set, and the measured residuals were regressed against a normal distribution with the same mean and variance as the sample. Using both techniques, the data passed the normality test with a confidence better than 97% (Appendix 2), and from this result, the normality assumption was applied to all other data in this chapter, which was acquired in a similar manner. With this requirement satisfied, the variation between runs was quantified by considering the standard deviation and range of mean sum load values as a function of position.
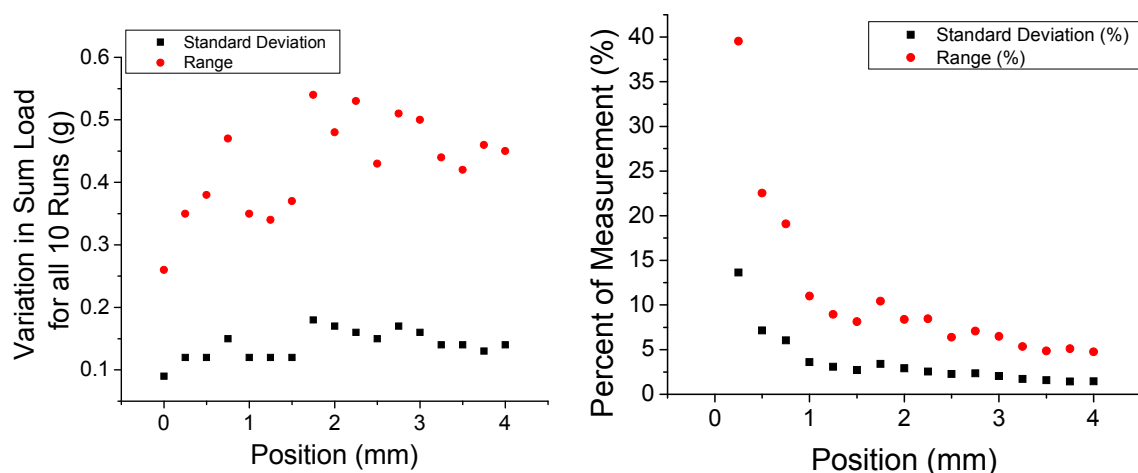
Figure 4.3: (left) Standard deviation (black) and range (red) in the average sum load for all ten runs, with no pins and no shoes. (right) Shows the standard deviation (black) and the range (red) as a percentage of the average sum load as a function of position.

The mean standard deviation, for all positions, was 0.14g, and the mean range was 0.43g. In other words, on average, the maximum difference in the position-hold sum load (of the magnetic load, with no pins and no shoes) over 10 runs was just under 0.5g.

Then, to determine the mean behavior, for each position-hold, a standard first order error propagation analysis was used (Bevington 1969), so that the average load and the standard uncertainty of the average load at each position was given by:

$$\overline{L}_j = \frac{1}{N}\sum_{i=1}^{N} L_{ij} \qquad\qquad \sigma_{L_j}^2 = \frac{1}{N}\sum_{i=1}^{N} \sigma_{L_{ij}}^2$$

Where

$\overline{L}_j$ = Average load at the j$^{\text{th}}$ position

N = Number of experiments = 10

L_{ij} = Average load for the i$^{\text{th}}$ measurement at the j$^{\text{th}}$ position

σ_{L_j} = Standard uncertainty of the average load at the j$^{\text{th}}$ position

$\sigma_{L_{ij}}$ = Standard deviation of the average load for the i$^{\text{th}}$ measurement at the j$^{\text{th}}$ position

A second degree polynomial was fit to the $\overline{L}_j$ vs. position profile. The best fit equation for the magnetic load with no tissue, no pins, and no shoes was found to be:

$$y = -0.244x^2 + 3.308x + 0.081$$

Where y is the magnetic load, and x is the position of the shoes.
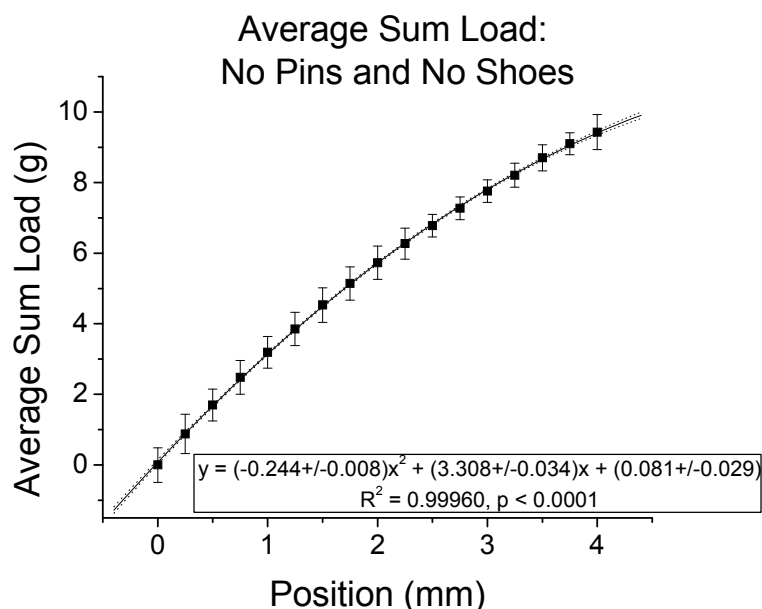
Figure 4.4: Average sum load (for all 10 experiments, with no pins and no shoes) as a function of position, where the error bars give the 95% confidence interval derived through a standard first order propagation of errors. A quadratic equation is fit to this data using a least squares regression technique (solid black line), and the 95% confidence intervals for each mean of the fit are shown (dotted black line). The quadratic equation and fit parameters are shown in the legend (bottom right).

4.2.1.4 Conclusions

The magnetic load gives a quadratic trend as a function of position. Since the standard uncertainty at each position is relatively constant, this indicates that, using these 10 measurements, the magnetic load with no pins and no shoes can be determined with a mean 95% confidence interval of ±0.43g. The magnetic load (with no pins and no shoes) can be determined at any position by the quadratic equation shown in Figure 4.6 with an uncertainty best approximated by ±0.43g.

4.2.2 With Pins and Shoes Stationary

4.2.2.1 Purpose

To determine the effect of the pins and shoes on the magnetic artifact, the magnetic load as a function of displacement with pins and shoes, while the position of the pins and shoes remains constant throughout all 10 experiments was characterized.

4.2.2.2 Methods

With the shoes (19mm) and pins mounted in EVASII, the same displacement profile as described previously was completed. In between each experiment, the motors were homed and the load was zeroed, and this process was repeated to obtain 10 measurements.

4.2.2.3 Results

The mean standard deviation, for all positions, was 0.18g, and the mean range was 0.58g. In other words, on average, the maximum difference in the position-hold sum load (with pins and shoes stationary) over 10 runs was just over 0.5g.

The best fit equation for the magnetic load with pins and shoes stationary was found to be:

$$y = -0.174x^2 + 2.458x + 0.064$$

Where y is the magnetic load, and x is the position of the shoes.
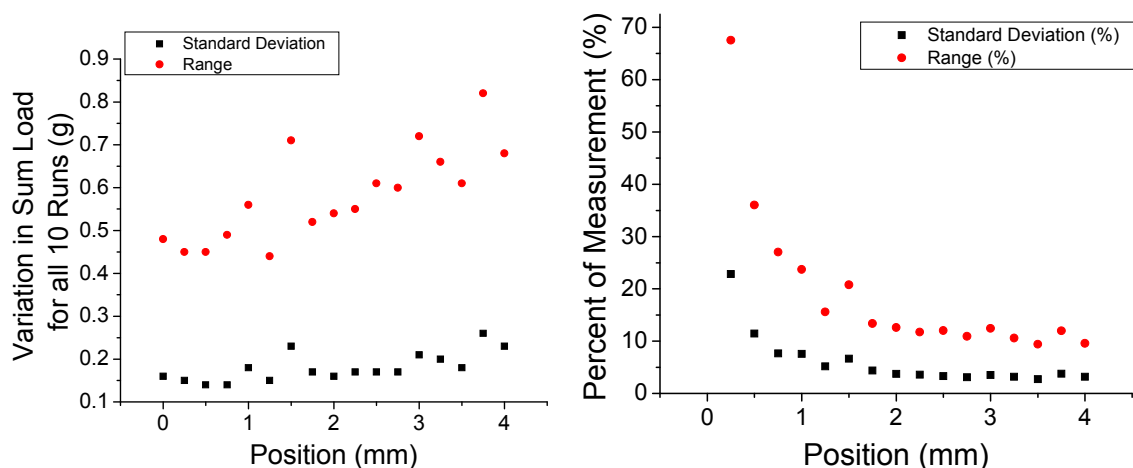
Figure 4.5: (left) Standard deviation (black) and range (red) in the average sum load for all ten runs, with pins and shoes stationary (stretch only). (right) Shows the standard deviation (black) and the range (red) as a percentage of the average sum load as a function of position.
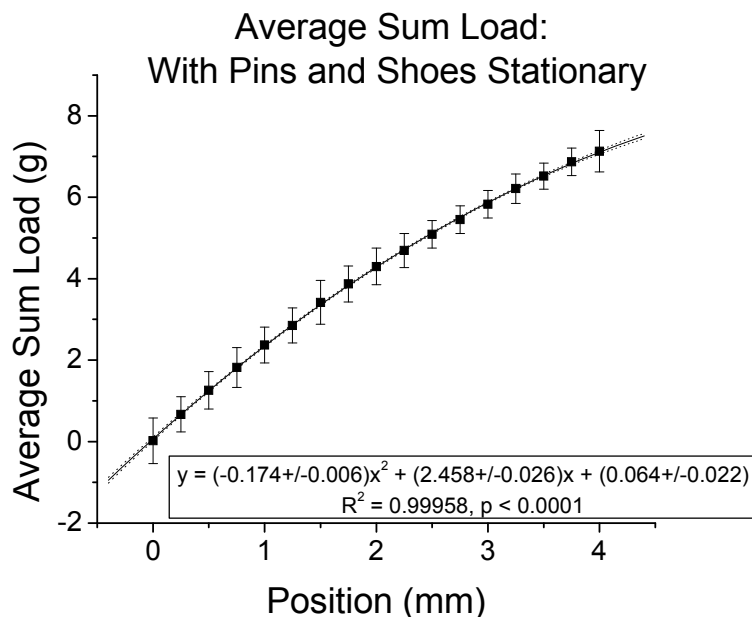
Figure 4.6: Average sum load (for all 10 experiments, with pins and shoes stationary) as a function of position, where the error bars give the 95% confidence interval derived through a standard first order propagation of errors. A quadratic equation is fit to this data using a least squares regression technique (solid black line), and the 95% confidence intervals for each mean of the fit are shown (dotted black line). The quadratic equation and fit parameters are shown in the legend (bottom right).

4.2.2.4 Conclusions

Again, the magnetic load gives a quadratic trend as a function of position. Since the standard uncertainty at each position is relatively constant, this indicates that, using these 10 measurements, the magnetic load with pins and shoes stationary can be determined with a mean 95% confidence interval of ±0.42g. Thus, the magnetic load (with pins and shoes stationary) can be determined at any position by the quadratic equation shown in Figure 4.8 with an uncertainty best approximated by ±0.42g.

4.2.3 With Pins and Shoes Randomly Rearranged

4.2.3.1 Purpose

To characterize the magnetic load as a function of stretch with pins and shoes, while the position of the pins and shoes are randomly rearranged between runs to

simulate the natural variation which may occur from one experiment to another. The results will then be used to compare the results with the pins and shoes stationary to determine if the variation in weights of the pins has a measurable affect on the magnetic loads. Also, these results will be compared to the results with no pins and no shoes to determine if the steel pins have a measurable affect on the magnetic load.

4.2.3.2 Methods

The same stretch profile as described previously was performed, but this time, the position of the pins and shoes were randomly rearranged between runs to access the effect of pin and shoe orientation, and this process was repeated for 10 measurements.

4.2.3.3 Results
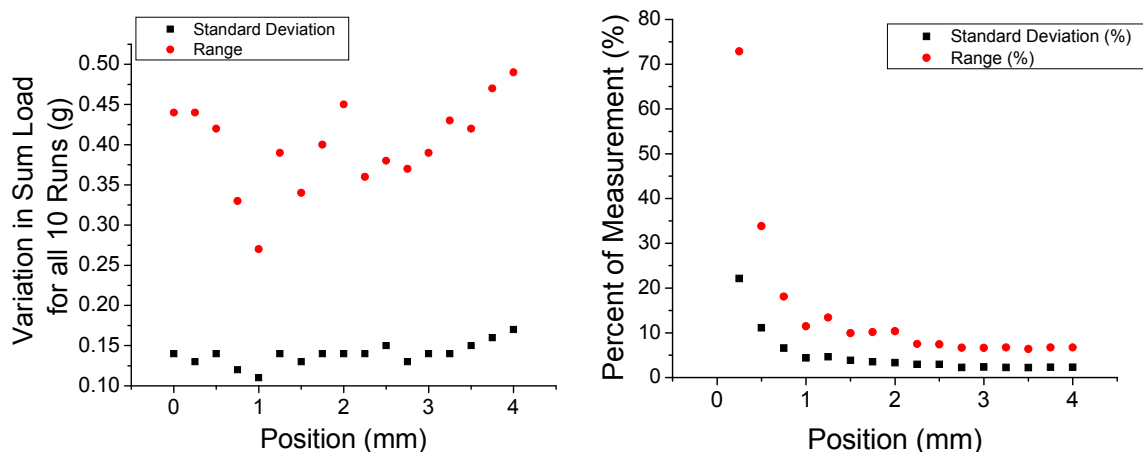
Figure 4.7: (left) Standard deviation (black) and range (red) in the average sum load for all ten runs, with pins and shoes randomly rearranged (stretch only). (right) Shows the standard deviation (black) and the range (red) as a percentage of the average sum load as a function of position.
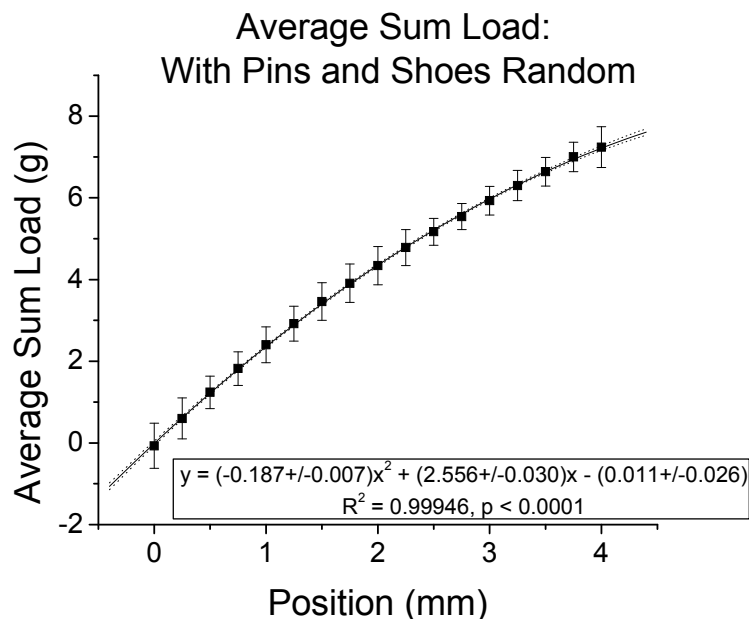
Figure 4.8: Average sum load (for all 10 experiments, with pins and shoes randomly rearranged) as a function of position, where the error bars give the 95% confidence interval derived through a standard first order propagation of errors. A quadratic equation is fit to this data using a least squares regression technique (solid black line), and the 95% confidence intervals for each mean of the fit are shown (dotted black line). The quadratic equation and fit parameters are shown in the legend (bottom right).

The mean standard deviation, for all positions, was 0.14g, and the mean range was 0.40g. Thus, on average, the maximum difference in the position-hold sum load (of the magnetic load, with pins and shoes randomly rearranged) over 10 runs was 0.40g.

The best fit equation for the magnetic load with pins and shoes randomly rearranged was found to be:

$$y = -0.187x^2 + 2.556x + 0.011$$

Where y is the magnetic load, and x is the position of the shoes.

4.2.3.4 Conclusions

The magnetic load gives a quadratic trend as a function of position. Since the standard uncertainty at each position is relatively constant, this indicates that, using these 10 measurements, the magnetic load with pins and shoes randomly rearranged can be

determined with a mean 95% confidence interval of ±0.42g. In other words, the magnetic load (with pins and shoes randomly rearranged) can be determined at any position by the quadratic equation shown in Figure 4.10 with an uncertainty best approximated by ±0.42g.

4.2.4 Comparison: Magnetic Load With and Without Pins

4.2.4.1 Purpose

The purpose of this analysis is to determine if the presence and position of the steel mounting pins has a significant effect on the magnetic load and on the variation in the magnetic load.

4.2.4.2 Methods

A Student's t-test has been performed for the load at each position, comparing three different configurations of EVASII: with no shoes and no pins, with shoes and pins stationary, and with shoes and pins randomly rearranged. (This and all other Student's t-tests herein were performed using Origin 7.0). Furthermore, a Student's t-test has been performed on the standard error of the magnetic load for each position, comparing the three configurations discussed above (Appendix 2).

4.2.4.3 Results
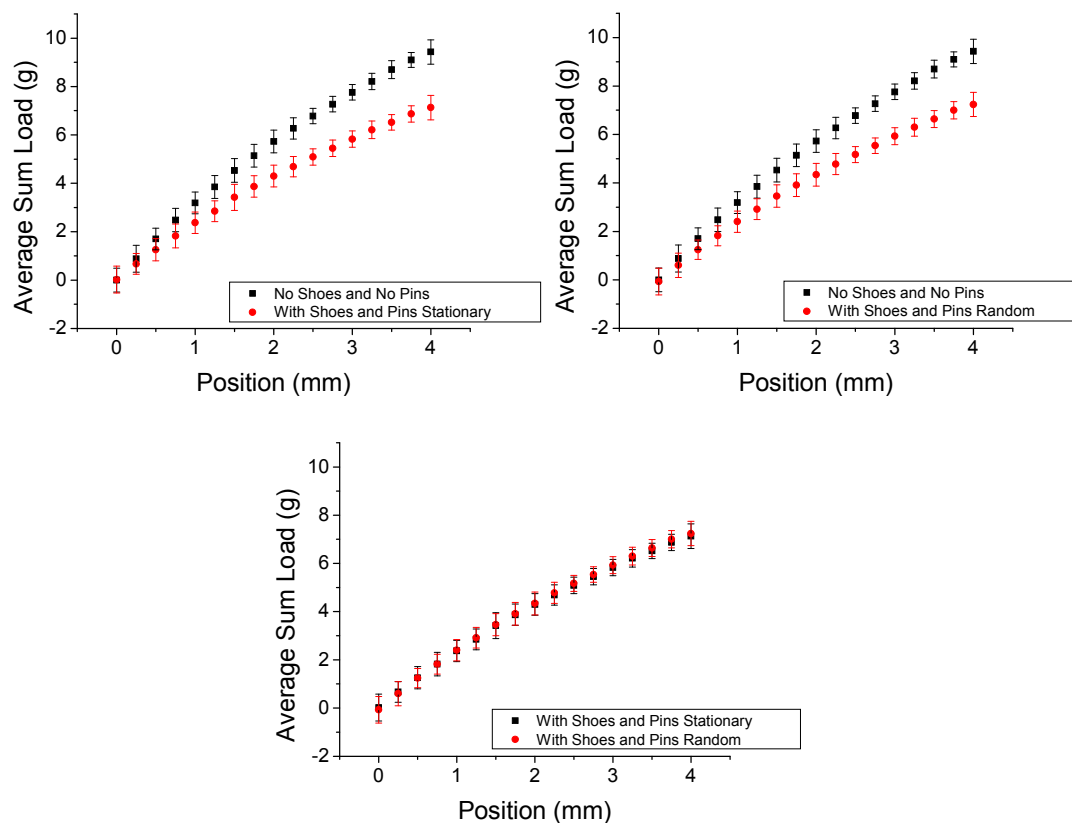
Figure 4.9: Average sum load (magnetic load) as a function of position comparing the magnetic load with no shoes and no pins to that with shoes and pins stationary (top left), the magnetic load with no shoes and no pins to that with shoes and pins randomly rearranged (top right), and the magnetic load with shoes and pins stationary to that with the shoes and pins randomly rearranged (bottom), where the error bars give the 95% confidence intervals.

The magnetic load with no pins and no shoes is significantly different than the magnetic load with pins and shoes stationary and also significantly different than the magnetic load with pins and shoes randomly rearranged for all positions, except for the initial position. The loads in the initial position are not significantly different since the load was zeroed between runs. Also, the magnetic load with the pins and shoes stationary is not significantly different from the magnetic load with the pins and shoes randomly rearranged.
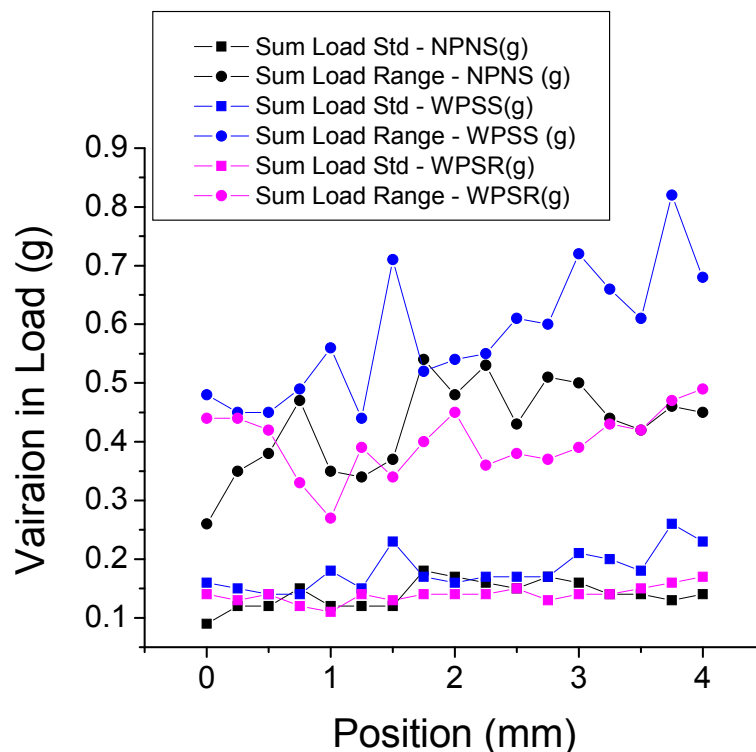
Figure 4.10: Comparison - variation in magnetic load with no pins and no shoes (black), with pins and shoes stationary (blue), and with pins and shoes randomly rearranged (purple), where the standard deviation (circle) and range (square) are shown as a function of position. NPNS = no pins and no shoes, WPSS = with pins and shoes stationary, and WPSR = with pins and shoes random.

The variation in magnetic load between runs with no shoes and pins is not significantly different from that with shoes and pins rearranged randomly. However, the variation in magnetic load between runs with shoes and pins stationary was significantly greater than the variation in either circumstance. This is likely due to external variations in the environment, and suggests the use of the sum loads obtained with the pins and shoes rearranged randomly for the magnetic load correction.

4.2.4.4 Conclusions

The presence of the pins has a significant effect on the magnetic load, but the positioning of the pins does not have a significant effect. The magnetic artifact can be

corrected by subtracting the following load offset from the measured load vs. displacement profile:

$$y = -0.187x^2 + 2.556x + 0.011$$

Where y is the load to be subtracted, and x is the corresponding position.

4.3 Calibration Ring

4.3.1 Purpose

To characterize the precision of the EVASII force measurement system using an elastic calibration ring (Figure 4.2) whose load-stretch behavior is repeatable over its elastic range.

4.3.2 Methods

The calibration ring was mounted in EVASII, and the ring was taken through a stretch cycle, stretching radially from 0 to 2mm in intervals of 0.25mm, with a 10s hold at each position. After reaching the 2mm plateau, the position returned to 0mm in a single step. In between each experiment, the positions of the pins were randomly rearranged, and the motors were homed and the load was zeroed. This process was repeated until 10 measurements were complete.

4.3.3 Results
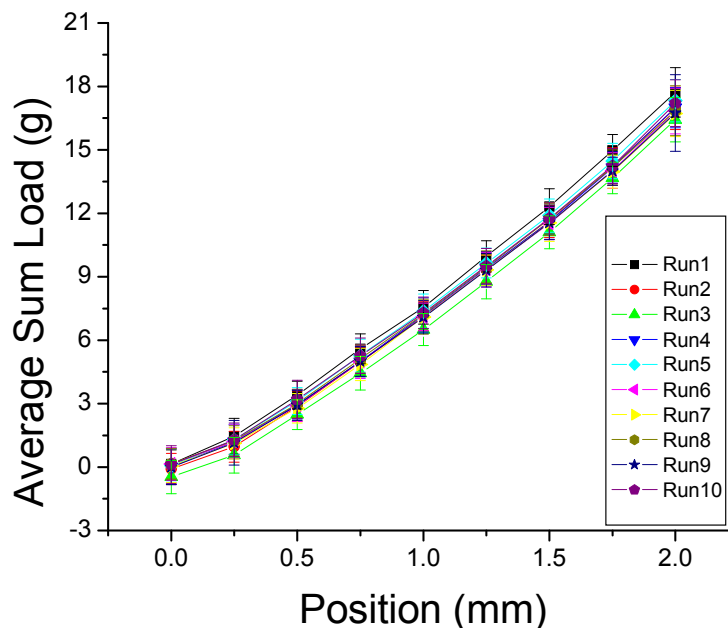
Figure 4.11: Calibration ring sum load. Each data point gives the average and standard error of the sum load during each position hold (after subtraction of the magnetic load), showing all 10 runs (0, 0.25, 0.5mm…).
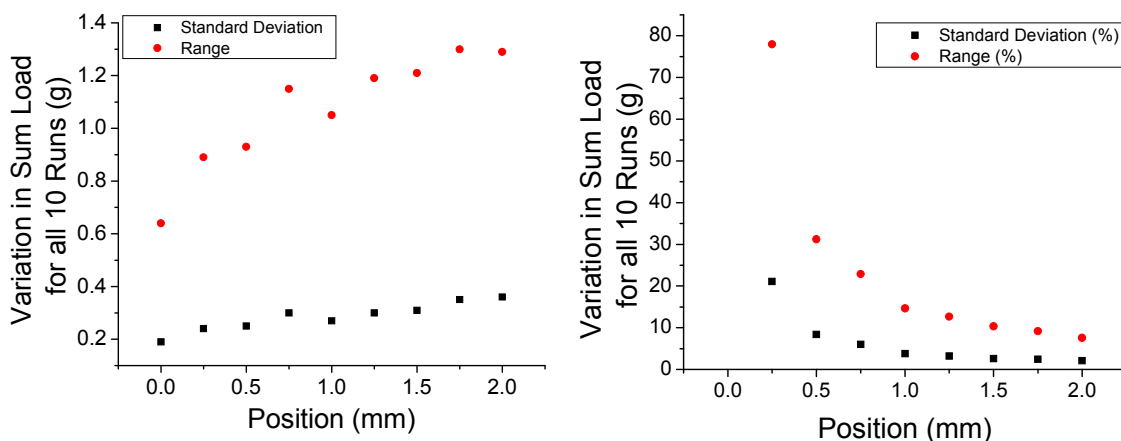
Figure 4.12: (left) Standard deviation (black) and range (red) in the calibration ring average sum load for all ten runs (stretch only). (right) Shows the standard deviation (black) and the range (red) as a percentage of the average sum load as a function of position.

The mean standard deviation, for all positions, was 0.29g, and the mean range was 1.07g. Hence, on average, the maximum difference in the position-hold sum load (of the calibration ring) over 10 runs was just over 1g. Also, the absolute maximum

difference in the position-hold sum load over 10 runs was 1.3g. The mean error in load,

across all runs and all positions, was ±0.81g (±0.64g to ±1.81g).
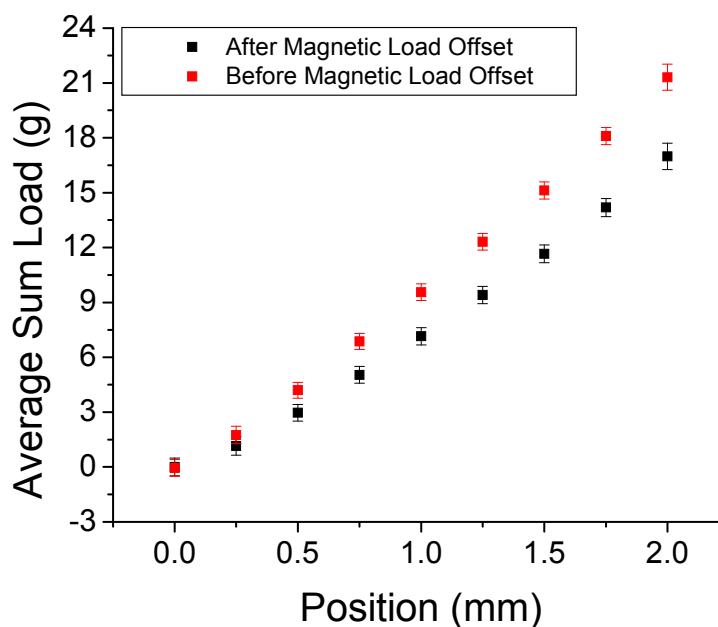
Figure 4.13: Calibration ring average sum load (for all 10 experiments) vs. position after (black) and before (red) magnetic load offset.
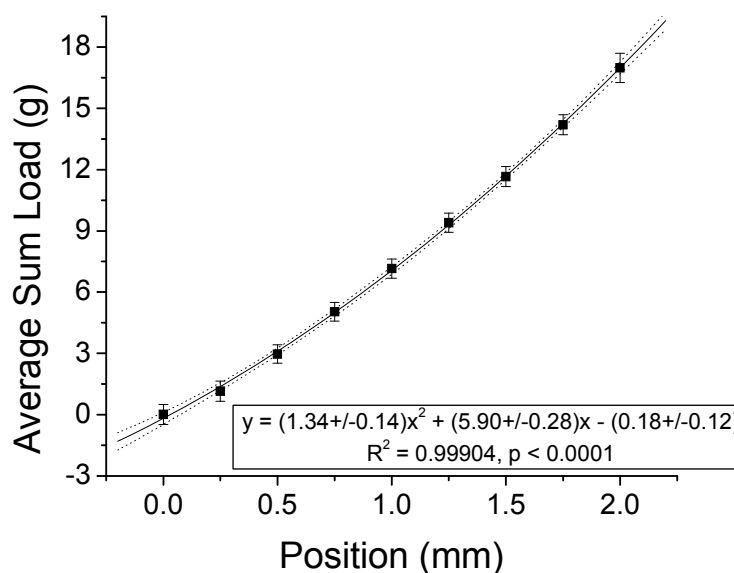
Figure 4.14: Average sum load (for all 10 experiments) as a function of position, where the error bars give the 95% confidence interval derived through a standard first order propagation of errors. A quadratic equation is fit to this data using a least squares regression technique (solid black line), and the 95% confidence intervals for each mean of the fit are shown (dotted black line). The quadratic equation and fit parameters are shown in the legend (bottom right).

4.3.4 Conclusions

The calibration ring load gives a quadratic trend as a function of position. Taking the average of 10 measurements, using the calibration ring as phantom tissue and after subtraction of the magnetic load, the calibration ring load can be determined with a mean 95% confidence interval of ±0.81g. In short, the calibration ring sum load can be determined at any position by the quadratic equation shown in Figure 4.14 with an uncertainty best approximated by ±0.81g.

4.4 Uncertainty Analysis

4.4.1 Purpose

The purpose of the uncertainty analysis was to:

- determine the effect of the additional calculation of the magnetic load offset on average sum load measurement uncertainty,

- estimate the overall sum load uncertainty of the EVASII force measurement system.

- characterize the effect on measurement uncertainty of using the sum of measurements from 8 transducers to calculate the sum load

- estimate the required resolution of each transducer for the smallest incremental loads of physiological concern for EVASII measurements.

4.4.2 Methods

A first order error propagation analysis was performed to assess the effect of the magnetic load offset and to characterize the effect of summing measurements from 8 transducers to determine the sum load. The variation in load during position hold was

assumed to be due to instrumental uncertainties, and thus distributed in a Gaussian nature. The Gaussian distribution, defined by the mean and the standard deviation, along with the model of overall system uncertainty, was used to calculate the required resolution for discerning an increase in load of 0.1g, which is typical increment in load during standard EVAS stretching with 0.25mm step intervals.

4.4.3 Results

For experiments performed in EVASII with magnetic arms, the measured load, $F_{measured}$, is the sum of the load applied to the tissue, F_{actual}, and the magnetic load, F_{offset}. Thus, to extract the load applied to the tissue, the magnetic load must first be subtracted

$$F_{actual} = F_{measured} - F_{offset}$$

Then, the uncertainty of the actual load becomes

$$\sigma_{F_{actual}} = \sqrt{\sigma_{F_{measured}}^2 + \sigma_{F_{offset}}^2}$$

However, in the case of a mechanical solution, without the magnetic loading, the uncertainty is simply given by $\sigma_{Fmeasured}$. Also, since the measurements of $F_{measured}$ and F_{offset} were preformed with the same instrument in an identical fashion, the standard deviations of these measurements are approximately equal. Thus, the added computation required to subtract the magnetic load adds a factor of $\sqrt{2}$ to the uncertainty in the sum load applied to the tissue. In other words, the use of magnets to mount the tissue added 42% to the overall force measurement uncertainty. Since, the 95% confidence interval of EVASII sum load measurements is approximately ±0.5g, the modified confidence interval for any load measurement after subtracting the magnetic load is ±0.71g, giving an increase in uncertainty of ±0.21g.

The measurement uncertainty of the sum load in EVASII is dictated by the behavior of each transducer, where the sum load is taken as the sum of all 8 transducer measurements. Any system using the sum of 8 signals will inherently have more uncertainty than a system using only one signal, assuming that the uncertainty in each individual signal is equivalent. Thus, in order for the system using 8 transducers (EVASII) to perform with a precision that is equal to that of the system using only one transducer (EVASI), each transducer must have greater precision than that used in the one transducer system. Following a first order propagation of errors, and assuming that each transducer has approximately the same standard deviation, σ, during position hold, it can be shown that

$$\sigma_{sum} = \sigma \cdot \sqrt{8}$$

Where, for a single transducer system, the uncertainty is given simply by σ. So, for a system with 8 transducers to perform with equal precision as a system with only one transducer, the following criterion must be satisfied

$$\sigma_{8\,Transducers} = \frac{1}{\sqrt{8}} \sigma_{1\,Transducer}$$

This result is very important for the goals of EVASII, which are to adequately resolve simulated accommodation force measurements, which are typically between 0.8 and 3g at the maximum position (2mm). Actually, a goal of EVAS is to confidently resolve each step, and the stretch protocol uses 9 steps, 0 to 2mm in increments of 0.25mm, giving a total of 8 divisions. Accordingly, for the smallest maximum loads, assuming a linear load vs. position curve, EVAS needs to adequately resolve 0.8/8 = 0.1g. Then, the required standard deviation of the sum load that gives a 95% confidence that two adjacent measurements are significantly different can be determined. The

general definition of the Gaussian probability distribution (of an individual measurement) is given by:

$$P(x) = \frac{1}{\sigma\sqrt{2\pi}} e^{-\left[(x-\mu)^2/(2\sigma^2)\right]}$$

Where, μ is the mean, and σ is the standard deviation. Then, for the case where the two means are $\mu = 0.0$g and $\mu = 0.1$g

$$P_{0.0}(x) = \frac{1}{\sigma\sqrt{2\pi}} e^{-\left[(x)^2/(2\sigma^2)\right]} \qquad ; \qquad P_{0.1}(x) = \frac{1}{\sigma\sqrt{2\pi}} e^{-\left[(x-0.1)^2/(2\sigma^2)\right]}$$

And the intercept of these two Gaussian distributions can be determined as

$$P_{0.0}(x) = \frac{1}{\sigma\sqrt{2\pi}} e^{-\left[(x)^2/(2\sigma^2)\right]} = P_{0.1}(x) = \frac{1}{\sigma\sqrt{2\pi}} e^{-\left[(x-0.1)^2/(2\sigma^2)\right]}$$

$$e^{-\left[(x)^2/(2\sigma^2)\right]} = e^{-\left[(x-0.1)^2/(2\sigma^2)\right]}$$

$$\frac{x^2}{2\sigma^2} = \frac{(x-0.1)^2}{2\sigma^2} \qquad ; \qquad x = 0.05$$

So, by the definition of the probability distribution

$$\int_{-\infty}^{\infty} P(x) = 1$$

And if a 95% confidence in the separation of the two measurements is imposed

$$0.05 = \int_{0.05}^{\infty} P_{0.0}(x) + \int_{-\infty}^{0.05} P_{0.1}(x) = 2\int_{0.05}^{\infty} P_{0.0}(x)$$

Where, in general

$$\int P(x)dx = \int \frac{1}{\sigma\sqrt{2\pi}} e^{-\left[(x-\mu)^2/(2\sigma^2)\right]}dx = \frac{1}{2}\left[1 + erf\left(\frac{x-\mu}{\sigma\sqrt{2}}\right)\right]$$

Therefore

$$0.05 = \left[1 + erf\left(\frac{x}{\sigma\sqrt{2}} \right) \right]_{0.05}^{\infty}$$

Where erf is the error function, given by

$$erf(x) = \frac{2}{\sqrt{\pi}} \int_0^x e^{-t^2} dt$$

Subsequently, with only one unknown, the 0.05 limit can be solved for analytically with the use of an error function look-up table, giving a required standard deviation of the sum load of, $\sigma = 0.026g$, as shown graphically below.

Thus, the required standard deviation during position hold for each individual transducer (for an 8 transducer system) is

$$\sigma_{8 Transducers} = \frac{1}{\sqrt{8}} \sigma_{1 Transducer} = \frac{0.026g}{\sqrt{8}} = 0.009g = 9mg$$
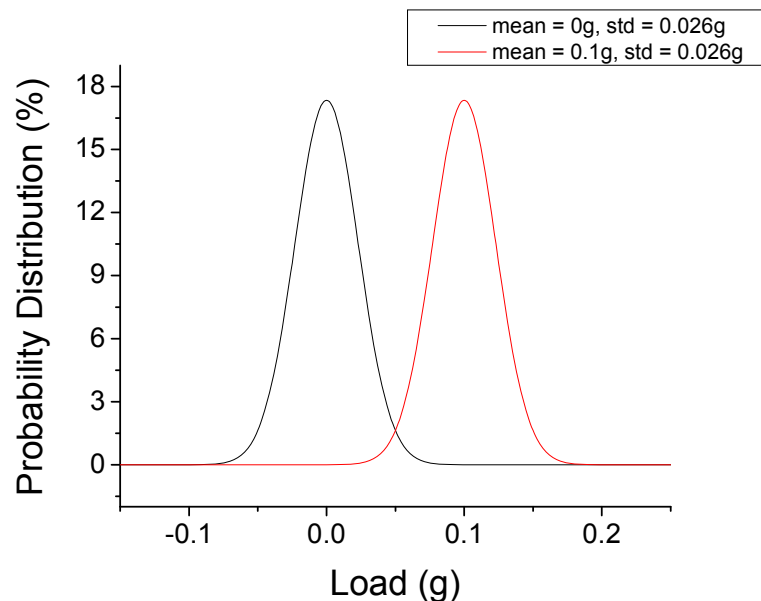
Figure 4.15: Two adjacent measurement probability distributions, separated by 0.1g, with a standard deviation of 0.026g, giving a 95% confidence that the measurements are different.

4.4.4 Conclusions

The use of magnets to mount the tissue added 42% to the overall force measurement uncertainty. Since, the 95% confidence interval of EVASII sum load measurements is approximately ±0.5g, the modified confidence interval for any load measurement after subtracting the magnetic load is ±0.71g, giving an increase in uncertainty of ±0.21g due to the magnetic load offset.

The use of an 8 transducer system to determine the sum load increases the overall uncertainty by a factor of √8 (182%). In other words, for an 8 transducer system to yield the same uncertainty in sum load as a single transducer system, the 8 transducer system must have individual transducers with a precision that is a factor of 1/√8 that of the transducer used in the single transducer system.

For the EVASII stretching profile, with 0.25mm step increments, the incremental increase in sum load is often as small as 0.1g. In order to resolve this increase in load with a confidence of 95% or better, the sum load standard deviation must be 26mg or less. Thus, with these resolution requirements, the standard deviation during position hold for each transducer must be 9mg or less, and this condition is not currently satisfied in EVASII.

4.5 Discussion

The magnetic load artifact can be subtracted using the following equation:

$$y = -0.187x^2 + 2.556x + 0.011$$

Implementation of the Mmgnetic load offset adds approximately ±0.2g of uncertainty to the sum load measurement. The mean uncertainty (95%) in the calibration ring sum load

is ±0.81g, and the mean range and standard deviation, over 10 runs, in calibration ring sum load as a function of position is 1.1±0.43g and 0.29±0.11g respectively.

The mean standard deviation of the sum load during position hold was approximately 0.8g. However, it has been shown that to be 95% confident that the measurement of sum load at two adjacent positions are different, when the step size gives an increase in load of 0.1g per position, as is often the case with tissue, a mean standard deviation of the sum load of 0.026g (or 0.009g per transducer) is required, and this condition is not currently satisfied in EVASII. The repeatability problem of the EVASII force measurement system is multi-factorial, where the use of 8 transducers inherently adds $\sqrt{8}$ times the uncertainty of a single transducer system, the additional calculation required to offset the magnetic load adds $\sqrt{2}$ times the uncertainty of a non-magnetic system.

The noise in the transducer is in part from vibrations due to the movement of the arms, from vibrations in the environment, and from the inherent noise in the balanced strain gauge transducer (resolution of the transducer is 10mg, with a variation in sensitivity of ±10% at 7μV/V/g). It is likely that variations in magnetic load due to magnetic hysteresis and positional error (±1μm) are minimal in comparison to the variations in sum load from the transducers. This suggests one or more of three potential courses to improve the repeatability of the EVASII load measurement system:

1. Install new transducers with better sensitivity and repeatability.

2. Revert to a mechanical mount (remove the magnets).

3. Mechanically (vibrationally) isolate the system (i.e. mount the system on a vibration isolation table).

Chapter 5: Optical Calibration

5.1 Purpose

As described in chapter 2, the EVASII optical measurement system utilizes the Scheiner principle to measure the dioptric power of crystalline lenses. The Scheiner system uses an 830nm laser beam, which is scanned using a set of x-y galvanometers to form a circular pattern on the anterior surface of the lens. The infrared ring is then refracted by the crystalline lens onto a CCD camera whose position is accurately measured. The camera is mounted on a computer controlled translation stage whose position is linearly related to the output voltage. The position of the camera is adjusted until the ring is focused into a single spot.

The objective of the optical calibration is to determine the voltage-dioptric power response of the EVASII optical measurement system, which will be used to derive the dioptric power of lenses mounted in EVASII.
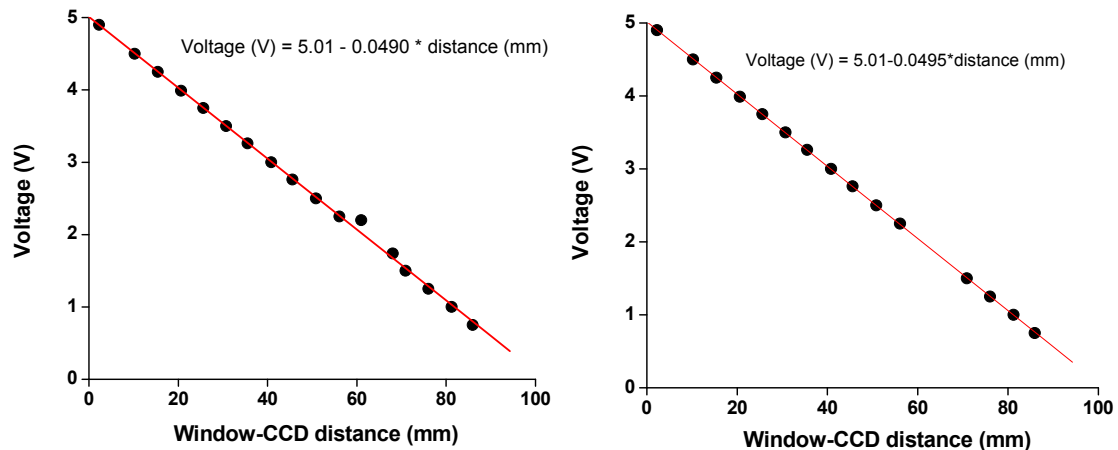
Figure 5.1: Voltage output as a function of CCD chip displacement. All points included (left), and with the two outliers removed (right). (Courtesy: David Borja and Fabrice Manns).

5.2 Theoretically derived formula

From paraxial optics, the formulas for the back focal length and back vertex power of a lens immersed in water in the EVASII cell are, with the notation of figure 5.3 (n_w=1 if the lenses are measured in air) (Manns et al. 2007):

$$f_b = n_w \cdot \left(x + \frac{t_g + t_{CCD}}{n_g} \right) + d_p \quad \text{(Eq. 1a)}$$

$$P_b = \frac{n_w}{f_b} = \frac{1}{x + \dfrac{d_p}{n_w} + \dfrac{t_g + t_{CCD}}{n_g}} \quad \text{(Eq. 1b)}$$

Where (see figure 5.3)

n_w = refractive index of water

x = distance from the back surface of the posterior window to the front surface of the CCD window

t_g = thickness of the posterior window

t_{CCD} = thickness of the CCD window

n_g = refractive index of the posterior window

d_p = distance from the posterior surface of the lens to the front surface of the posterior window
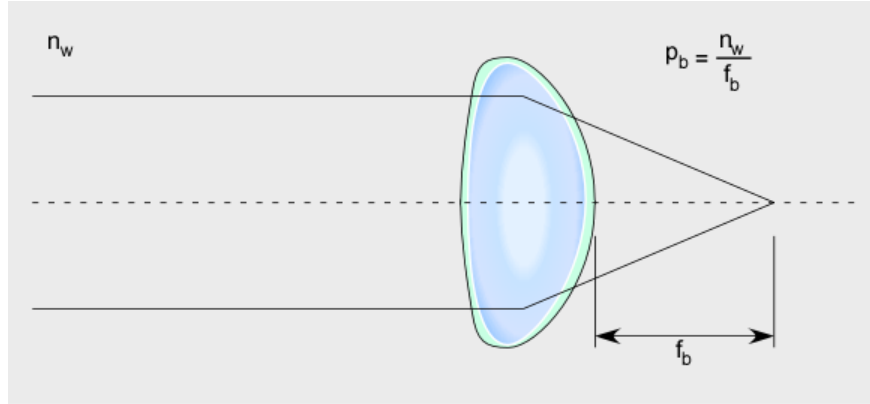
Figure 5.2: Ray diagram illustrating the back vertex power, P_b.

Since the camera position, x, is a linear function of voltage, V, Eq (1) can be written:

$$f_b = n_w \cdot \left(m \cdot V + b + \frac{t_g + t_{CCD}}{n_g} \right) + d_p \quad \text{(Eq. 2a)}$$

$$P_b = \frac{1}{m \cdot V + b + \dfrac{d_p}{n_w} + \dfrac{t_g + t_{CCD}}{n_g}} \quad \text{(Eq. 2b)}$$

Using the measurements of the dimensions and distances of the cell (t_g=3.3mm, t_{CCD}=1mm, n_g=1.510 and n_w=1.328 at 830nm, m=-20.204mm/V, b=101.32mm) the following theoretically-derived equation is obtained for lenses immersed in water:

$$f_b = 1.328 \cdot \left(-20.204 \cdot V + 104.17 \right) + d_p \quad \text{(Eq. 3a)}$$

$$P_b = \frac{1000}{-20.204 \cdot V + 104.17 + \dfrac{d_p}{1.328}} \quad \text{(Eq. 3b)}$$

The purpose of the following experiment is to verify the accuracy of equation 3b.
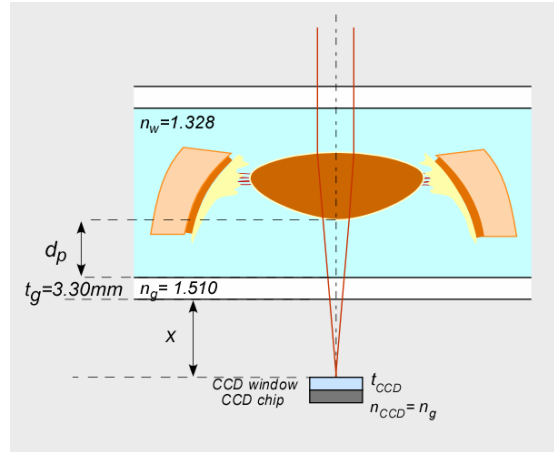
Figure 5.3: EVASII optical measurement setup and notation. Refractive index values are provided for a wavelength of 830nm (Manns et al. 2007).

5.3 Calibration procedure

The back focal length of plano-convex (PCX) lenses of known paraxial characteristics (e.g., Edmund Scientific, TechSpec PCX lenses) was measured with the Scheiner system. Measurements were performed in air and in water. The lenses were placed in the cell on custom-made ring holders at a known distance (d_p) from the bottom glass window of the cell.

The voltage was measured and plotted as a function of the known back focal length. A linear regression of the focal length versus voltage response was used to confirm the validity of Eqs. (2) and (3). In air, the linear regression can be written:

$$f_b(V) = m \cdot V + c + d_p \text{ (Eq. 4)}$$

If Eq. (3) is correct, then the values of m and c should be: m=-20.204mm/V and c=104.17mm.

Measurements were performed at four different positions of the lens (d_p= 2.5, 4, 6, 8mm), for two different optical zone diameters (2mm and 3mm). The measurements

were repeated in water. The measured spacer thicknesses were 2.42, 4.02, 7.97, and 6.01mm.

The procedure was as follows:

1.   Select 2.5 mm spacer

2.   Select lens of known focal length/power

3.   Place lens on spacer

4.   Use a 2 mm zone diameter

5.   Find the focus of the lens

6.   Record the voltage

7.   Repeat steps 5-6 for a 3 mm zone diameter

8.   Repeat steps 2-7 for all lenses in the calibration set

9.   Repeat steps 2-8 with a 4 mm spacer

10.   Repeat steps 2-8 with a 6 mm spacer

11.   Repeat steps 2-8 with an 8mm spacer

12.   Repeat steps 1-11 in water

The lens manufacturer data was used to simulate the lenses using Optics Software for Layout and Optimization (OSLO). The paraxial back focal length at 830nm of each lens was calculated using OLSO (simulations courtsey: David Borja). The calculation was performed for the lens surrounded by air and for the lens immersed in water. The results of the simulations at 830nm in air and in water will be used as a reference to quantify the measurement error.

Catalog Number	EFL Specification at 589.3nm (mm)	OSLO EFL at 830nm (mm)	BFL Specification at 589.3nm (mm)	OSLO BFL at 830nm (mm)	OSLO BFL in water at 830nm (mm)
47-329	12.00	12.34	9.76	10.07	25.73
47-330	15.00	15.19	12.03	12.21	52.51
47-331	18.00	18.42	16.22	16.61	46.40
47-332	24.00	24.34	22.15	22.49	88.04
47-333	30.00	30.38	28.02	28.39	110.30
47-334	36.00	36.53	34.07	34.55	130.72
47-335	42.00	42.55	40.22	38.76	153.82
47-336	48.00	48.65	46.36	44.99	176.65
47-337	54.00	54.70	52.02	50.72	198.73
47-338	60.00	60.80	58.37	57.14	221.83
47-339	72.00	72.93	70.42	69.34	267.02
47-340	84.00	85.12	82.39	81.47	312.26
47-341	100.00	101.29	98.35	97.64	372.37

Table 5.1: Plano convex lens paraxial specifications. The paraxial effective focal length (EFL) and back focal length (BFL) in air at 830nm and the BFL in water at 830nm were calculated using a ray -tracing simulation (courtsey: David Borja).

5.4 Experimental results in air

Results obtained on plano-convex lenses are included in Table 5.1. The table provides the voltage recorded for each measurement.

Spacer Distance, dp (mm)	2.5		4		6		8	
Optical Zone (mm)	2	3	2	3	2	3	2	3
#47-341 Fb=97.64mm	1.11	0.75	1.43	1.03	1.06	1.01	1.31	1.23
#47-339 Fb=69.34mm	2.09	2.03	2.10	2.02	2.24	2.16	2.26	2.19
#47-338 Fb=57.14mm	2.65	2.47	2.53	2.49	2.69	2.56	2.79	2.74
#47-337 Fb=50.72mm	2.77	2.72	2.83	2.86	2.98	2.99	3.12	3.00
#47-336 Fb=44.99mm	3.04	2.98	3.13	3.09	3.24	3.18	3.33	3.27
#47-335 Fb=38.76mm	3.32	3.30	3.41	3.38	3.46	3.47	3.60	3.57
#47-334 Fb=34.55mm	3.44	3.50	3.58	3.62	3.67	3.70	3.90	3.89
#47-333 Fb=28.39mm	3.83	3.87	3.90	3.94	4.02	4.05	4.16	4.13
#47-332 Fb=22.49mm	4.14	4.18	4.26	4.29	4.38	4.36	4.47	4.45
#47-331 Fb=16.61mm	4.59	4.52	4.62	4.59	4.69	4.64	4.69	4.74
#47-330 Fb=12.21mm	4.68	4.69	4.77	4.75	4.77	4.80	4.87	4.87
#47-329 Fb=10.07mm	4.72	4.73	4.78	4.80	4.86	4.87	N/A	N/A

Table 5.2: Experimental results in air showing the voltage recorded for each lens for 2mm and 3mm diameter optical zones with 2.5, 4, 6, and 8mm spacers.

The back focal length in air as a function of measured voltage gave a linear response. For each spacer and for each optical zone, the back focal length vs. voltage response was fit with a line using a least squares regression, optimizing both the slope and intercept. Further, since the voltage-displacement response was found to be perfectly linear with a slope that matches the specifications, the linear regressions of the focal-length versus voltage response were redone with a fixed value of the slope, equal to the predicted value of -20.204mm/V. For the curves where d_p = 8mm, the system was unable to measure the highest power lenses with f_b = 10.07mm, so this point is not present on these graphs.
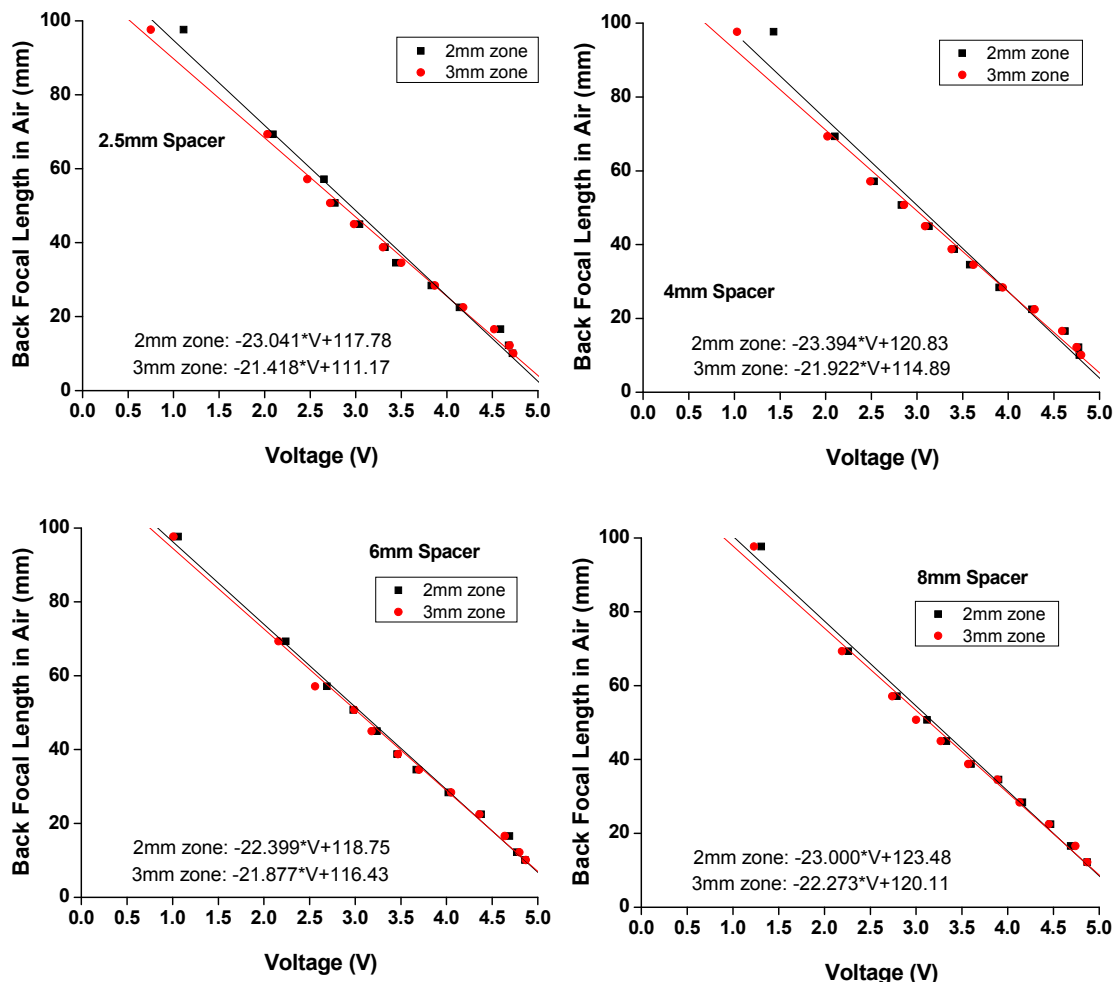
Figure 5.4: Back focal length versus voltage for all spacers with 2mm optical zone (black) and 3mm optical zone (red). The spacer thickness is the distance d$_p$.
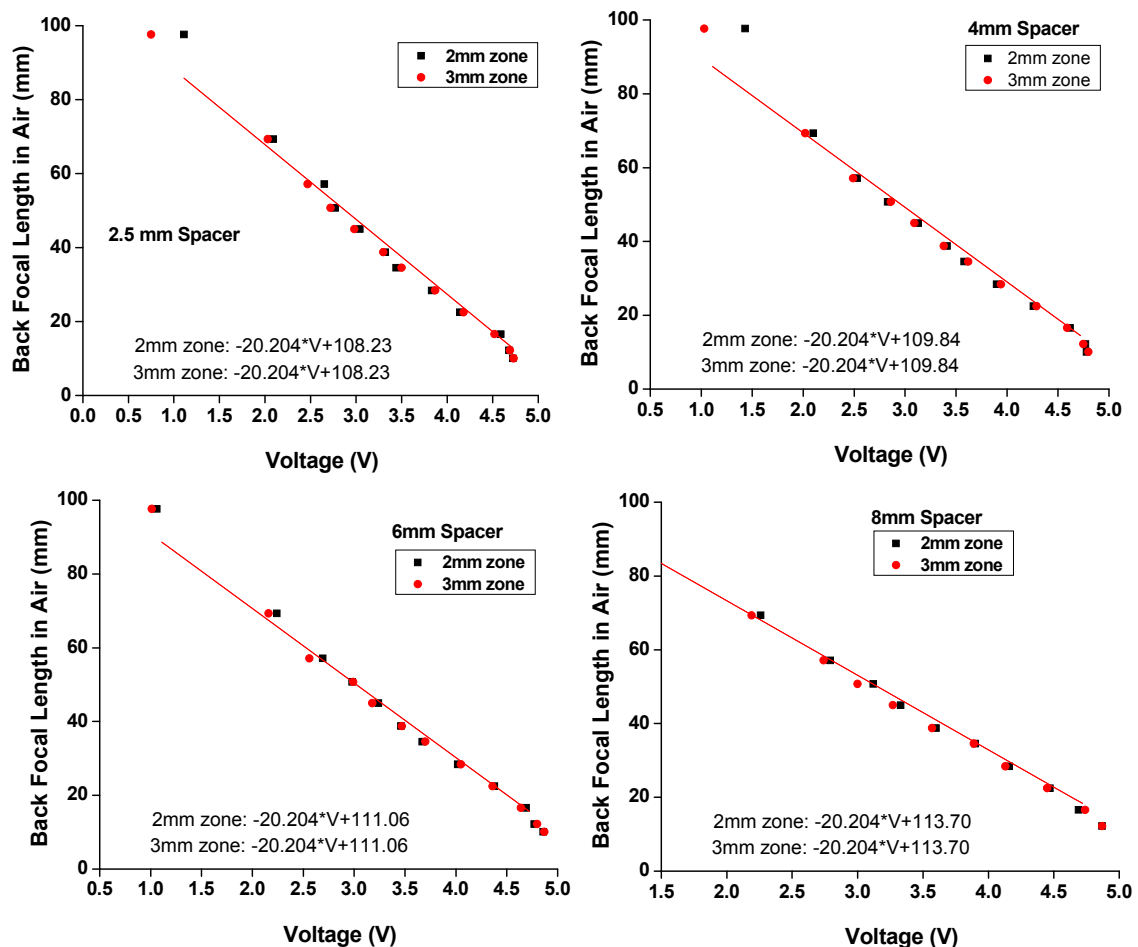
Figure 5.5: Regression analysis using the measured voltage-displacement response (49.5mV/mm, 20.204mm/V). The linear regression provides the value of the intercept.

In figure 5.4, the slopes and intercepts are different from what is expected from the predicted formula (Eq. 3). According to the voltage-displacement calibration, the slope should be equal to -20.204mm/V and the offset should be equal to 104.16mm. In addition, according to the OLSO simulations, the results obtained from measurements with 2 and 3mm diameter optical zones should be approximately equal. The discrepancies could be due to the uncertainty of the linear regression, error in measurement due to misalignment of the calibration lens, and non-linearities at high power because the paraxial assumption becomes less accurate for thicker lenses.

Actual spacer thickness, d_p (mm)	I, Intercept (mm)	c, Offset (mm)
2.42	108.23	105.81
4.02	109.84	105.82
6.01	111.06	105.05
7.97	113.7	105.73

Table 5.3: Summary of the intercepts obtained from the regression analysis of Figure 5.5, which uses the measured voltage-displacement response (49.5mV/mm, 20.204mm/V).

In figure 5.5, the linear regressions of the focal-length versus voltage response were redone with a fixed value of the slope, equal to the predicted value of -20.204mm/V. For all spacers, the values of the intercepts were almost exactly the same with the 2 and 3 mm diameter optical zones. The values of the intercepts and the corresponding offset (intercept minus d_p) are listed in Table 5.3.

The mean value of the offset is 105.60±0.37mm. This value is in good agreement with the value expected from the theoretical derivation and measurements of EVASII dimensions (104.16mm). These results suggest that the following equation can be used to compute the back focal length:

$$f_b(V) = -20.204 \cdot V + 105.60 + d_p \ \text{(Eq. 5)}$$

5.5 Fine tuning of the calibration equation

A separate experiment was conducted on the glass lenses to determine the accuracy of, and if necessary fine-tune, the calibration equation (Eq.5). The focal length of each lens was measured 5 times (in order to reduce the uncertainty by taking multiple measurements) in air with the 2.5 mm spacer (d_p=2.42mm) and the 8mm spacer (d_p=7.97mm) and a 3 mm optical zone diameter. The results are shown in Table 5.4

(2.5mm spacer) and Table 5.5 (8mm spacer). The average of the error between the measured and actual focal length (data from Table 5.4 and 5.5) is 2.57±0.90mm with the 2.5mm spacer and 1.59±1.13mm with the 8mm spacer. The average error for all measurements is 2.25±0.97mm. If Eq. 5 is corrected to take into account this offset, the new calibration equation becomes:

$$f_b(V) = -20.204 \cdot V + 103.35 + d_p \text{ (Eq. 6)}$$

The difference between the values of focal length and power provided by Eq. (6) and the specified values are given in Table 5.6. With the 2.5mm spacer, the error for all lenses with power ranging from 12 to 60D is less than 0.5D, except for 1 lens (f_b=25.8D). With the 8mm spacer, the error is less than 0.5D for all lenses with a power ranging up to 25.8D and less than 2 D for all other lenses.

Calculated Back Focal Length (mm)	M1 (V)	M2 (V)	M3 (V)	M4 (V)	M5 (V)	AVG	STDEV	Measured back focal length, from Eq.5 (mm)	Error (mm)
81.47	1.11	1.08	1.32	1.31	1.23	**1.21**	**0.11**	83.57	2.10
69.34	1.79	1.73	1.89	1.79	1.75	**1.79**	**0.06**	71.85	2.51
57.14	2.32	2.41	2.31	2.32	2.35	**2.34**	**0.04**	60.74	3.60
50.72	2.90	2.63	2.56	2.75	2.62	**2.69**	**0.14**	53.67	2.95
44.99	3.15	2.92	2.93	2.93	2.94	**2.97**	**0.10**	48.01	3.02
38.76	3.29	3.19	3.10	3.16	3.20	**3.19**	**0.07**	43.57	4.81
34.55	3.55	3.55	3.51	3.50	3.66	**3.55**	**0.06**	36.30	1.75
28.39	3.82	3.81	3.90	3.84	3.84	**3.84**	**0.03**	30.44	2.05
22.49	4.14	4.13	4.11	4.16	4.10	**4.13**	**0.02**	24.58	2.09
16.61	4.44	4.40	4.44	4.42	4.40	**4.42**	**0.02**	18.72	2.11
12.21	4.63	4.65	4.62	4.63	4.67	**4.64**	**0.02**	14.27	2.06
10.07	4.76	4.74	4.76	4.76	4.76	**4.76**	**0.01**	11.85	1.78

Table 5.4: Voltage recorded during repeated measurements in air with a 3mm diameter optical zone and the 2mm spacer (d_p=2.42mm). The measured back focal length was calculated using Eq. (5). The error is the difference between the measured back focal length and the actual back focal length at 830nm.

Calculated Back Focal Length (mm)	M1 (V)	M2 (V)	M3 (V)	M4 (V)	M5 (V)	AVG	STDEV	Measured back focal length, from Eq.5 (mm)	Error (mm)
81.47	1.53	1.67	1.77	1.63	1.45	**1.61**	**0.12**	81.04	-0.4
69.34	2.1	2.03	2.13	2.17	2.24	**2.13**	**0.08**	70.45	1.11
57.14	2.67	2.17	2.85	2.7	2.74	**2.63**	**0.26**	60.51	3.37
50.72	3.02	3.19	3.14	2.87	3.03	**3.05**	**0.12**	51.95	1.23
44.99	3.25	3.34	3.21	3.45	3.22	**3.29**	**0.1**	47.02	2.03
38.76	3.53	3.58	3.58	3.57	3.67	**3.59**	**0.05**	41.12	2.36
34.55	3.82	3.91	3.95	3.82	3.89	**3.88**	**0.06**	35.22	0.67
28.39	4.16	4.19	4.19	4.14	4.2	**4.18**	**0.03**	29.2	0.81
22.49	4.35	4.33	4.44	4.36	4.37	**4.37**	**0.04**	25.28	2.79
16.61	4.7	4.73	4.69	4.72	4.67	**4.7**	**0.02**	18.57	1.96
12.21									
10.07									

Table 5.5: Voltage recorded during repeated measurements in air with a 3mm diameter optical zone and the 8mm spacer (d_p=7.97mm). The measured back focal length was calculated using Eq. (5). The error is the difference between the measured back focal length and the actual back focal length at 830nm. The lenses with back focal length of 12.21 and 10.07mm were outside the measurable range.

Calculated Back Focal Length (mm)	Back Vertex Power (D)	Fb error (mm), 2.5mm spacer	Fb Error (mm), 8mm spacer	**Pb error (D), 2.5mm spacer**	**Pb Error (D), 8mm spacer**
81.47	12.3	-0.15	-2.68	**0**	**0.4**
69.34	14.4	0.26	-1.14	**-0.1**	**0.2**
57.14	17.5	1.35	1.12	**-0.4**	**-0.3**
50.72	19.7	0.7	-1.02	**-0.3**	**0.4**
44.99	22.2	0.77	-0.22	**-0.4**	**0.1**
38.76	25.8	2.56	0.11	**-1.6**	**-0.1**
34.55	28.9	-0.5	-1.58	**0.4**	**1.4**
28.39	35.2	-0.2	-1.44	**0.3**	**1.9**
22.49	44.5	-0.16	0.54	**0.3**	**-1**
16.61	60.2	-0.14	-0.29	**0.5**	**1.1**
12.21	81.9	-0.19		**1.3**	
10.07	99.3	-0.47		**4.9**	

Table 5.6: Difference between the values of focal length and power predicted using Eq. 6 and the values calculated from the lens specifications. With the 2.5mm spacer, the error for all lenses with power ranging from 12 to 60D is less than 0.5D, except for one lens (P_b=25.8D). With the 8mm spacer, the error is less than 0.5D for all lenses with a power ranging up to and including 25.8D and less than 2D for all other lenses.

5.6 Experimental results in water

The back focal lengths of the glass lenses immersed in water were calculated from measurements with the EVASII Scheiner system using Eq. 6. The equation was modified to take into account immersion in water:

$$f_b(V) = 1.328 \cdot (-20.204 \cdot V + 103.35) + d_p \text{ (Eq. 7)}$$

Each lens was measured 5 times with a 3mm diameter optical zone and the 2.5mm spacer, where the 2.5mm spacer was choosen because more lenses in the lens set used could be measured using this spacer as opposed to the 8mm spacer. The results are shown in Table 5.7. In water, only five lenses had a focal length in the measurement

range. According to these results, Eq. (7) underestimates the focal length by an average of 3.5mm and overestimates the power by an average of 1.5D. The increased error compared to the measurements in air is partly due to the fact that any error in the coefficients of the regression line is increased by a factor equal to the refractive index of water (1.328). In addition, there can be a difference between the assumed (1.328) and actual value of the refractive index of water, which would introduce an error in the reference value of the back focal length. For instance, using a refractive index of 1.340 (extreme value at 830nm) instead of 1.328 produces a difference of +1.06mm in the back focal length of the f=12mm lens. The increased difficulty in precisely positioning the lens in water could also contribute to the increased error.

Calculated Back Focal Length in Water (mm)	M1 (V)	M2 (V)	M3 (V)	M4 (V)	M5 (V)	AVG	STDEV	Measured Back Focal Length, from Eq.7 (mm)	Error (mm)
110.3	1.27	1.33	1.59	1.1	1.34	**1.33**	**0.18**	103.98	-6.32
88.04	2.05	2.04	2	2.04	2.34	**2.09**	**0.14**	83.59	-4.45
46.4	3.49	3.58	3.58	3.61	3.47	**3.55**	**0.06**	44.42	-1.98
52.51	3.29	3.48	3.39	3.48	3.26	**3.38**	**0.10**	48.98	-3.53
25.73	4.33	4.29	4.26	4.32	4.32	**4.30**	**0.03**	24.30	-1.43

Table 5.7: Voltage recorded during repeated measurements in water with a 3mm diameter optical zone and the 2mm spacer (d_p=2.42mm). The error is the difference between the value of the back focal length or back vertex power calculated using Eq.(7) and the actual value.

5.7 Summary

The following equation is recommended to calculate the back focal length and back vertex power from recorded voltage measurements:

$$f_b(V) = n \cdot (-20.204 \cdot V + 103.35) + d_p \quad \text{(Eq. 8)}$$

$$P_b = \frac{1000}{-20.204 \cdot V + 103.35 + \dfrac{d_p}{n}} \quad \text{(Eq. 9)}$$

Where n = 1 if the lens under test is placed in air and n = 1.328 at 830nm if the lens is immersed in water.

The experiments show that the focal length can be measured as long as the point of focus is more than approximately 4mm below the inside surface of the EVASII bottom window. For instance, with an 8mm spacer, the minimum focal length that can be measured is approximately 13mm (76D). However, the lenses used in the calibration are plano-convex, but the crystalline lens is biconvex, thereby bringing the posterior surface of the crystalline lens closer to the window (approximately 4mm) than the PCX lens with the 8mm spacer.

Considering lenses in the 12 to 60D range, the experiments with the lenses placed in air suggest that Eq. (9) provides the lens power with an accuracy of 0.5D or better, for most glass lenses. The error was more than 0.5D in only 5 out of 20 lens measurements. Overall, the error ranged from -1.6D to +1.9D, with a mean absolute error of 0.56±0.54D.

Chapter 6: Comparison and Validation of EVASII vs. EVASI

6.1 Purpose

EVASI and EVASII are both lens stretching systems; however, the mechanism of stretching, force transduction, and force measurement, are performed differently by each system. More than 100 eyes have been tested with EVASI. The goal of this study is to determine if the results of EVASII are similar to and interchangeable with that of EVASI. The load, power, and the lens and ciliary body response obtained in EVASI and EVASII are compared.

6.2 Methods: Overview

The load, power, lens diameter, and ciliary body diameter for 4 monkey eyes were measured (3 runs each) in EVASI and the same was measured for the contralateral eye in EVASII. For all eyes, a stretch protocol of 0 to 2mm of radial scleral stretch with 0.25mm intervals was used. The performance of the load, lens power, lens diameter, and ciliary body diameter were compared (EVASI vs. EVASII) for each eye. The tissue preparation was performed as described in chapter 2. All experiments in chapter 6 were performed before the addition of the magnetic mounts and modification of the shoes.

Species	Eye Number	Date of Experiment	Age (years)	PMT (hours)	Sex	Weight (kg)
Cyno	113-217	2/21/2007	8.3	24	Male	7.07
Baboon	5P56	8/16/07	2.8	2	Male	6.26
Cyno	124Y	8/22/2007	7	2	Male	5.28
Cyno	125-72	3/28/2007	7	2	Male	6.6

Table 6.1: Species, eye number, date of experiment, age, post-mortem time (PMT), sex and weight of all 4 monkeys used in this study.

6.3 Initial Lens and Ciliary Body Diameter and Initial Lens Power

6.3.1 Methods

The average and standard deviation of the unstretched (0.00mm position) lens diameter, ciliary body diameter, and lens power has been determined from the 3 runs. The difference (EVASI - EVASII) of the unstretched lens diameter, ciliary body diameter, and lens power were calculated for each eye, and the mean of this difference was determined using all 4 eyes. To determine if the unstretched lens diameters, ciliary body diameters, and lens powers are significantly different between the two systems, a Student's t-test was performed. It is important to note that, in EVASI, the slack in the sutures was removed by increasing the stretch to obtain the initial experimental condition, but in EVASII, this step was not necessary, and this difference in procedure may influence the results of the comparison of the initial conditions of the lens and ciliary body.

6.3.2 Results

Eye Number	Stretcher	Unstretched Lens Diameter (mm)					Difference
		Run1	Run2	Run3	Avg	Stdev	
CY 113-217	EVASI	7.57	7.62	7.62	7.61	0.03	0.25
	EVASII	7.37	7.35	7.33	7.35	0.02	
Baboon 5P56	EVASI	7.26	7.15	7.16	7.19	0.06	-0.57
	EVASII	7.76	N/A	7.77	7.77	N/A	
CY 124Y	EVASI	7.45	7.46	7.46	7.46	<0.01	-0.24
	EVASII	7.79	7.64	7.66	7.70	0.08	
CY 125-72	EVASI	7.49	7.52	7.51	7.51	0.01	0.36
	EVASII	7.13	7.13	7.17	7.15	0.02	
					Average Difference		-0.05
					Non-Zero Difference? p-value		0.83252

Table 6.2: Unstretched lens diameter for each eye. Each run, and the average and standard deviation of all 3 runs is shown for both EVASI and EVASII. The mean difference (EVASI - EVASII) is shown at the right, and the results of a Student's t-test (p-value) are shown to check if the difference was significantly different than zero.

Eye Number	Stretcher	Unstretched Ciliary Body Diameter (mm)					
		Run1	Run2	Run3	Avg	Stdev	Difference
CY 113-217	EVASI	9.16	9.16	9.19	9.17	0.02	0.92
	EVASII	8.45	8.15	8.15	8.25	0.17	
Baboon 5P56	EVASI	8.45	8.55	8.55	8.52	0.06	-0.29
	EVASII	8.81	N/A	N/A	8.81	N/A	
CY 124Y	EVASI	8.97	8.99	8.98	8.98	0.01	-0.05
	EVASII	9.18	8.94	8.99	9.04	0.13	
CY 125-72	EVASI	9.05	9.11	9.11	9.09	0.03	1.33
	EVASII	7.79	7.90	7.61	7.76	0.15	
		Average Difference					0.48
		Non-Zero Difference? p-value					0.30429

Table 6.3: Unstretched ciliary body diameter for each eye. Each run, and the average and standard deviation of all 3 runs is shown for both EVASI and EVASII. The mean difference (EVASI - EVASII) is shown at the right, and the results of a Student's t-test (p-value) are shown to check if the difference was significantly different than zero.

Eye Number	Stretcher	Unstretched Lens Power (D)					
		Run1	Run2	Run3	Avg	Stdev	Difference
CY 113-217	EVASI	50.05	51.92	50.66	50.88	0.95	3.40
	EVASII	47.33	47.33	47.78	47.48	0.26	
Baboon 5P56	EVASI	52.38	52.19	51.87	52.15	0.26	-6.84
	EVASII	59.22	58.52	59.22	58.99	0.40	
CY 124Y	EVASI	54.64	53.33	53.94	53.97	0.66	0.19
	EVASII	57.17	50.72	53.46	53.78	3.23	
CY 125-72	EVASI	58.72	55.40	55.25	56.46	1.96	-2.84
	EVASII	58.52	62.20	57.17	59.29	2.60	
		Average Difference					-1.52
		Non-Zero Difference? p-value					0.53569

Table 6.4: Unstretched lens power for each eye. Each run, and the average and standard deviation of all 3 runs is shown for both EVASI and EVASII. The mean difference (EVASI - EVASII) is shown at the right, and the results of a Student's t-test (p-value) are shown to check if the difference was significantly different than zero.

The difference in the unstretched lens diameter (EVASI - EVASII), unstretched ciliary body diameter, and the unstretched lens power is not consistent among samples, and none of these are significantly different than zero.

6.3.3 Conclusions

The unstretched lens diameters, ciliary body diameters, and lens powers are not significantly different among contralateral eyes in EVASI and EVASII.

6.4 Load vs. Stretch

6.4.1 Methods

The average of the sum load was calculated in each position for all three runs, and this was done for all four eyes. In EVASII, the sum load was obtained by adding the load measured on each individual transducer, 1 through 8, and in EVASI the sum load was directly measured. In both EVASI and II, the averages of the sum loads were obtained by averaging the sum load during each position hold (i.e. while the positions of the arms are held constant).

In all experiments in EVASII, the initial (0.00mm position) load is greater than the load at the next position (0.25mm position), as this load always becomes negative. The negative load is an artifact due to insufficient electrical power for two devices, the stepper motors and the signal amplifiers, which were sharing the same power supply. Once each device was given its own power supply, the artifactual initial decrease in load was eliminated. To compensate for this artifact, the loads were offset to set the 0.25mm position load to zero.

6.4.2 Results
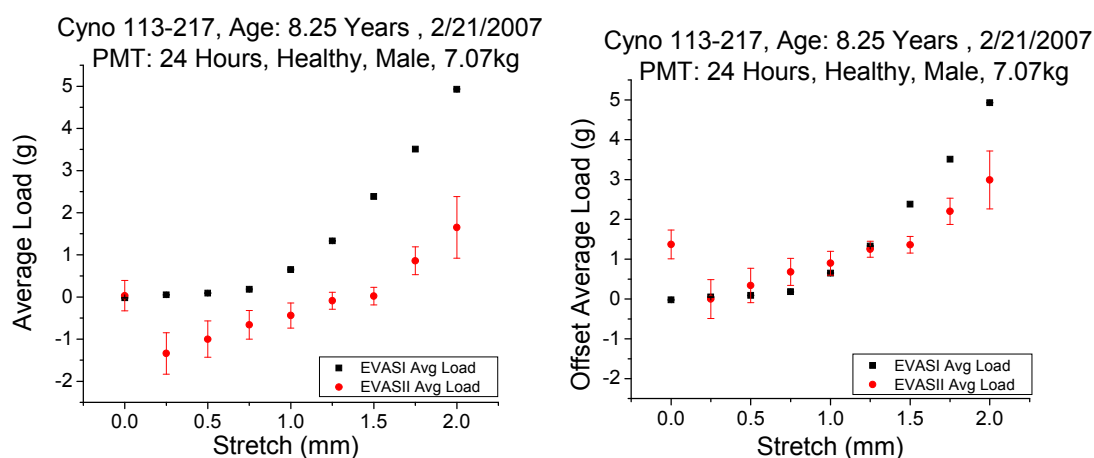
Figure 6.1: Average load vs. stretch for one eye before (left) and after (right) offset. The plotted values and error bars give the average and standard deviation of all 3 runs.
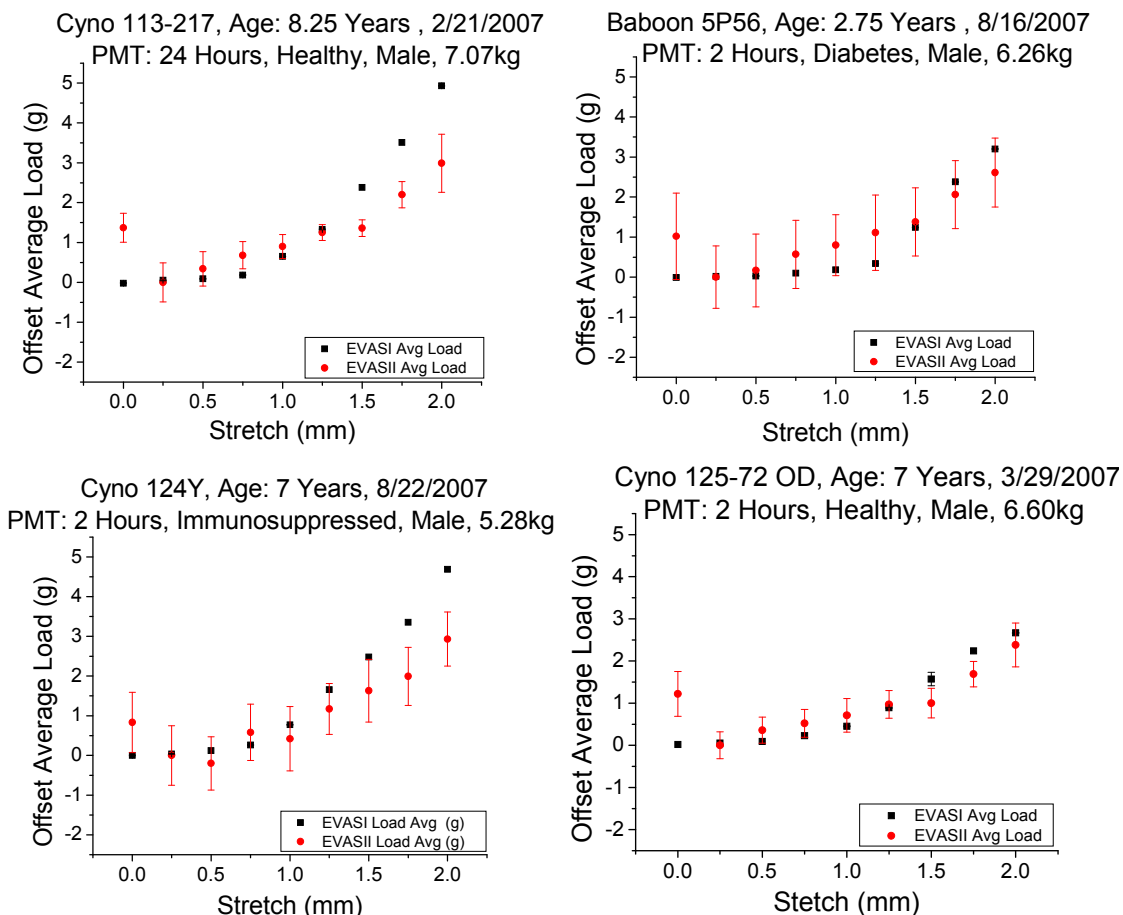
Figure 6.2: Offset average load vs. stretch for each eye, where the offset was implemented to set the 0.25mm position load to zero. The plotted values and error bars give the average and standard deviation of all 3 runs.

The maximum load in EVASI is greater than in EVASII, and the variation in load between runs is considerably higher in EVASII. Also, the EVASI load data is smoother than the EVASII load data.

6.4.3 Discussion

Even after the offset, the maximum load in EVASI is still greater than the maximum load in EVASII. Overlapping load values (within one standard deviation) occurred in 25/36 (69.4%) of all of the averaged measurements. This discrepancy is likely due to the differences between the mechanical transduction mechanisms of the two

systems, as the EVASII system is less susceptible to friction than EVASI. Also, the EVASII system utilizes mechanical components (aluminum arms) whose compliance is much less than those used in EVASI (nylon monofilament sutures, which tend to act as springs when loaded heavily).

The variation in load between runs is an order of magnitude greater in EVASII than in EVASI (approximate average standard deviation: 0.08g in EVASI and 0.8g in EVASII). This is likely due the differences between the force measurement mechanisms of the two systems. As demonstrated in chapter 4, the use of 8 transducers (in EVASII) inherently adds more uncertainty to the force measurement, and this also reduces the measured loads by a factor of 8, pushing the measurements closer to the noise level of the EVASII force transducers. Furthermore, the increased variability of the EVASII load measurements influenced the overall load-stretch behavior so that the EVASI load-stretch data is smoother than the EVASII data.

6.4.4 Conclusions

The EVASI and EVASII load-stretch behavior are significantly different, and the EVASII load data is more variable between runs than the EVASI load data.

6.5 Total Change in Lens and Ciliary Body Diameter and Lens Power
6.5.1 Methods

The total change in the lens diameter, ciliary body diameter, and lens power was determined as the difference between the 0.00mm and 2.00mm positions. The average and standard deviation of the total change in the lens diameter, ciliary body diameter, and lens power was determined from the 3 runs for all 4 eyes. The difference in the total

change parameters (EVASI - EVASII) were calculated for each eye, and the mean of this difference was determined for all four eyes. To determine if the total change parameters are significantly different between the two systems, a Student's t-test was performed.

6.5.2 Results

Change in Lens Diameter (mm)				
Eye Number	Stretcher	Avg	Error	Difference
CY 113-217	EVASI	0.24	0.03	-0.27
	EVASII	0.51	0.02	
Baboon 5P56	EVASI	0.15	0.06	-0.51
	EVASII	0.66	0.09	
CY 124Y	EVASI	0.23	0.01	-0.59
	EVASII	0.82	0.08	
CY 125-72	EVASI	0.13	0.01	-0.24
	EVASII	0.37	0.02	
Average Difference				-0.40
Non-Zero Difference? p-value				0.01897

Table 6.5: Total change in lens diameter for each eye. The average and standard error of all 3 runs is shown for both EVASI and EVASII. The mean difference (EVASI - EVASII) is shown at the right, and the results of a Student's t-test (p-value) are shown to check if the difference was significantly different than zero.

Change in Ciliary Body Diameter (mm)				
Eye Number	Stretcher	Avg	Error	Difference
CY 113-217	EVASI	0.39	0.03	-0.92
	EVASII	1.31	0.17	
Baboon 5P56	EVASI	0.24	0.07	-1.34
	EVASII	1.57	0.02	
CY 124Y	EVASI	0.25	0.03	-1.25
	EVASII	1.50	0.20	
CY 125-72	EVASI	0.30	0.03	-0.64
	EVASII	0.94	0.15	
Average Difference				-1.04
Non-Zero Difference? p-value				0.00749

Table 6.6: Total change in ciliary body diameter for each eye. The average and standard error of all 3 runs is shown for both EVASI and EVASII. The mean difference (EVASI - EVASII) is shown at the right, and the results of a Student's t-test (p-value) are shown to check if the difference was significantly different than zero.

Change in Lens Power (D)				
Eye Number	Stretcher	Avg	Error	Difference
CY 113-217	EVASI	-13.28	1.04	1.28
	EVASII	-14.56	1.51	
Baboon 5P56	EVASI	-5.09	1.02	12.27
	EVASII	-17.36	0.45	
CY 124Y	EVASI	-12.14	1.81	4.40
	EVASII	-16.54	3.32	
CY 125-72	EVASI	-7.92	2.04	7.53
	EVASII	-15.45	2.67	
Average Difference				6.37
Non-Zero Difference? p-value				0.07271

Table 6.7: Total change in lens power for each eye. The average and standard error of all 3 runs is shown for both EVASI and EVASII. The mean difference (EVASI - EVASII) is shown at the right, and the results of a Student's t-test (p-value) are shown to check if the difference was significantly different than zero.

The total change in lens diameter, ciliary body diameter, and lens power are significantly greater in EVASII than in EVASI.

6.5.3 Conclusions

The total change in lens and ciliary body diameter was significantly greater in EVASII than in EVASI at 2mm of stretch, and the magnitude of the change in power is also much greater in EVASII. Thus, as a function of stretch, EVASII is much more efficient than EVASI in producing changes in lens diameter, ciliary body diameter, and lens power. The discrepancy between the change in these parameters for these two systems could be due to the differences between the mechanical transduction mechanisms of the two systems, as the EVASII system utilizes mechanical components (aluminum arms) whose compliance is much less than those used in EVASI (sutures), and the starting position in EVASI may have slack in some of the sutures. Consequently, the reported displacement in EVASI potentially overestimates the actual displacement of the tissue since the system must first eliminate the slack in the sutures and since the strain in the sutures is not accounted for.

It is interesting to note that the difference (EVASI - EVASII) for the change in lens and ciliary body diameter are significantly different (p = 0.01311). In other words, both the lens and ciliary body diameters changed more as a function of stretch in EVASII, but the increase was more pronounced for the ciliary body. Perhaps the difference between the starting positions of the tissue in EVASI and EVASII is responsible for the additional increase in ciliary body distension in EVASII, since a slight pre-stretch was used to obtain the initial position in EVASI, while in EVASII, no pre-stretch was applied.

6.6 Diameter and Power Repeatability

6.6.1 Methods

The standard deviation of the lens diameter, ciliary body diameter, and the lens power was determined for each position based on the 3 runs. The mean of this standard deviation has been determined for each parameter. A Student's t-test was performed to check if the mean standard deviation is significantly different for EVASI and EVASII.

6.6.2 Results

Standard Deviation in Lens Diameter (mm)				
Eye Number	Stretcher	Avg	Error	Difference
CY 113-217	EVASI	0.018	0.011	0.005
	EVASII	0.013	0.006	
Baboon 5P56	EVASI	0.041	0.013	-0.002
	EVASII	0.043	0.034	
CY 124Y	EVASI	0.009	0.004	-0.066
	EVASII	0.076	0.024	
CY 125-72	EVASI	0.009	0.003	-0.002
	EVASII	0.011	0.006	
Average Difference				-0.016
Non-Zero Difference? p-value				0.40143

Table 6.8: Standard deviation in lens diameter for each eye. The average and standard error of all 3 runs is shown for both EVASI and EVASII. The mean difference (EVASI - EVASII) is shown at the right, and the results of a Student's t-test (p-value) are shown to check if the difference was significantly different than zero.

Standard Deviation in Ciliary Body Diameter (mm)				
Eye Number	Stretcher	Avg	Error	Difference
CY 113-217	EVASI	0.027	0.015	-0.018
	EVASII	0.045	0.052	
Baboon 5P56	EVASI	0.046	0.020	-0.068
	EVASII	0.113	0.122	
CY 124Y	EVASI	0.018	0.006	-0.131
	EVASII	0.150	0.014	
CY 125-72	EVASI	0.016	0.014	-0.019
	EVASII	0.035	0.045	
Average Difference				-0.059
Non-Zero Difference? p-value				0.11401

Table 6.9: Standard deviation in ciliary body diameter for each eye. The average and standard error of all 3 runs is shown for both EVASI and EVASII. The mean difference (EVASI - EVASII) is shown at the right, and the results of a Student's t-test (p-value) are shown to check if the difference was significantly different than zero.

Standard Deviation in Lens Power (D)				
Eye Number	Stretcher	Avg	Error	Difference
CY 113-217	EVASI	0.949	0.635	-0.795
	EVASII	1.744	1.419	
Baboon 5P56	EVASI	0.352	0.258	-0.851
	EVASII	1.203	0.657	
CY 124Y	EVASI	1.226	0.700	-0.182
	EVASII	1.407	0.838	
CY 125-72	EVASI	1.271	0.610	-0.144
	EVASII	1.415	0.882	
Average Difference				-0.493
Non-Zero Difference? p-value				0.08172

Table 6.10: Standard deviation in lens power for each eye. The average and standard error of all 3 runs is shown for both EVASI and EVASII. The mean difference (EVASI - EVASII) is shown at the right, and the results of a Student's t-test (p-value) are shown to check if the difference was significantly different than zero.

The mean standard deviation was 0.019 ± 0.007mm in EVASI and 0.036 ± 0.015mm in EVASII for the lens diameter, 0.027 ± 0.007mm in EVASI and 0.086 ± 0.027mm in EVASII for the ciliary body diameter, and 0.949 ± 0.211D in EVASI and 1.442 ± 0.112D in EVASII for the lens power.

6.6.3 Conclusion

Although the variability of the lens diameter, ciliary body diameter, and lens power is consistently higher in EVASII, the difference between the variability of the diameter and power measurements of the two systems is not statistically significant.

6.7 Lens and Ciliary Body Diameter and Lens Power vs. Load: Slopes

6.7.1 Methods

The load was plotted as a function of average lens diameter, ciliary body diameter, and lens power for all four eyes for both EVASI and EVASII. Each trend gave a linear result, and the best fit line was obtained through least squares linear regression. It is important to note that the fits in EVASII were performed after removal of the initial

load, which otherwise would have significantly altered the fit. The mean slope of each eye was used to calculate the slope difference (EVASI - EVASII). To determine if the slopes are significantly different between the two systems, a Student's t-test was performed.

6.7.2 Results
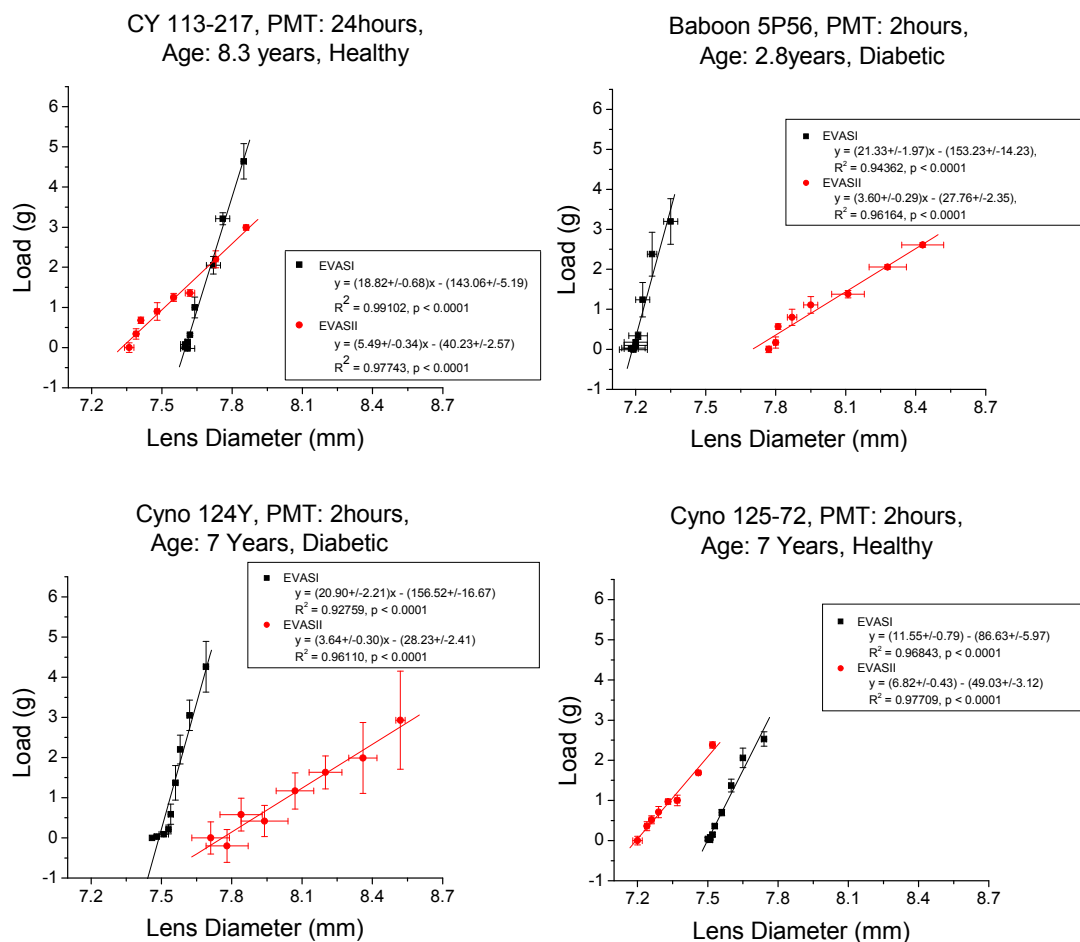
Figure 6.3: Load vs. lens diameter for all 4 eyes. The best fit line is shown for both EVASI (black) and EVASII (red). The equation of the line and the fit parameters are given in the legend.

Load vs. Lens Diameter Slopes (g/mm)				
Eye Number	Stretcher	Avg	Error	Difference
CY 113-217	EVASI	18.82	0.68	13.33
	EVASII	5.49	0.34	
Baboon 5P56	EVASI	21.33	1.97	17.73
	EVASII	3.60	0.29	
CY 124Y	EVASI	20.90	2.21	17.26
	EVASII	3.64	0.30	
CY 125-72	EVASI	11.55	0.79	4.73
	EVASII	6.82	0.43	
Average Difference				13.26
Non-Zero Difference? p-value				0.02169

Table 6.11: Load vs. lens diameter slopes for each eye. The average and standard error of all 3 runs is shown for both EVASI and EVASII. The mean difference (EVASI - EVASII) is shown at the right, and the results of a Student's t-test (p-value) are shown to check if the difference was significantly different than zero.
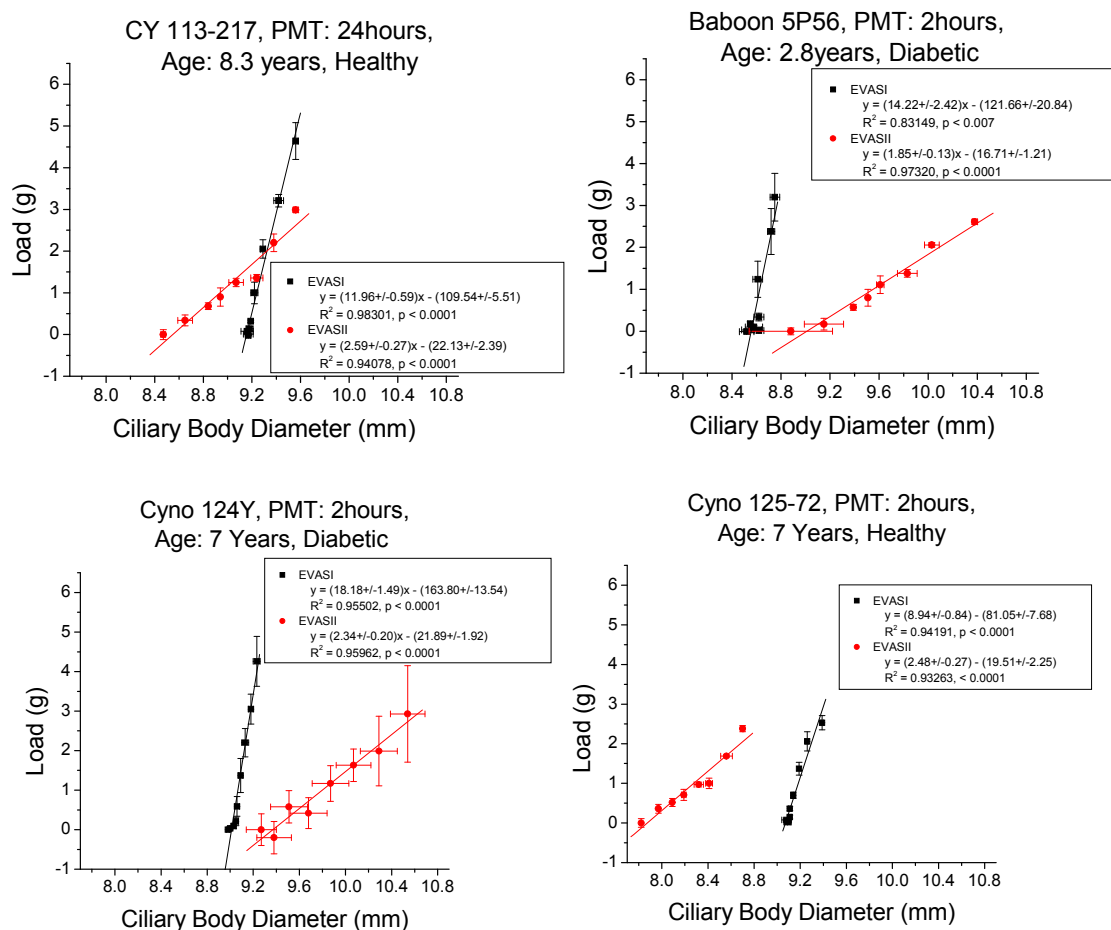
Figure 6.4: Load vs. ciliary body diameter for all 4 eyes. The best fit line is shown for both EVASI (black) and EVASII (red). The equation of the line and the fit parameters are given in the legend.

Load vs. Ciliary Body Diameter Slopes (g/mm)				
Eye Number	Stretcher	Avg	Error	Difference
CY 113-217	EVASI	11.96	0.59	9.37
	EVASII	2.59	0.27	
Baboon 5P56	EVASI	14.22	2.42	12.37
	EVASII	1.85	0.13	
CY 124Y	EVASI	18.18	1.49	15.84
	EVASII	2.34	0.20	
CY 125-72	EVASI	8.94	0.84	6.46
	EVASII	2.48	0.27	
Average Difference				11.01
Non-Zero Difference? p-value				0.01200

Table 6.12: Load vs. ciliary body diameter slopes for each eye. The average and standard error of all 3 runs is shown for both EVASI and EVASII. The mean difference (EVASI - EVASII) is shown at the right, and the results of a Student's t-test (p-value) are shown to check if the difference was significantly different than zero.
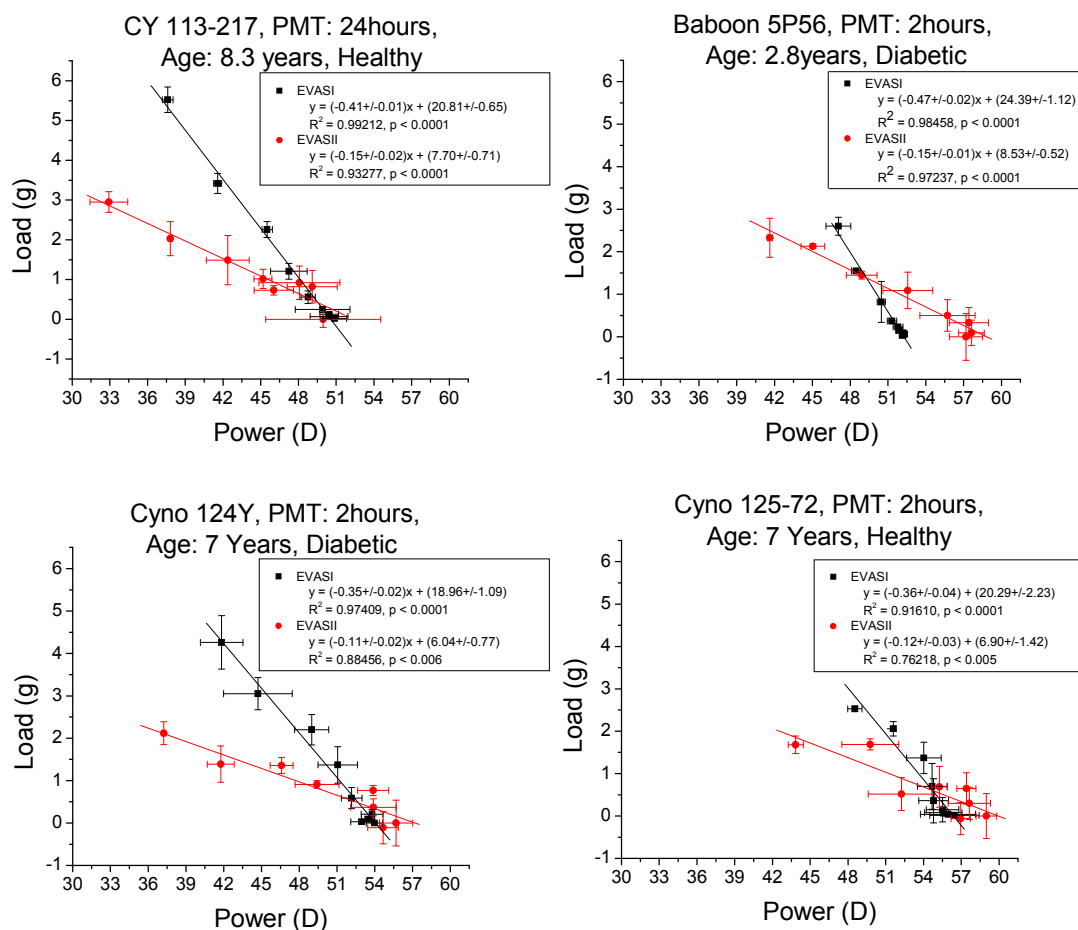
Figure 6.5: Load vs. lens power for all 4 eyes. The best fit line is shown for both EVASI (black) and EVASII (red). The equation of the line and the fit parameters are given in the legend.

Load vs. Lens Power Slopes (g/D)				
Eye Number	Stretcher	Avg	Error	Difference
CY 113-217	EVASI	-0.41	0.01	-0.26
	EVASII	-0.15	0.02	
Baboon 5P56	EVASI	-0.47	0.02	-0.32
	EVASII	-0.15	0.01	
CY 124Y	EVASI	-0.35	0.02	-0.24
	EVASII	-0.11	0.02	
CY 125-72	EVASI	-0.36	0.04	-0.24
	EVASII	-0.12	0.03	
Average Difference				-0.27
Non-Zero Difference? p-value				0.00079

Table 6.13: Load vs. lens power slopes for each eye. The average and standard error of all 3 runs is shown for both EVASI and EVASII. The mean difference (EVASI - EVASII) is shown at the right, and the results of a Student's t-test (p-value) are shown to check if the difference was significantly different than zero.

The mean (of all 4 eyes) load/lens diameter slope was 18.15 ± 4.53g/mm in EVASI and 4.89 ± 1.56g/mm in EVASII. The mean (of all 4 eyes) load/ciliary body diameter slope was 13.33 ± 3.89g/mm in EVASI and 2.32 ± 0.33g/mm in EVASII. The mean (of all 4 eyes) of the load/power slope was -0.40 ± 0.06g/D in EVASI and -0.13 ± 0.02g/D in EVASII.

6.7.3 Conclusions

The lens and ciliary body diameter, and lens power as a function of load are significantly different for EVASI and EVASII. EVASI requires more load for an equivalent amount of stretch in EVASII, and it is therefore intuitive that EVASI requires more load for an equivalent amount of lens or ciliary body distension in EVASII.

6.8 EVASII vs. EVASI Curves

6.8.1 Methods

EVASII vs. EVASI curves were generated with EVASI data on the abscissa and EVASII data on the ordinate for each of the following parameters: lens diameter, ciliary

body diameter, and lens power. When appropriate, a linear fit of the data was conducted in order to retrieve the slope and the slope error, where a slope of unity would reflect a perfect correlation between the two systems as a function of stretch.

6.8.2 Results
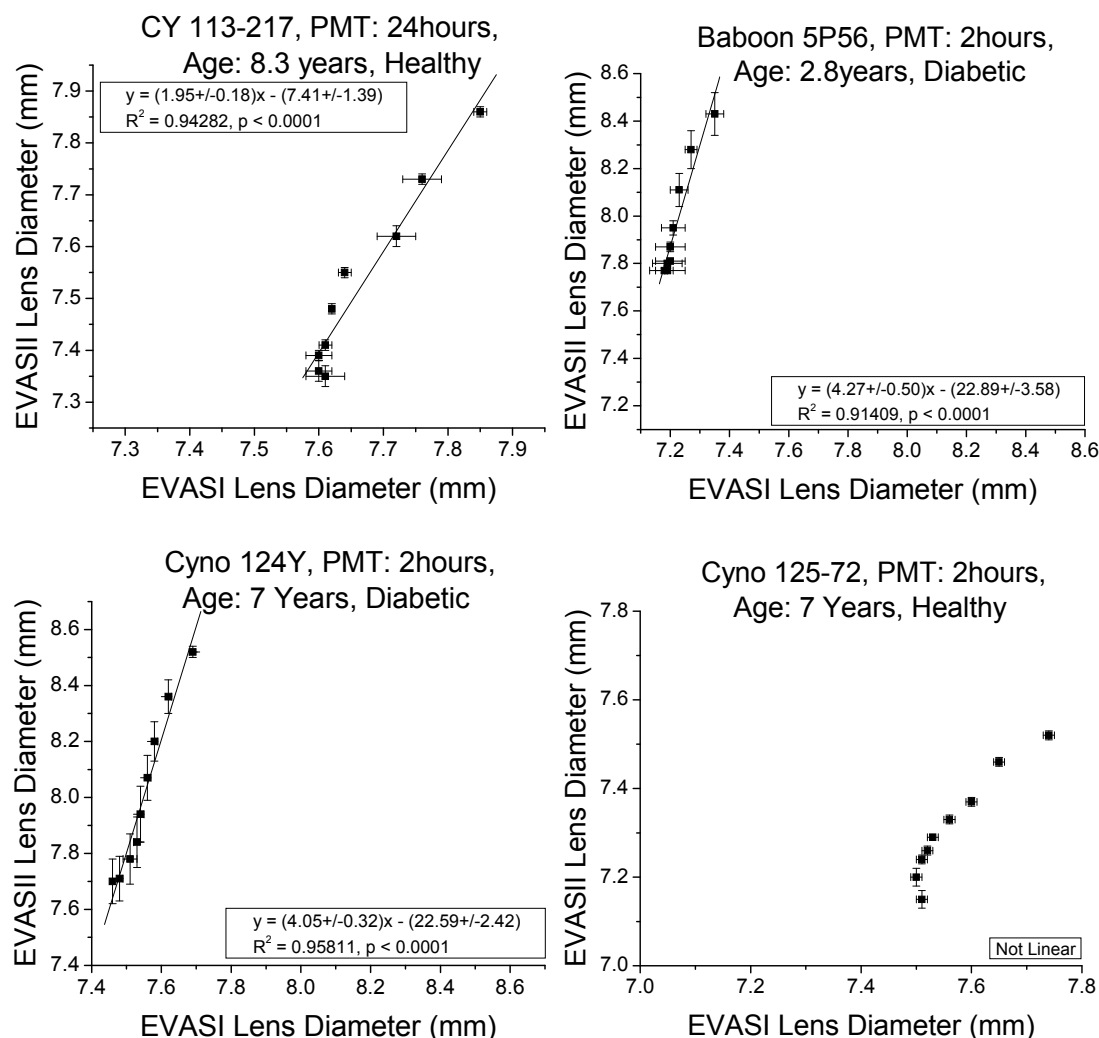
Figure 6.6: EVASII vs. EVASI curves for the lens diameter of all 4 eyes. The equation of the best fit line and the fit parameters are given in the legend.
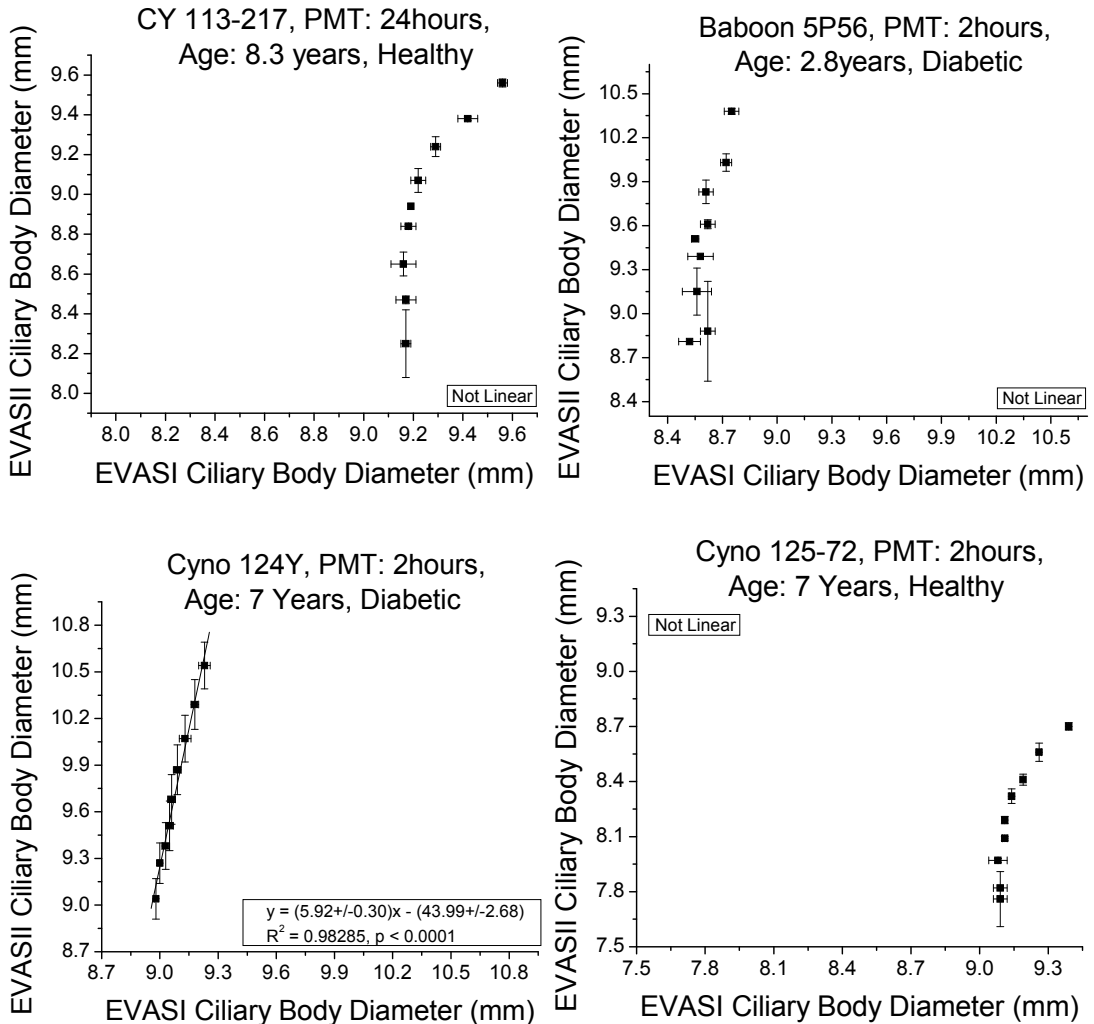
Figure 6.7: EVASII vs. EVASI curves for the ciliary body diameter of all 4 eyes. The equation of the best fit line and the fit parameters are given in the legend.
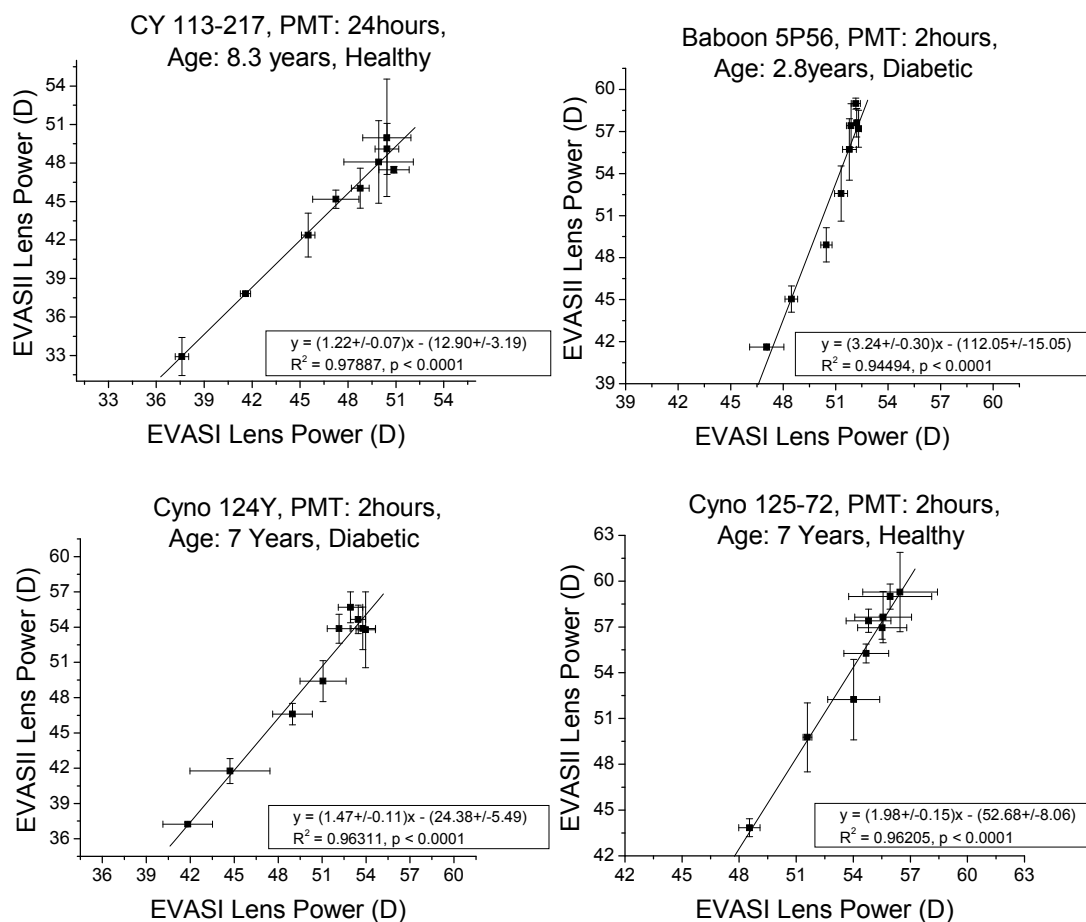
Figure 6.8: EVASII vs. EVASI curves for the lens power of all 4 eyes. The equation of the best fit line and the fit parameters are given in the legend.

The EVASII vs. EVASI curves for the lens diameter are linear for 3 of 4 eyes, and all of the linear curves have a slope that is significantly greater than unity. The EVASII vs. EVASI curves for the ciliary body diameter are linear for 1 of 4 eyes, and the single linear curve has a slope that is significantly greater than unity. Furthermore, by inspection, the mean slope of the EVASII vs. EVASI curves for the ciliary body diameter is larger than for the lens diameter. The EVASII vs. EVASI curves for the lens power are linear for 4 of 4 eyes, and all these curves have a slope that is significantly greater than unity. The non-linear trends Figures 6.6 and 6.7 are due to differences between the order of the diameter vs. sclera stretch curves. For example, the lens diameter vs. stretch trend for CY 125-72 was linear in EVASII and quadratic in EVASI.

6.8.3 Conclusions

This result indicates that, as a function of stretch EVASII is more efficient at producing changes in the lens diameter, ciliary body diameter, and lens power than EVASI. The EVASII vs. EVASI curves are not consistent among different eyes; and thus, no correction factor can be implemented to render the results of the two systems interchangeable.

6.9 EVASI and EVASII Results Compared

6.9.1 Methods

Plots showing the total change in lens diameter, ciliary body diameter, and lens power were created using the total database (as of 11/3/08) of EVASI and EVASII human results to qualitatively compare the two systems. Similar plots were made for the load-lens diameter slope, the load-ciliary body diameter slope, and the power-load slope.

6.9.2 Results
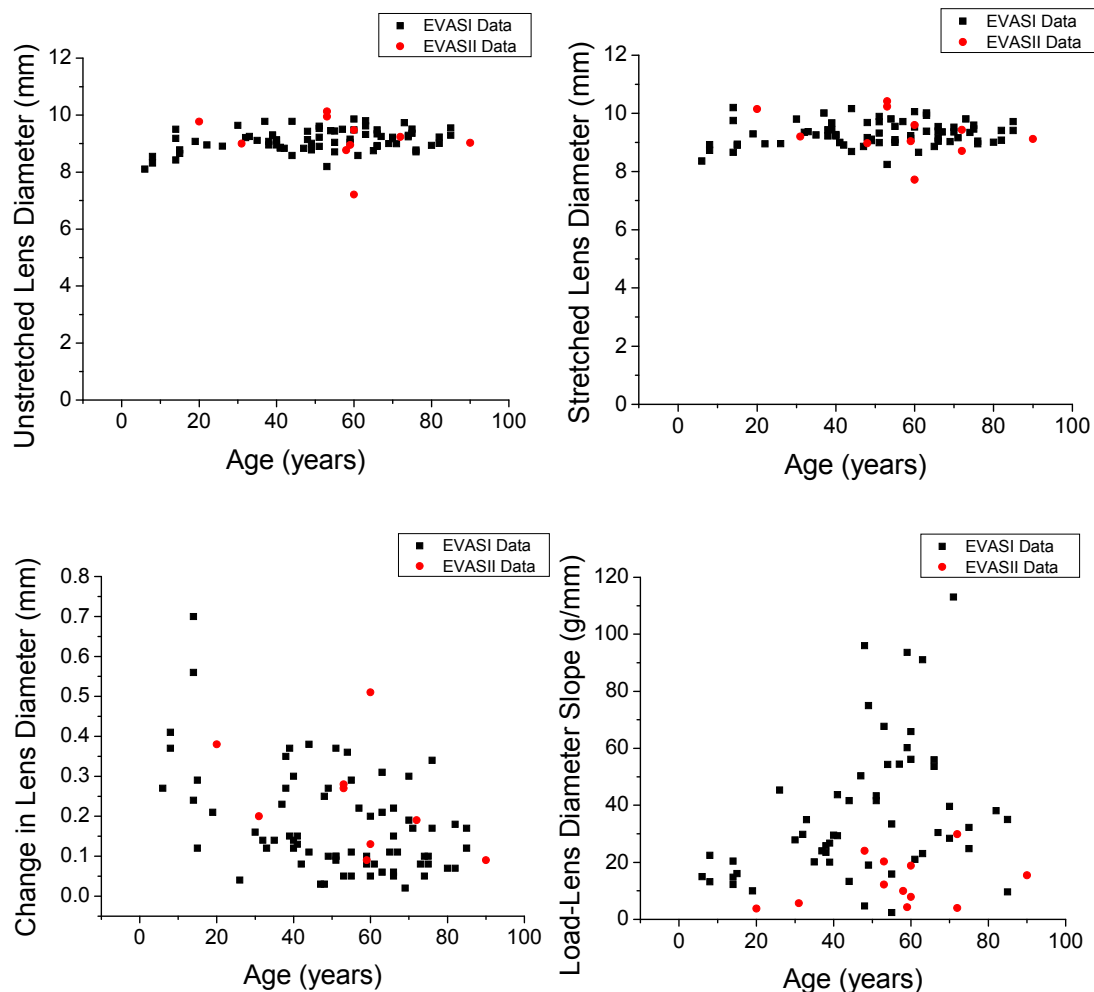
Figure 6.9: Unstretched lens diameter (top left), stretched lens diameter (top right), change in lens diameter (bottom right), and load-lens diameter slope (bottom right) for all human eyes tested in EVASI (black) and EVASII (red).

The unstretched lens diameter and the stretched lens diameter are not significantly different for EVASI and EVASII. The change in lens diameter decreases as a function of age in both systems; however, when sorted into 5 bins (1 bin = 20 years), the change in lens diameter is consistently higher in EVASII except for the last bin, which has only one data point. The load-lens diameter is significantly less in EVASII than in EVASI.
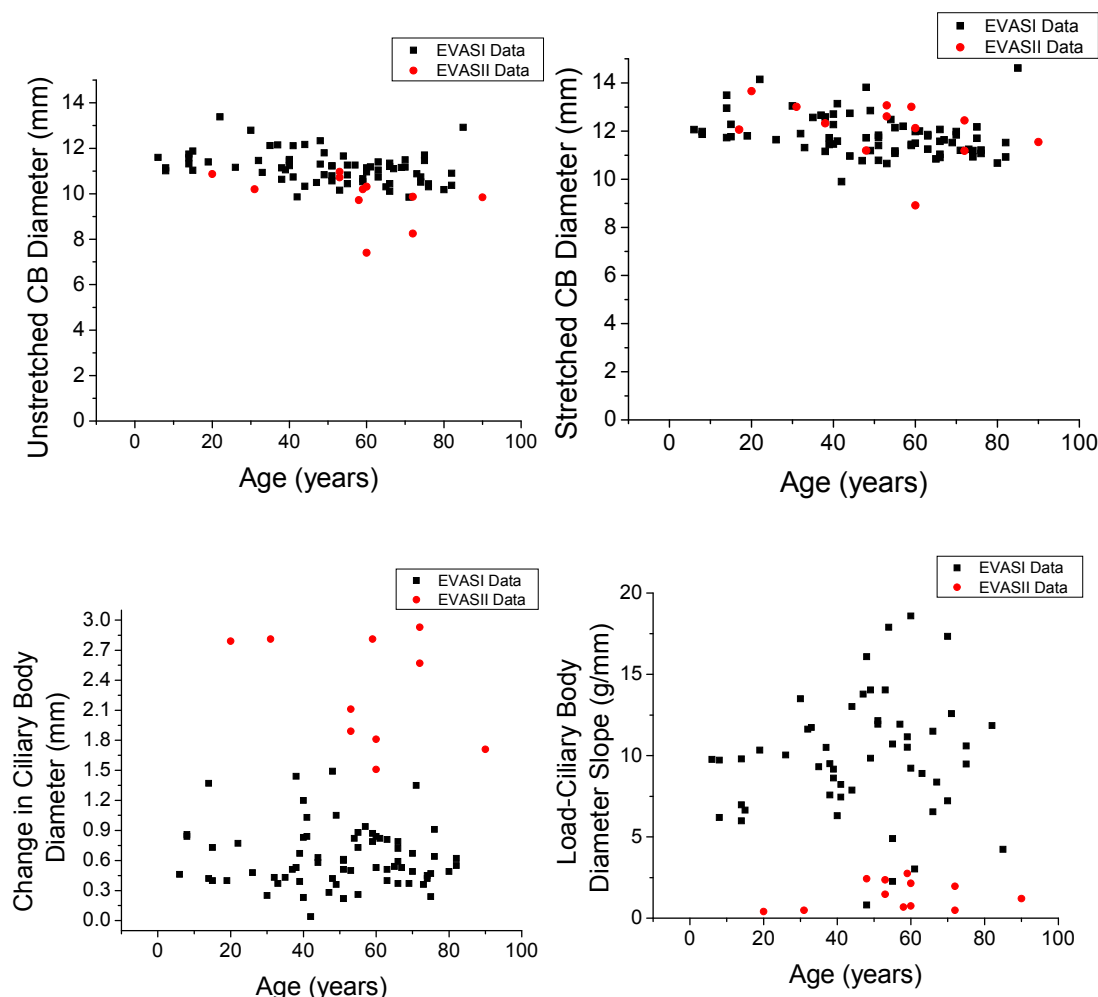
Figure 6.10: Unstretched ciliary body diameter (top left), stretched ciliary body diameter (top right), change in ciliary body diameter (bottom right), and load-ciliary body diameter slope (bottom right) for all human eyes tested in EVASI (black) and EVASII (red).

The unstretched ciliary body diameter is significantly smaller in EVASII than in EVASI, and this is likely due to the initial suture slack removal in the latter. The stretched ciliary body diameter is not significantly different, and thus, the change in ciliary body diameter is significantly greater in EVASII, and the load-ciliary body diameter is significantly less in EVASII.
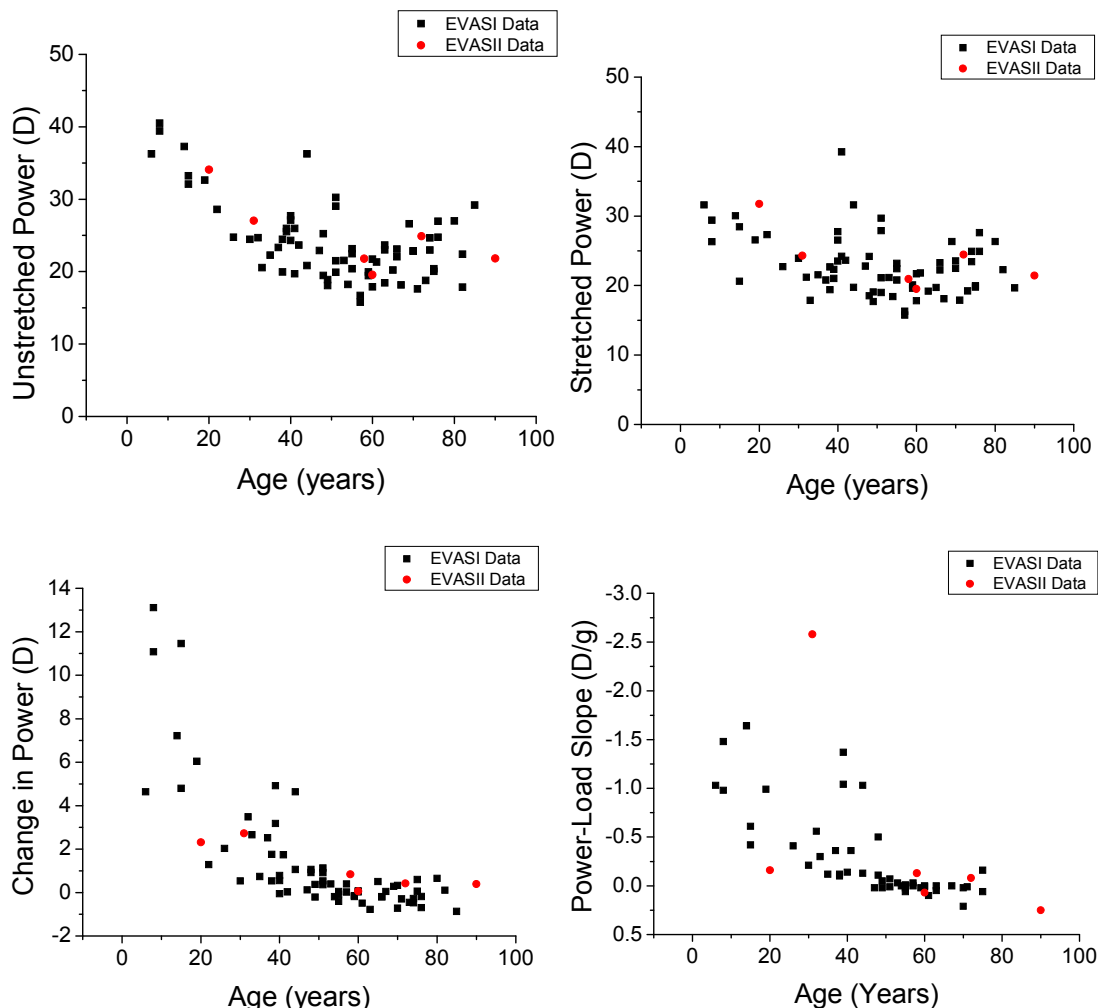
Figure 6.11: Unstretched lens power (top left), stretched lens power (top right), change in lens power (bottom right), and power-load slope (bottom right) for all human eyes tested in EVASI (black) and EVASII (red).

The unstretched power, stretched power, change in power, and power-load slope are decreasing as a function of age. When sorted into 5 bins (1 bin = 20 years), the unstretched power, stretched power, and power-load slope is not significantly different, but the change in power is consistently greater in EVASII than in EVASI.

6.9.3 Conclusions

Both as a function of stretch and as a function of load, EVASII is more efficient than EVASI in producing changes in lens diameter, ciliary body diameter, and lens power.

6.10 Summary

Overall, EVASI and EVASII results are significantly different both as a function of stretch and as a function of load. As a function of stretch, EVASII is more efficient than EVASI in producing changes in lens diameter, ciliary body diameter, and lens power. The discrepancy between the change in these parameters could be due to the differences between the mechanical transduction mechanisms of the two systems, as the EVASII system utilizes mechanical components (aluminum arms) whose compliance is much less than those used in EVASI (sutures), and the starting position in EVASI may have slack in some of the sutures. Then, the reported displacement in EVASI potentially overestimates the actual displacement of the tissue since the system must first eliminate the slack in the sutures and since the strain in the sutures is not accounted for.

Furthermore, both the lens and ciliary body diameters changed more as a function of stretch in EVASII, but the increase was more pronounced for the ciliary body. Perhaps the difference between the starting positions of the tissue in EVASI and EVASII is responsible for the additional increase in ciliary body distension in EVASII, since a slight pre-stretch was used to obtain the initial position in EVASI, while in EVASII, no pre-stretch was applied.

The maximum load in EVASI is greater than the maximum load in EVASII. This discrepancy is likely due to the differences between the mechanical transduction mechanisms of the two systems, and because the EVASII system is less susceptible to friction than EVASI. In turn, EVASI requires more load for an equivalent amount of lens or ciliary body distension in EVASII; and thus, the load-lens diameter, load-ciliary body diameter, and load-lens power slopes are significantly smaller in EVASII.

The variation in load between runs is an order of magnitude greater in EVASII than in EVASI (approximate average standard deviation: 0.08g in EVASI and 0.8g in EVASII). This is likely due the differences between the force measurement mechanisms of the two systems. As demonstrated in chapter 4, the use of 8 transducers (in EVASII) inherently adds more uncertainty to the force measurement, and this also reduces the measured loads by a factor of 8, pushing the measurements closer to the noise level of the EVASII force transducers. The variability of lens diameter, ciliary body diameter, and lens power are consistently higher in EVASII as well, but the differences are not statistically significant.

Finally, the EVASII vs. EVASI plots of the lens diameter, ciliary body diameter, and lens power induced by EVASI and EVASII are not consistent among different eyes; and thus, results of the two systems cannot be used interchangeability, and no correction factor can be implemented to make the results interchangeable. However, both systems share a common qualitative trend of increasing lens and ciliary body diameter and decreasing lens power with increasing scleral stretch and applied load. Thus, general trends concerning efficacy and optimization of surgical procedures as well as age related accommodative changes can be compared for each individual system.

Chapter 7: Summary and Conclusion

Presbyopia is the condition of insufficient accommodative amplitude for clear near vision; it is a symptom of ocular senescence, which affects all people living beyond 50 years of age. It implies a major loss of visual function, and the estimated economic impact of this is staggering, since people with presbyopia are likely to lose productivity due to this impairment; thus, the study of accommodation is of paramount importance. Presbyopia can potentially be cured by surgical procedures such as lens refilling, and this hope provides a driving force behind understanding accommodation. As part of the work currently underway on accommodation, presbyopia, and lens refilling, at the Ophthalmic Biophysics Center, two different ex-vivo accommodation simulation instruments, EVASI and EVASII, were developed.

The goal of this project was to design, fabricate, and validate a mechanical mounting system for post-mortem human and higher-primate tissue for use in EVASII experiments, to characterize and calibrate both the optical and mechanical measurement systems of EVASII, and to compare the results of EVASII to that of EVASI.

A tissue mounting mechanism utilizing magnetic force was designed, fabricated, and implemented, and has proven successful in a number of experiments. The magnetic mounts produced a measurement artifact however, as the measured load included that contributed by magnetic interference of the 8 arm system of EVASII. The magnetic load artifact has been characterized and this characterization provided the means for compensation during post processing of EVASII data. This additional computation contributes to the overall measurements system uncertainty, and this contribution has been determined, giving a total sum load uncertainty of ±0.81g.

90

Further, an optical calibration of the EVASII lens power measurement system has been performed, giving a system accuracy of 0.5D for most lenses and 2D for all lenses. Overall, the error ranged from -1.6D to +1.9D, with a mean absolute error of 0.56±0.54D.

Finally, a study directly comparing EVASII to EVASI using 4 primates (8 eyes), and a comparison of the total database of human eyes measured in EVASII and EVASI was performed. Both as a function of displacement and load, EVASII is much more efficient than EVASI in producing changes in lens diameter, ciliary body diameter, and lens power. The discrepancy between these parameters could be due to the differences between the mechanical transduction mechanisms of the two systems, as the EVASII system utilizes mechanical components (aluminum arms) whose compliance is much less than those used in EVASI (sutures), and the starting position in EVASI may have slack in some of the sutures.

Furthermore, the variation in load between runs is an order of magnitude greater in EVASII than in EVASI, and this is likely due the differences between the force measurement mechanisms of the two systems. The use of 8 transducers (in EVASII) inherently adds more uncertainty to the force measurement, and this also reduces the measured loads by a factor of 8, pushing the measurements closer to the noise level of the EVASII force transducers.

All and all, the results of the two systems are significantly different, they cannot be used interchangeability, and no correction factor can be implemented to make the results interchangeable. However, both systems share a common trend of increasing lens and ciliary body diameter and decreasing lens power with increasing scleral stretch and applied load. Thus, general trends concerning efficacy and optimization of surgical

procedures as well as age related accommodative changes can be compared for each individual system.

References

Bevington PR, "Estimates of Means and Errors," *Data Reduction and Error Analysis for the Physical Sciences*, Bevington PR, McGraw-Hill Book Company, New York NY, 1969, 66-91.

Coleman DJ, Fish SK, "Presbyopia, Accommodation, and the Mature Catenary," *Ophthalmology*, 2001;108 (9):1544-1551.

Coleman DJ, "On the Hydraulic Suspension Theory of Accommodation," *Trans Am Ophthalmol Soc.* 1986;84:846-68.

Cramer A, "Het Accommodatievermogen der Oogen Physiologisch Toegelicht," *Haarlem. De Erven Loosjes*, 1853; 35-37.

Croft MA, Glasser A, Heatley G, et al., "The Zonula, Lens, and Circumlental Space in Normal Iridectomized Rhesus Monkey Eyes," *Invest Ophthalmol Vis Sci*, 2006;47:1087-1095.

Denham DB, Fernandez V, Billotte C, et al., "Method for Ex-Vivo Assesment of Accommodation Forces," *Invest Ophthalmol Vis Sci*, 2002;43: E-Abstract 403.

Donders FC, "On the anomalies of accommodation and refraction of the eye," *The New Sydenham Society, London,* 1864; 10–19.

Duane, A, "Normal values of the accommodation at all ages," *J Am Med Assoc,* 59, 1912.

Ehrmann K, Ho A, Parel J-M, "Biomechanical analysis of the accommodative apparatus in primates," *Clin Exp Optom*, 2008; 91: 3: 302–312

Fincham, EF, "The Mechanism of Accommodation," *Br J Ophthalmol*, 1937;(Suppl. 8):5-80.

Fisher RF, "Presbyopia and the Changes with Age in the Human Crystalline Lens," *J Physiol,* 1973; 228, 765-779.

Fisher RF, "The Force of Contraction of the Human Ciliary Muscle during Accommodation," *J Physiol,* 1977; 270, 51-74.

Gilmartin B, "The Aetiology of Presbyopia: A Summary of the Role of Lenticular and Extralenticular Structures," *Ophthal Physiol Opt*, 1995, 15:5, 431-437.

Glasser A, Campbell MCW, "Presbyopia and the Optical Changes in the Human Crystalline Lens with Age," *Vision Res,* 1998; 38, 209-229.

Glasser A, Kaufman PL, "The Mechanism of Accommodation in Primates," *Ophthalmology*, 1999;106:863-872.

Glasser A, "Edinger-Westphal Stimulated Accommodation in Monkeys," Guthoff R, Ludwig K, *Current Aspects of Human Accommodation*, Heidelberg/Germany, 2001;53-69.

Glasser A, "Restoration of Accommodation: Surgical Options for the Correction of Presbyopia," *Clin Exp Optom*, 2008, 91:3:279-295.

Helmholtz H, "Uber die Akkommodation des Auges," *Albrecht von Grafes Arch Ophthalmol*, 1855; 1:1.

Kaufman PL, "Accommodation and Presbyopia: Neuromusclar and Biophysical Aspects," *Adler's Physiology of the Eye*, Ninth Edition, Hart, William M., Mosby Year Book, Missouri: St. Louis, 1992. 391-411.

Kessler J, "Experiments in Refilling the Lens," *Arch Ophthalmol*, 1964, 71:412-417.

Koretz JF, Handelman GH, Brown NP, "Analysis of Human Crystalline Lens Curvature as a Function of Accommodative State and Age," *Vision Res*, 1984; 24:1141.

Koretz JF, Bertasso AM, Neider MW, True-Gabelt B, Kaufman PL, "Slit-lamp Studies of the Rhesus Monkey Eye, II, Changes in Crystalline Lens Shape, Thickness and Position during Accommodation and Aging," *Exp Eye Res*, 1987; 45:317.

Ludwig K, Wegscheider E, Hoops JP, Kampik A, "In Vivo Imaging of the Human Zonular Apparatus with High-Resolution Ultrasound Biomicroscopy," *Graefes Arch Clin Exp Ophthalmol*, 1999;237:361-371.

Manns F, Nankivil D, Borja D, et al., "Calibration of EVASII Power Measurements," *Internal OBC Report*, August 2007.

Manns F, Parel J-M, Denham D, et al., "Optomechanical Response of Human and Monkey Lenses in a Lens Stretcher," *Invest Ophthalmol Vis Sci*, 2007;48:3260-3268.

Menapace R, Findl O, Kriechbaum K, "Accommodating Intraocular Lenses: A Critical Review of Present and Future Concepts," *Graefe's Arch Clin Exp Ophth* (2007) 245:473-489.

Nishi O, "Restoration of Accommodation by Refilling the Lens Capsule after Endocapsular Phacoemulsification," In: Guthoff R, Ludwig K, eds. *Current Aspects of Human Accommodation II*, Heidelberg: Kaden Verlag, 2003.

Norrby S, Koopmans S, Terwee T, "Artificial Crystalline Lens," *Ophthalmol Clin North Am*, 2006, 19: 142-146, vii.

94

Pardue MT, Sivak JG, "Age-Related Changes in Human Ciliary Muscle," *Optom Vis Sci,* 2000;77:204-210.

Parel J-M, Gelender H, Treffers WF, Norton EWD, "Phaco-ersatz," *Graefes Arch Clin Exp Ophthalmol.* 1986;224:165-173.

Pau H, Kranz J, "The Increasing Sclerosis of the Human Lens with Age and its Relevance to Accommodation and Presbyopia," *Graefes Arch Clin Exp Ophthalmol.* 1991;229,294-296.

Schachar RA, Cudmore DP, "The Effect of Gravity on the Amplitude of Accommodation," *Ann Ophthalmol*, 1994;26:65-70.

Strenk SA, Semmlow JL, Strenk LM, et al., "Age-Related Changes in Human Ciliary Muscle and Lens: A Magnetic Resonance Imaging Study," *Invest Ophthalmol Vis Sci*, 1999;40:1162-1169.

Suresh K. Pandey, Jaya Thakur, Liliana Werner, Edward M. Wilson, Leonardo P. Werner, Andrea M. Izak, David J. Apple, "The Human Crystalline Lens, Ciliary Body, and Zonules," *Presbyopia*, Agarwal, Amar, Slack Incorporated, New Jersey: Thorofare, 2002. 17-27.

Weale RD, "Presbyopia Toward the End of the 20th Century," *Surv Ophthalmol*, 1989. 34:1, 15-30.

Werner LP, Werner L, Pandey SK, Apple DJ, "Physiology of Accommodation and Presbyopia," *Presbyopia*, Agarwal, Amar, Slack Incorporated, New Jersey: Thorofare, 2002. 29-34.

Young T, "Observations on Vision," *Phil Trans R Soc*, 1793; 83:169-181.

Appendix 1: EVASII Load Data Program

```
%%%%%%%%%%%%%%%%%%%%%%%%%%%%%%%%%%%%%%%%%%%%%%%%%%%%%%%%%%%%%%%%%%%%%%%
%%%%
%%%%%                      -EVASII Load Data Plotter-
%%%%%
%%%%%          Created by: Derek Nankivil, On: 10-15-2007
%%%%%
%%%%%%%%%%%%%%%%%%%%%%%%%%%%%%%%%%%%%%%%%%%%%%%%%%%%%%%%%%%%%%%%%%%%%%%
%%%%

%%%%% Instructions: (Takes ~ 3-4min)
%%%%% 1.) Open .txt data file (generated by EVASII software) with excel
%%%%% 2.) Save file as an excel workbook.
%%%%% 3.) Using Matlab, drive to File: Import Data,
%%%%%     then drive to the file location, and select the file.
%%%%% 4.) Run EVASIILoadDataPlotter.M.
%%%%% 5.) Copy the 25 figures to the eye data folder by run number.
%%%%% 6.) Use output data in: transpositionsubset, transavgsumload and
%%%%%     transstdsumload (located in Matlab workspace) in excel eye
%%%%%     data table.
%%%%%     (Note: these values are not offset to give the first step of
%%%%%     the first run in the series a zero load).
%%%%%     *****Code terminates if step size is not satisfied


%%%%% Operations and Functions:
%%%%% 1.) Plots position vs time profile.
%%%%% 2.) Plots all 8 individual piezos load data as a function of
%%%%%     time: all 8 plots have the same load range to make comparison
%%%%%     straight-forward.
%%%%% 3.) Sums individual piezos and plots sum load vs time.
%%%%% 4.) Calculates the average and standard deviation of the sum load
%%%%%     during each position-hold.
%%%%% 5.) Plots average and standard deviation of the sum load vs
%%%%% position.
%%%%% 6.) Calculates the average and standard deviation of the 8
%%%%%     individual piezo loads during each position hold.
%%%%% 7.) Plots average and standard deviation of the 8 individual
%%%%%     piezo loads vs position: all 8 plots have the same load range
%%%%%     to make comparison straight-forward.
%%%%% 8.) Calculates the FFT and sampling interval of the sum load data
%%%%%     and obtains the frequency spectrum.
%%%%% 9.) Plots the sampling interval, and frequency spectrum two
%%%%%     plots,where the second plot is a close-up whose zoom window
%%%%% is based on the variation in the mean power of the frequency
%%%%% response.
%%%%% 10.)Filteres the sum load with an 0.2, 0.5, and 0.7Hz elliptical
%%%%%     lowpass filter
%%%%% 11.)Plots the sum load with the filter response superimposed


%%%%% -Initialize Variables-
i=45; j=1;                              %counter
time=[]; position=[]; sumload=[];       %time, position & sum load
f1=[]; f2=[]; f3=[]; f4=[];             %individual piezo loads
f5=[]; f6=[]; f7=[]; f8=[];
```

96

```matlab
maxindivload=[]; minindivload=[];        %used of setting the limits of
individual piezo load vs time graph so that all 8 graphs have the same
scale
avgsumload=[];                           %position-hold avg sum loads
(sum of all 8 piezos)
stdsumload=[];                           %std of position-hold avg loads
loadsubset=[];                           %used in loop for grabbing
loads during position-hold intervals
lowerlimit=[]; upperlimit=[];            %used for setting the limits of
position-hold avg sum load graph
checker=[];                              %used for terminating code if
step size is not satsified
samplinginterval=[];
avgsumloadf1=[]; avgsumloadf2=[]; avgsumloadf3=[];  %individual piezo
position hold avg sum loads
avgsumloadf4=[]; avgsumloadf5=[]; avgsumloadf6=[];
avgsumloadf7=[]; avgsumloadf8=[]; avgsumloadf9=[];
lowerlimitI=[]; upperlimitI=[];          %used for setting the limits of
individual piezo position hold avg sum load graphs so that all 8 graphs
have the same scale
pausetime=5;                             %pause has been introduced to
eliminate errors due to processing overload during saving
sos1=[]; g1=[]; sos2=[]; g2=[]; sos3=[]; g3=[];     %elliptical filter
characteristics
filtered1=[]; filtered2=[]; filtered3=[];           %filtered response
avesamplinginterval=[]; stdsamplinginterval=[];     %used for giving a
warning when the sampling interval is not reasonably constant


%%%%% -Get Data from Excel File-
[m,n]=size(data);                        %get size of data
eyeinfo1=cat(2,textdata(8,2),textdata(9,2));        %get eye info:
species, eye number, run number
eyeinfo2=cat(2,textdata(30,1),data(26,2));
eyeinfo=cat(2,eyeinfo1,eyeinfo2);
stepsize=data(31,2);                     %get step size


%%%%% -Main: Define Loops to Parse and Calculate Data for Plotting-
while (i<=m)                             %define time array
    time(j)=data(i,1);
    i=i+1;
    j=j+1;
end
timeaxisinterval=max(time)/10;           %define time axis interval
for plotting, either 10, 20, 30, 40, 50 or 60s intervals
if(timeaxisinterval>0 && timeaxisinterval<15)
    timeaxisinterval=10;
end
if(timeaxisinterval>=15 && timeaxisinterval<25)
    timeaxisinterval=20;
end
if(timeaxisinterval>=25 && timeaxisinterval<35)
    timeaxisinterval=30;
end
if(timeaxisinterval>=35 && timeaxisinterval<45)
    timeaxisinterval=40;
end
```

```matlab
if(timeaxisinterval>=45 && timeaxisinterval<55)
    timeaxisinterval=50;
end
if(timeaxisinterval>=55 && timeaxisinterval<65)
    timeaxisinterval=60;
end
i=45; j=1;                                  %reset counter
while (i<=m)                                 %define position array
    position(j)=data(i,2);
    i=i+1;
    j=j+1;
end
i=45; j=1;                                  %reset counter
while (i<=m)                                 %define f1 array
    f1(j)=data(i,4);
    i=i+1;
    j=j+1;
end
i=45; j=1;                                  %reset counter
while (i<=m)                                 %define f2 array
    f2(j)=data(i,5);
    i=i+1;
    j=j+1;
end
i=45; j=1;                                  %reset counter
while (i<=m)                                 %define f3 array
    f3(j)=data(i,6);
    i=i+1;
    j=j+1;
end
i=45; j=1;                                  %reset counter
while (i<=m)                                 %define f4 array
    f4(j)=data(i,7);
    i=i+1;
    j=j+1;
end
i=45; j=1;                                  %reset counter
while (i<=m)                                 %define f5 array
    f5(j)=data(i,8);
    i=i+1;
    j=j+1;
end
i=45; j=1;                                  %reset counter
while (i<=m)                                 %define f6 array
    f6(j)=data(i,9);
    i=i+1;
    j=j+1;
end
i=45; j=1;                                  %reset counter
while (i<=m)                                 %define f7 array
    f7(j)=data(i,10);
    i=i+1;
    j=j+1;
end
i=45; j=1;                                  %reset counter
while (i<=m)                                 %define f8 array
    f8(j)=data(i,11);
```

```
        i=i+1;
        j=j+1;
    end
    [o,p]=size(f8);                          %get size of load data
    i=1; j=1;                                %reset counter
    f1=f1/9.81;                              %convert individual loads
    to grams
    f2=f2/9.81;
    f3=f3/9.81;
    f4=f4/9.81;
    f5=f5/9.81;
    f6=f6/9.81;
    f7=f7/9.81;
    f8=f8/9.81;
    maxindivload(1)=max(f1);                 %define max of individual
    loads
    maxindivload(2)=max(f2);
    maxindivload(3)=max(f3);
    maxindivload(4)=max(f4);
    maxindivload(5)=max(f5);
    maxindivload(6)=max(f6);
    maxindivload(7)=max(f7);
    maxindivload(8)=max(f8);
    minindivload(1)=min(f1);                 %define min of individual
    loads
    minindivload(2)=min(f2);
    minindivload(3)=min(f3);
    minindivload(4)=min(f4);
    minindivload(5)=min(f5);
    minindivload(6)=min(f6);
    minindivload(7)=min(f7);
    minindivload(8)=min(f8);
    while (j<=p)                             %define sum load
        sumload(j)=f1(j)+f2(j)+f3(j)+f4(j)+f5(j)+f6(j)+f7(j)+f8(j);
        j=j+1;
    end
    [maxposition,index]=max(position);       %define max position
    positionsubset=(0:stepsize:maxposition);
    [c,d]=max(positionsubset);               %c=maxposition,
    d=index=number of steps during stretching
    i=1; j=1; k=1; l=0;                       %reset counter
    while(i<=d)              %define average sum load during position-hold
        while(j<=p)
            while(position(j)==l)
                loadsubset(k)=sumload(j);
                if(j==p)
                else
                    k=k+1;
                    j=j+1;
                end
            end
            avgsumload(i)=mean(loadsubset);
            stdsumload(i)=std(loadsubset);
            if(avgsumload(i)==NaN)
                warning('Step Size Requirement Not Met');
            end
            clear loadsubset;
```

```
        loadsubset=[];
        if(l+stepsize<=maxposition)
                l=l+stepsize;
        end
        k=1;
        while(j<=p && position(j)<l)
            j=j+1;
        end
        i=i+1;
    end
end
checker=isnan(avgsumload);                      %checker is used to
terminate code if avg sum load returns NaN, which happens when EVASII
does not stop at designated step intervals
i=1;
while(i<=d)      %loop to display warning if a step interval is not found
    if(checker(i)==1)
        warning('Step Interval Requirement Not Satisfied')
    end
    i=i+1;
end
if(sum(checker)==0)                    %all further operations come under
this if statement so code is aborted if a step interval is not found
    i=1;
    while(i<=d)                                  %define upper and lower
limits for position vs avg sum load plot
        lowerlimit(i)=avgsumload(i)-1.5*stdsumload(i);
        upperlimit(i)=avgsumload(i)+1.5*stdsumload(i);
        i=i+1;
    end
    i=1; j=1; k=1; l=0;                          %reset counter
    while(i<=d)         %define f1 average sum load during position-hold
        while(j<=p)
            while(position(j)==l)
                loadsubset(k)=f1(j);
                if(j==p)
                else
                    k=k+1;
                    j=j+1;
                end
            end
            avgsumloadf1(i)=mean(loadsubset);
            stdsumloadf1(i)=std(loadsubset);
            clear loadsubset;
            loadsubset=[];
            if(l+stepsize<=maxposition)
                l=l+stepsize;
            end
            k=1;
            while(j<=p && position(j)<l)
                j=j+1;
            end
            i=i+1;
        end
    end
    i=1; j=1; k=1; l=0;                          %reset counter
    while(i<=d)
```

```matlab
    while(j<=p)        %define f2 average sum load during position-hold
        while(position(j)==l)
            loadsubset(k)=f2(j);
            if(j==p)
            else
                k=k+1;
                j=j+1;
            end
        end
        avgsumloadf2(i)=mean(loadsubset);
        stdsumloadf2(i)=std(loadsubset);
        clear loadsubset;
        loadsubset=[];
        if(l+stepsize<=maxposition)
            l=l+stepsize;
        end
        k=1;
        while(j<=p && position(j)<l)
            j=j+1;
        end
        i=i+1;
    end
end
i=1; j=1; k=1; l=0;                              %reset counter
while(i<=d)          %define f3 average sum load during position-hold
    while(j<=p)
        while(position(j)==l)
            loadsubset(k)=f3(j);
            if(j==p)
            else
                k=k+1;
                j=j+1;
            end
        end
        avgsumloadf3(i)=mean(loadsubset);
        stdsumloadf3(i)=std(loadsubset);
        clear loadsubset;
        loadsubset=[];
        if(l+stepsize<=maxposition)
            l=l+stepsize;
        end
        k=1;
        while(j<=p && position(j)<l)
            j=j+1;
        end
        i=i+1;
    end
end
i=1; j=1; k=1; l=0;                              %reset counter
while(i<=d)          %define f4 average sum load during position-hold
    while(j<=p)
        while(position(j)==l)
            loadsubset(k)=f4(j);
            if(j==p)
            else
                k=k+1;
                j=j+1;
```

```matlab
                end
            end
            avgsumloadf4(i)=mean(loadsubset);
            stdsumloadf4(i)=std(loadsubset);
            clear loadsubset;
            loadsubset=[];
            if(l+stepsize<=maxposition)
                l=l+stepsize;
            end
            k=1;
            while(j<=p && position(j)<l)
                j=j+1;
            end
            i=i+1;
        end
    end
    i=1; j=1; k=1; l=0;                              %reset counter
    while(i<=d)          %define f5 average sum load during position-hold
        while(j<=p)
            while(position(j)==l)
                loadsubset(k)=f5(j);
                if(j==p)
                else
                    k=k+1;
                    j=j+1;
                end
            end
            avgsumloadf5(i)=mean(loadsubset);
            stdsumloadf5(i)=std(loadsubset);
            clear loadsubset;
            loadsubset=[];
            if(l+stepsize<=maxposition)
                l=l+stepsize;
            end
            k=1;
            while(j<=p && position(j)<l)
                j=j+1;
            end
            i=i+1;
        end
    end
    i=1; j=1; k=1; l=0;                              %reset counter
    while(i<=d)          %define f6 average sum load during position-hold
        while(j<=p)
            while(position(j)==l)
                loadsubset(k)=f6(j);
                if(j==p)
                else
                    k=k+1;
                    j=j+1;
                end
            end
            avgsumloadf6(i)=mean(loadsubset);
            stdsumloadf6(i)=std(loadsubset);
            clear loadsubset;
            loadsubset=[];
            if(l+stepsize<=maxposition)
```

```matlab
            l=l+stepsize;
        end
        k=1;
        while(j<=p && position(j)<l)
            j=j+1;
        end
        i=i+1;
    end
end
i=1; j=1; k=1; l=0;                          %reset counter
while(i<=d)        %define f7 average sum load during position-hold
    while(j<=p)
        while(position(j)==l)
            loadsubset(k)=f7(j);
            if(j==p)
            else
                k=k+1;
                j=j+1;
            end
        end
        avgsumloadf7(i)=mean(loadsubset);
        stdsumloadf7(i)=std(loadsubset);
        clear loadsubset;
        loadsubset=[];
        if(l+stepsize<=maxposition)
            l=l+stepsize;
        end
        k=1;
        while(j<=p && position(j)<l)
            j=j+1;
        end
        i=i+1;
    end
end
i=1; j=1; k=1; l=0;                          %reset counter
while(i<=d)        %define f8 average sum load during position-hold
    while(j<=p)
        while(position(j)==l)
            loadsubset(k)=f8(j);
            if(j==p)
            else
                k=k+1;
                j=j+1;
            end
        end
        avgsumloadf8(i)=mean(loadsubset);
        stdsumloadf8(i)=std(loadsubset);
        clear loadsubset;
        loadsubset=[];
        if(l+stepsize<=maxposition)
            l=l+stepsize;
        end
        k=1;
        while(j<=p && position(j)<l)
            j=j+1;
        end
        i=i+1;
```

```matlab
        end
    end
    i=1;
    while(i<=d)                                  %define upper and lower
limits of position vs individual avg load plot
        lowerlimit1(i)=avgsumloadf1(i)-1.5*stdsumloadf1(i);
        upperlimit1(i)=avgsumloadf1(i)+1.5*stdsumloadf1(i);
        lowerlimit2(i)=avgsumloadf2(i)-1.5*stdsumloadf2(i);
        upperlimit2(i)=avgsumloadf2(i)+1.5*stdsumloadf2(i);
        lowerlimit3(i)=avgsumloadf3(i)-1.5*stdsumloadf3(i);
        upperlimit3(i)=avgsumloadf3(i)+1.5*stdsumloadf3(i);
        lowerlimit4(i)=avgsumloadf4(i)-1.5*stdsumloadf4(i);
        upperlimit4(i)=avgsumloadf4(i)+1.5*stdsumloadf4(i);
        lowerlimit5(i)=avgsumloadf5(i)-1.5*stdsumloadf5(i);
        upperlimit5(i)=avgsumloadf5(i)+1.5*stdsumloadf5(i);
        lowerlimit6(i)=avgsumloadf6(i)-1.5*stdsumloadf6(i);
        upperlimit6(i)=avgsumloadf6(i)+1.5*stdsumloadf6(i);
        lowerlimit7(i)=avgsumloadf7(i)-1.5*stdsumloadf7(i);
        upperlimit7(i)=avgsumloadf7(i)+1.5*stdsumloadf7(i);
        lowerlimit8(i)=avgsumloadf8(i)-1.5*stdsumloadf8(i);
        upperlimit8(i)=avgsumloadf8(i)+1.5*stdsumloadf8(i);
        i=i+1;
    end
    lowerlimitI(1)=min(lowerlimit1);            %define upper and lower
limits of position vs individual avg load plot to make all 8 graphs
have the same scale
    lowerlimitI(2)=min(lowerlimit2);
    lowerlimitI(3)=min(lowerlimit3);
    lowerlimitI(4)=min(lowerlimit4);
    lowerlimitI(5)=min(lowerlimit5);
    lowerlimitI(6)=min(lowerlimit6);
    lowerlimitI(7)=min(lowerlimit7);
    lowerlimitI(8)=min(lowerlimit8);
    upperlimitI(1)=max(upperlimit1);
    upperlimitI(2)=max(upperlimit2);
    upperlimitI(3)=max(upperlimit3);
    upperlimitI(4)=max(upperlimit4);
    upperlimitI(5)=max(upperlimit5);
    upperlimitI(6)=max(upperlimit6);
    upperlimitI(7)=max(upperlimit7);
    upperlimitI(8)=max(upperlimit8);
    transpositionsubset=positionsubset';        %define transpose of
output for direct copying into excel data sheet
    transavgsumload=avgsumload';
    transstdsumload=stdsumload';
    i=1; j=2;
    while(i<p)                                  %sampling interval in ms
        samplinginterval(i)=1000*(time(j)-time(i));
        i=i+1; j=j+1;
    end
    avesamplinginterval=mean(samplinginterval);
    stdsamplinginterval=std(samplinginterval);
    if(stdsamplinginterval>6)                   %Used to check the
constancy of the sampling interval
        disp('Warning: Sampling interval is inconsistant')  %Warning
generated if sampling interval is inconsistant
```

```matlab
        disp('Warning: This may cause errors in the FFT and in the
Filtered Result')
    end
    F=fft(sumload,2048);            %Fourier transform and power spectrum
    N=length(F);
    F(1)=[];
    power=abs(F(1:N/2)).^2;
    power(N/2)=0;
    power=power/max(power);
    nyquist = 8.33;
    freq = (1:N/2)/(N/2)*nyquist;
    sos1 = [1 -1.7384 1 1 -1.9701 0.97057; 1 -1.9632 1 1 -1.9755
0.97775; 1 -1.9818 1 1 -1.9829 0.98731; 1 -1.986 1 1 -1.9904 0.996];
    g1 = [0.0017361; 0.062256; 0.24101; 0.40251; 1];        %0.2Hz
Lowpass Filter
    Hd1=dfilt.df2sos(sos1,g1);
    filtered1 = filter(Hd1,sumload);
    sos2 = [1 -1.6321 1 1 -1.9316 0.93846; 1 -1.8752 1 1 -1.9392
0.95809; 1 -1.9213 1 1 -1.9481 0.97759; 1 -1.9341 1 1 -1.9579 0.99314;
1 1 0 1 -0.96415 0];
    g2 = [0.0030967; 0.15106; 0.3748; 0.53416; 0.10808; 1];   %0.5Hz
Lowpass Filter
    Hd2=dfilt.df2sos(sos2,g2);
    filtered2 = filter(Hd2,sumload);
    sos3 = [1 -0.38508 1 1 -1.9046 0.90959; 1 -1.6734 1 1 -1.9075
0.93006; 1 -1.8364 1 1 -1.9118 0.9564; 1 -1.8802 1 1 -1.917 0.97786; 1
-1.8939 1 1 -1.9245 0.99337];
    g3 = [0.002736; 0.069168; 0.27279; 0.5078; 0.64899; 1];   %0.7Hz
Lowpass Filter
    Hd3=dfilt.df2sos(sos3,g3);
    filtered3 = filter(Hd3,sumload);

%%%%% -Plot Figures-
    fig1=figure;
    plot(time, f1);                              %plot f1 vs time
    set(gca,'XTick',0:timeaxisinterval:max(time));        %set x-
axis tickmark labels
    xlabel('Time(s)','FontSize',18);                      %set x-
axis label
    ylabel('F1 - Load(g)','FontSize',18);                 %set y-
axis label
    title(eyeinfo,'FontSize',18);                         %set
title
    axis([min(time) max(time) min(minindivload) max(maxindivload)]);
    fig2=figure;
    plot(time, f2);                              %plot f2 vs time
    set(gca,'XTick',0:timeaxisinterval:max(time));        %set x-
axis tickmark labels
    xlabel('Time(s)','FontSize',18);          %set x-axis label
    ylabel('F2 - Load(g)','FontSize',18);     %set y-axis label
    title(eyeinfo,'FontSize',18);             %set title
    axis([min(time) max(time) min(minindivload) max(maxindivload)]);
    fig3=figure;
    plot(time, f3);                              %plot f3 vs time
    set(gca,'XTick',0:timeaxisinterval:max(time));        %set x-
axis tickmark labels
    xlabel('Time(s)','FontSize',18);          %set x-axis label
```

```
ylabel('F3 - Load(g)','FontSize',18);          %set y-axis label
title(eyeinfo,'FontSize',18);                  %set title
axis([min(time) max(time) min(minindivload) max(maxindivload)]);
fig4=figure;
plot(time, f4);                                %plot f4 vs time
set(gca,'XTick',0:timeaxisinterval:max(time));          %set x-
axis tickmark labels
xlabel('Time(s)','FontSize',18);               %set x-axis label
ylabel('F4 - Load(g)','FontSize',18);          %set y-axis label
title(eyeinfo,'FontSize',18);                  %set title
axis([min(time) max(time) min(minindivload) max(maxindivload)]);
fig5=figure;
plot(time, f5);                                %plot f5 vs time
set(gca,'XTick',0:timeaxisinterval:max(time));          %set x-
axis tickmark labels
xlabel('Time(s)','FontSize',18);               %set x-axis label
ylabel('F5 - Load(g)','FontSize',18);          %set y-axis label
title(eyeinfo,'FontSize',18);                  %set title
axis([min(time) max(time) min(minindivload) max(maxindivload)]);
fig6=figure;
plot(time, f6);                                %plot f6 vs time
set(gca,'XTick',0:timeaxisinterval:max(time));          %set x-
axis tickmark labels
xlabel('Time(s)','FontSize',18);               %set x-axis label
ylabel('F6 - Load(g)','FontSize',18);          %set y-axis label
title(eyeinfo,'FontSize',18);                  %set title
axis([min(time) max(time) min(minindivload) max(maxindivload)]);
fig7=figure;
plot(time, f7);                                %plot f7 vs time
set(gca,'XTick',0:timeaxisinterval:max(time));          %set x-
axis tickmark labels
xlabel('Time(s)','FontSize',18);               %set x-axis label
ylabel('F7 - Load(g)','FontSize',18);          %set y-axis label
title(eyeinfo,'FontSize',18);                  %set title
axis([min(time) max(time) min(minindivload) max(maxindivload)]);
fig8=figure;
plot(time, f8);                                %plot f8 vs time
set(gca,'XTick',0:timeaxisinterval:max(time));          %set x-
axis tickmark labels
xlabel('Time(s)','FontSize',18);               %set x-axis label
ylabel('F8 - Load(g)','FontSize',18);          %set y-axis label
title(eyeinfo,'FontSize',18);                  %set title
axis([min(time) max(time) min(minindivload) max(maxindivload)]);
fig9=figure;
plot(time, position);                          %plot position vs time
set(gca,'XTick',0:timeaxisinterval:max(time));          %set x-
axis tickmark labels
xlabel('Time(s)','FontSize',18);               %set x-axis label
ylabel('Position(mm)','FontSize',18);          %set y-axis label
title(eyeinfo,'FontSize',18);                  %set title
axis([min(time) max(time) min(position) max(position)]);
fig10=figure;
plot(time, sumload);                           %plot sumload vs time
set(gca,'XTick',0:timeaxisinterval:max(time));          %set x-
axis tickmark labels
xlabel('Time(s)','FontSize',18);               %set x-axis label
ylabel('Sum Load(g)','FontSize',18);           %set y-axis label
```

```matlab
    title(eyeinfo,'FontSize',18);                %set title
    axis([min(time) max(time) min(sumload) max(sumload)]);
    fig11=figure;
    errorbar(positionsubset,avgsumload,stdsumload,'--
bs','LineWidth',2,'MarkerEdgeColor','k','MarkerFaceColor','g','MarkerSi
ze',10);          %plot sumload vs time
    set(gca,'XTick',0:stepsize:maxposition);     %set x-axis tickmark
labels
    xlabel('Position(mm)','FontSize',18);         %set x-axis label
    ylabel('Avg Sum Load(g)','FontSize',18);      %set y-axis label
    title(eyeinfo,'FontSize',18);                 %set title
    axis([(min(positionsubset)-stepsize) (max(positionsubset)+stepsize)
min(lowerlimit) max(upperlimit)]);
    fig12=figure;
    errorbar(positionsubset,avgsumloadf1,stdsumloadf1,'--
bs','LineWidth',2,'MarkerEdgeColor','k','MarkerFaceColor','g','MarkerSi
ze',10);          %plot sumload vs time
    set(gca,'XTick',0:stepsize:maxposition);     %set x-axis tickmark
labels
    xlabel('Position(mm)','FontSize',18);         %set x-axis label
    ylabel('Avg Load - F1(g)','FontSize',18);     %set y-axis label
    title(eyeinfo,'FontSize',18);                 %set title
    axis([(min(positionsubset)-stepsize) (max(positionsubset)+stepsize)
min(lowerlimitI) max(upperlimitI)]);
    fig13=figure;
    errorbar(positionsubset,avgsumloadf2,stdsumloadf2,'--
bs','LineWidth',2,'MarkerEdgeColor','k','MarkerFaceColor','g','MarkerSi
ze',10);          %plot sumload vs time
    set(gca,'XTick',0:stepsize:maxposition);      %set x-axis tickmark
labels
    xlabel('Position(mm)','FontSize',18);          %set x-axis label
    ylabel('Avg Load - F2(g)','FontSize',18);      %set y-axis label
    title(eyeinfo,'FontSize',18);                  %set title
    axis([(min(positionsubset)-stepsize) (max(positionsubset)+stepsize)
min(lowerlimitI) max(upperlimitI)]);
    fig14=figure;
    errorbar(positionsubset,avgsumloadf3,stdsumloadf3,'--
bs','LineWidth',2,'MarkerEdgeColor','k','MarkerFaceColor','g','MarkerSi
ze',10);          %plot sumload vs time
    set(gca,'XTick',0:stepsize:maxposition);     %set x-axis tickmark
labels
    xlabel('Position(mm)','FontSize',18);          %set x-axis label
    ylabel('Avg Load - F3(g)','FontSize',18);      %set y-axis label
    title(eyeinfo,'FontSize',18);                  %set title
    axis([(min(positionsubset)-stepsize) (max(positionsubset)+stepsize)
min(lowerlimitI) max(upperlimitI)]);
    fig15=figure;
    errorbar(positionsubset,avgsumloadf4,stdsumloadf4,'--
bs','LineWidth',2,'MarkerEdgeColor','k','MarkerFaceColor','g','MarkerSi
ze',10);          %plot sumload vs time
    set(gca,'XTick',0:stepsize:maxposition);     %set x-axis tickmark
labels
    xlabel('Position(mm)','FontSize',18);         %set x-axis label
    ylabel('Avg Load - F4(g)','FontSize',18);     %set y-axis label
    title(eyeinfo,'FontSize',18);                 %set title
    axis([(min(positionsubset)-stepsize) (max(positionsubset)+stepsize)
min(lowerlimitI) max(upperlimitI)]);
```

```matlab
    fig16=figure;
    errorbar(positionsubset,avgsumloadf5,stdsumloadf5,'--
bs','LineWidth',2,'MarkerEdgeColor','k','MarkerFaceColor','g','MarkerSi
ze',10);          %plot sumload vs time
    set(gca,'XTick',0:stepsize:maxposition);    %set x-axis tickmark
labels
    xlabel('Position(mm)','FontSize',18);       %set x-axis label
    ylabel('Avg Load - F5(g)','FontSize',18);   %set y-axis label
    title(eyeinfo,'FontSize',18);               %set title
    axis([(min(positionsubset)-stepsize) (max(positionsubset)+stepsize)
min(lowerlimitI) max(upperlimitI)]);
    fig17=figure;
    errorbar(positionsubset,avgsumloadf6,stdsumloadf6,'--
bs','LineWidth',2,'MarkerEdgeColor','k','MarkerFaceColor','g','MarkerSi
ze',10);          %plot sumload vs time
    set(gca,'XTick',0:stepsize:maxposition);    %set x-axis tickmark
labels
    xlabel('Position(mm)','FontSize',18);       %set x-axis label
    ylabel('Avg Load - F6(g)','FontSize',18);   %set y-axis label
    title(eyeinfo,'FontSize',18);               %set title
    axis([(min(positionsubset)-stepsize) (max(positionsubset)+stepsize)
min(lowerlimitI) max(upperlimitI)]);
    fig18=figure;
    errorbar(positionsubset,avgsumloadf7,stdsumloadf7,'--
bs','LineWidth',2,'MarkerEdgeColor','k','MarkerFaceColor','g','MarkerSi
ze',10);          %plot sumload vs time
    set(gca,'XTick',0:stepsize:maxposition);    %set x-axis tickmark
labels
    xlabel('Position(mm)','FontSize',18);       %set x-axis label
    ylabel('Avg Load - F7(g)','FontSize',18);   %set y-axis label
    title(eyeinfo,'FontSize',18);               %set title
    axis([(min(positionsubset)-stepsize) (max(positionsubset)+stepsize)
min(lowerlimitI) max(upperlimitI)]);
    fig19=figure;
    errorbar(positionsubset,avgsumloadf8,stdsumloadf8,'--
bs','LineWidth',2,'MarkerEdgeColor','k','MarkerFaceColor','g','MarkerSi
ze',10);          %plot sumload vs time
    set(gca,'XTick',0:stepsize:maxposition);    %set x-axis tickmark
labels
    xlabel('Position(mm)','FontSize',18);       %set x-axis label
    ylabel('Avg Load - F8(g)','FontSize',18);   %set y-axis label
    title(eyeinfo,'FontSize',18);               %set title
    axis([(min(positionsubset)-stepsize) (max(positionsubset)+stepsize)
min(lowerlimitI) max(upperlimitI)]);
    fig20=figure;
    plot(samplinginterval);                     %plot the sampling
interval
    xlabel('Data Number','FontSize',18);        %set x-axis label
    ylabel('Sampling Interval (ms)','FontSize',18);         %set y-
axis label
    title(eyeinfo,'FontSize',18);               %set title
    axis([min(0-(p/100)) max(p+(p/100)) min(samplinginterval)
max(samplinginterval)]);
    fig21=figure;                               %plot frequency
spectrum of sum load
    plot(freq,power);
    title('Periodogram of Sum Load','FontSize',18);
```

```matlab
    xlabel('Frequency (Hz)','FontSize',18);
    ylabel('Normalized Power Spectrum','FontSize',18);
    axis([min(0) max(8.33) min(0) max(1)]);
    fig22=figure;                               %plot close-up of
frequency spectrum of sum load
    plot(freq,power);
    title('Periodogram of Sum Load (Close-Up)','FontSize',18);
    xlabel('Frequency (Hz)','FontSize',18);
    ylabel('Normalized Power Spectrum','FontSize',18);
    axis([min(0) max(8.33) min(0) max(mean(power)+3*std(power))]);
    fig23=figure;                               %plot 0.2Hz cutoff
elliptical filtered result
    plot(time, sumload, 'Color', 'b')
    hold on;
    plot((time-4.9), filtered1, 'Color', 'r', 'LineWidth',2);
    hold off;
    set(gca,'XTick',0:timeaxisinterval:max(time));          %set x-
axis tickmark labels
    xlabel('Time(s)','FontSize',18);                %set x-axis label
    ylabel('Sum Load(g)','FontSize',18);            %set y-axis label
    title(eyeinfo,'FontSize',18);                   %set title
    axis([min(time) max(time) min(sumload) max(sumload)]);
    legend('Raw Signal','0.2Hz Lowpass Filtered','Location','Best');
    fig24=figure;                               %plot 0.5Hz cutoff
elliptical filtered result
    plot(time, sumload, 'Color', 'b')
    hold on;
    plot((time-1.2), filtered2, 'Color', 'r', 'LineWidth',2);
    hold off;
    set(gca,'XTick',0:timeaxisinterval:max(time));          %set x-
axis tickmark labels
    xlabel('Time(s)','FontSize',18);                %set x-axis label
    ylabel('Sum Load(g)','FontSize',18);            %set y-axis label
    title(eyeinfo,'FontSize',18);                   %set title
    axis([min(time) max(time) min(sumload) max(sumload)]);
    legend('Raw Signal','0.5Hz Lowpass Filtered','Location','Best');
    fig25=figure;                               %plot 0.7Hz cutoff
elliptical filtered result
    plot(time, sumload, 'Color', 'b')
    hold on;
    plot((time-0.5), filtered3, 'Color', 'r', 'LineWidth',2);
    hold off;
    set(gca,'XTick',0:timeaxisinterval:max(time));          %set x-
axis tickmark labels
    xlabel('Time(s)','FontSize',18);                %set x-axis label
    ylabel('Sum Load(g)','FontSize',18);            %set y-axis label
    title(eyeinfo,'FontSize',18);                   %set title
    axis([min(time) max(time) min(sumload) max(sumload)]);
    legend('Raw Signal','0.7Hz Lowpass Filtered','Location','Best');
else
    warning('Code Terminated - Perform Calculations Manually')
end
```

Appendix 2: EVASII Test and Validation

Appendix 2.1 Normality Tests

Shapiro-Wilk Normality Test	
Position (mm)	Normal?
0.00	Normal at 0.01 level
0.25	Normal at 0.01 level
0.50	Normal at 0.01 level
0.75	Normal at 0.01 level
1.00	Normal at 0.01 level
1.25	Normal at 0.01 level
1.50	Normal at 0.01 level
1.75	Normal at 0.01 level
2.00	Normal at 0.01 level

Table A2.1: Shapiro-Wilk normality test results by position for data acquired with no pins and no shoes.

Figure A2.1: Measured residuals regressed against a normal distribution with the same mean and variance as the sample for all positions 0 to 0.75mm, where an R^2 of unity gives a perfect Gaussian distribution.

Figure A2.2: Measured residuals regressed against a normal distribution with the same mean and variance as the sample for all positions 1 to 2.25mm, where an R^2 of unity gives a perfect Gaussian distribution.
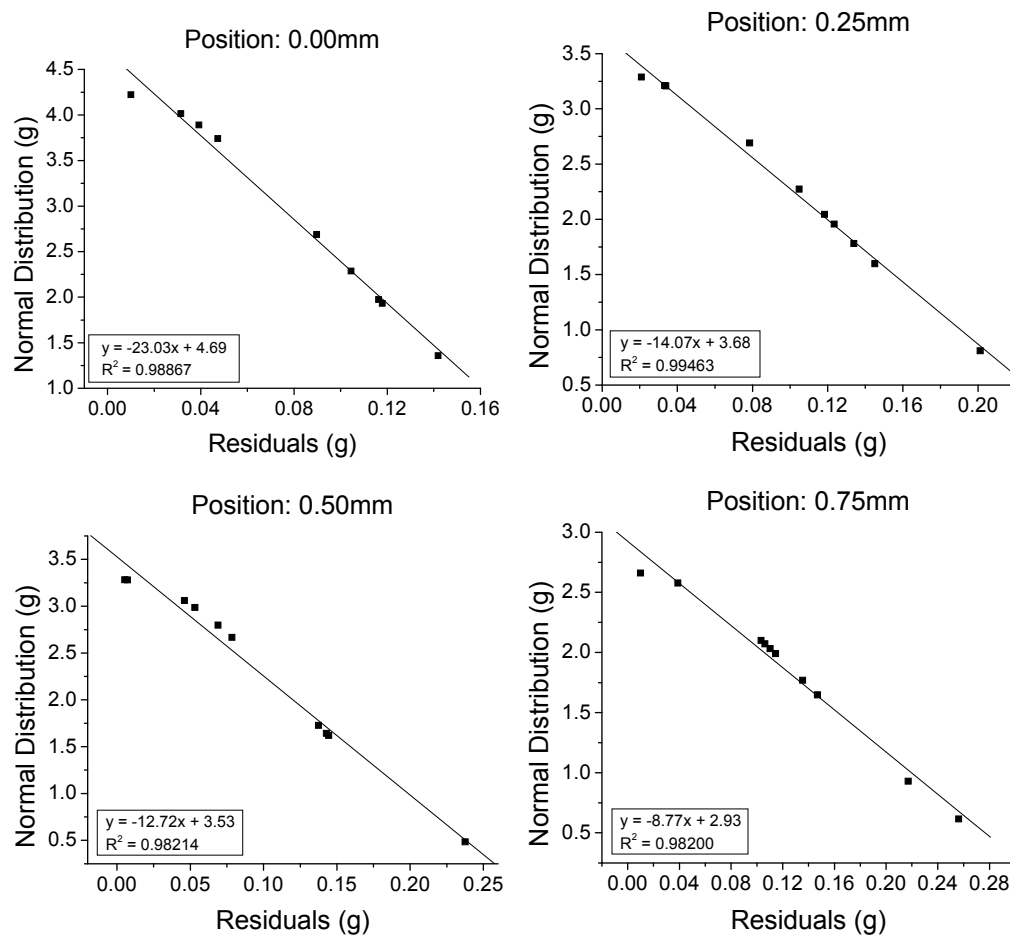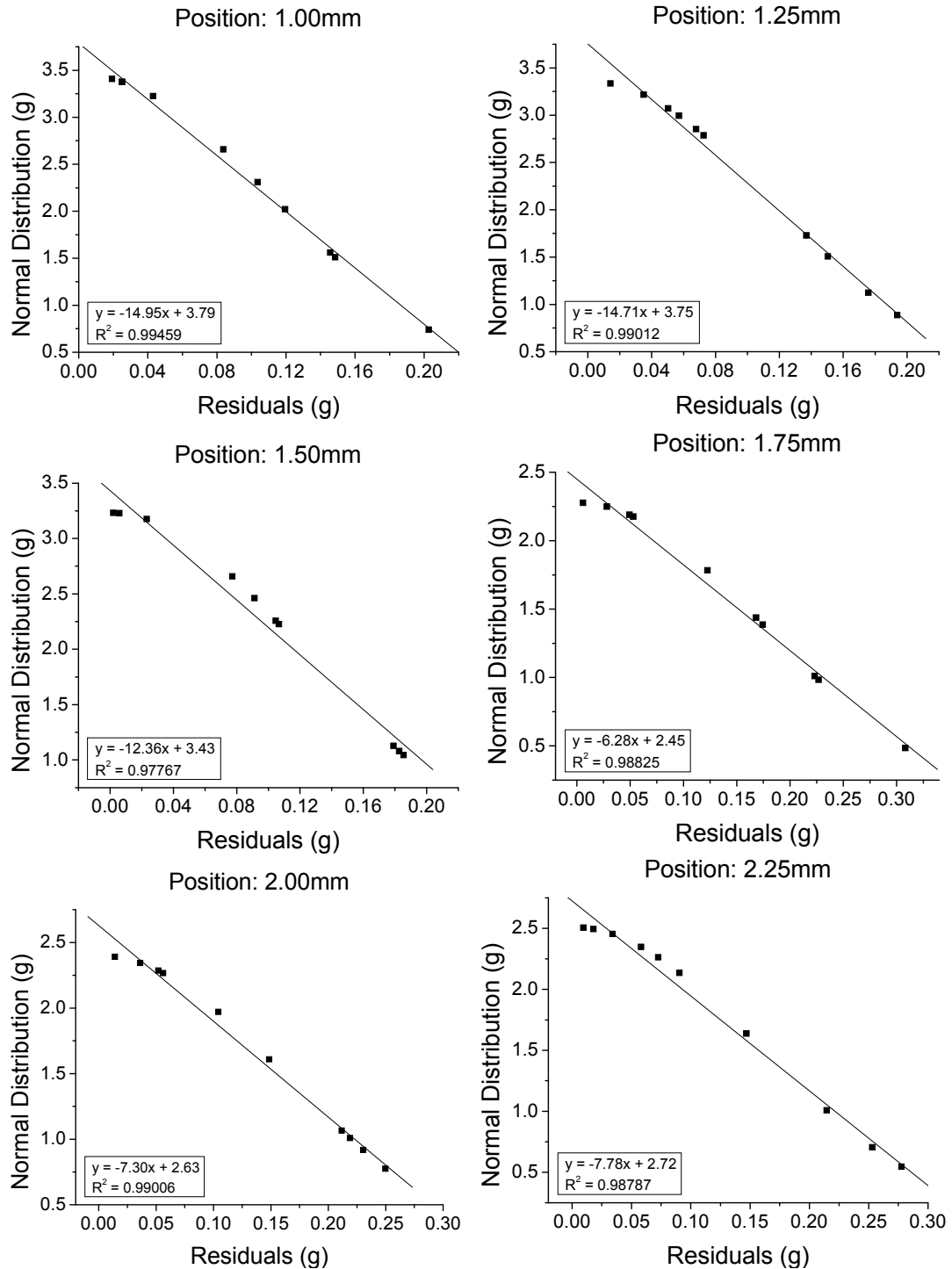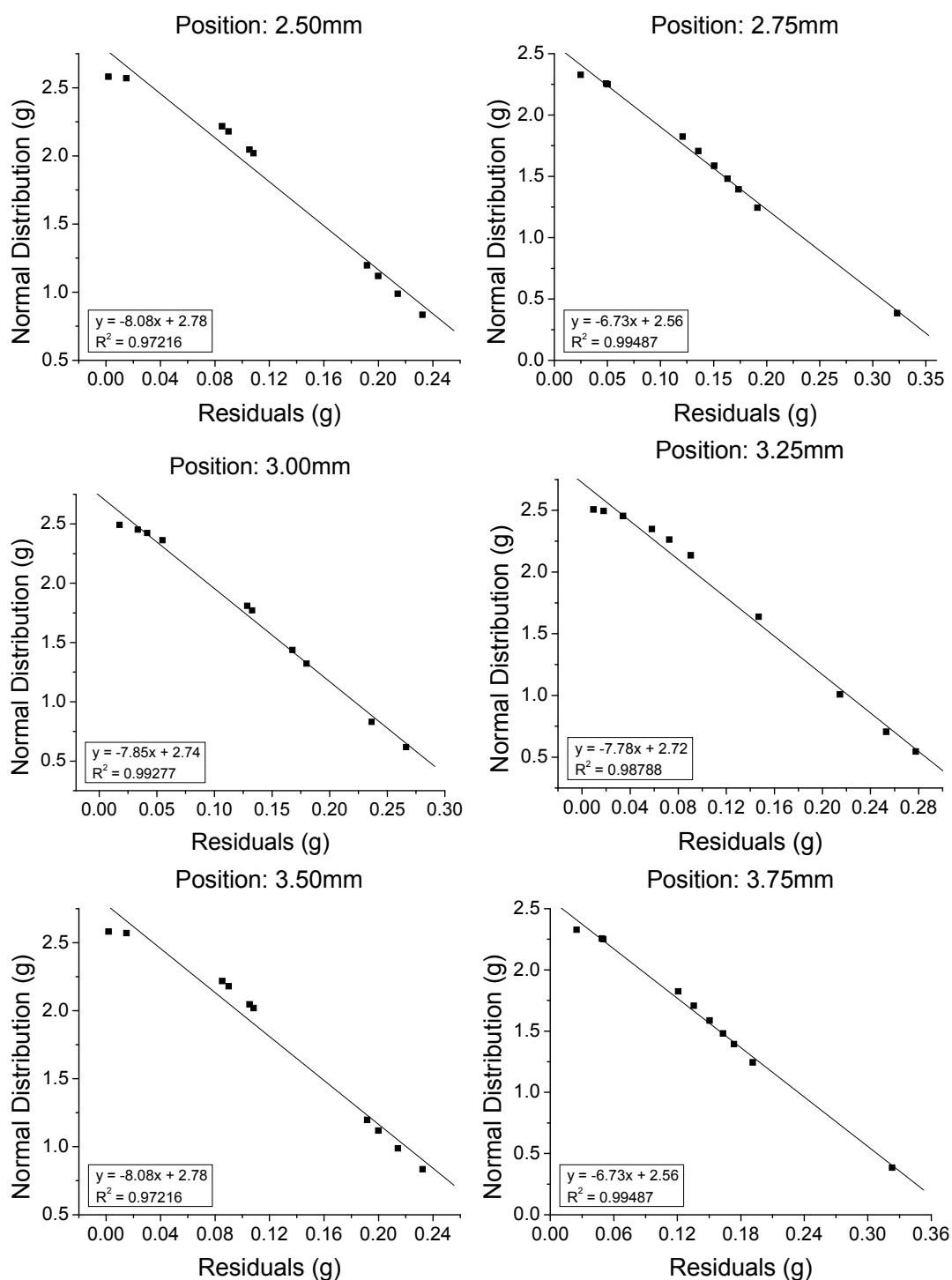
Figure A2.3: Measured residuals regressed against a normal distribution with the same mean and variance as the sample for all positions 2.5 to 3.75mm, where an R^2 of unity gives a perfect Gaussian distribution.
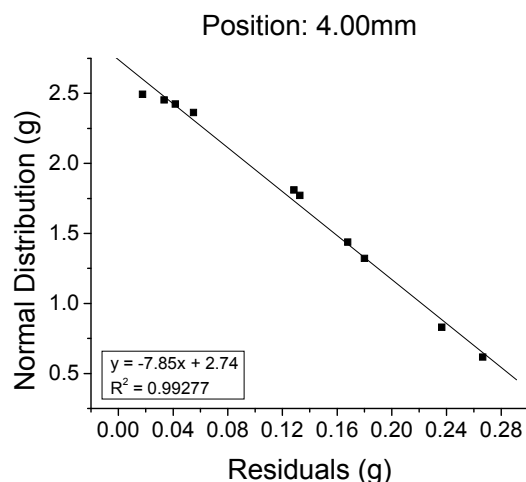
Figure A2.4: Measured residuals regressed against a normal distribution with the same mean and variance as the sample for the 4mm position, where an R^2 of unity gives a perfect Gaussian distribution.

Appendix 2.2 Comparing Magnetic Load

Position (mm)	Sum Load (g)				Different? P =
	No Pins and No Shoes		With Pins and Shoes Stationary		
	Average	95% Error	Average	95% Error	
0.00	0.00	0.49	0.02	0.56	0.77694
0.25	0.88	0.56	0.67	0.43	0.00358
0.50	1.70	0.45	1.26	0.46	8.90E-07
0.75	2.48	0.48	1.82	0.49	6.96E-09
1.00	3.19	0.45	2.37	0.44	2.20E-14
1.25	3.85	0.47	2.85	0.43	1.75E-05
1.50	4.53	0.49	3.42	0.54	7.36E-11
1.75	5.14	0.47	3.87	0.44	2.67E-12
2.00	5.73	0.47	4.30	0.45	1.46E-13
2.25	6.27	0.44	4.69	0.42	2.64E-14
2.50	6.78	0.32	5.09	0.34	6.85E-15
2.75	7.27	0.32	5.45	0.34	3.98E-15
3.00	7.76	0.32	5.83	0.34	6.30E-15
3.25	8.21	0.34	6.21	0.36	1.10E-15
3.50	8.70	0.37	6.52	0.32	5.67E-17
3.75	9.10	0.31	6.87	0.34	3.28E-15
4.00	9.43	0.50	7.13	0.51	4.44E-16

Table A2.2: Comparison - magnetic load with no pins and no shoes vs. magnetic load with pins and shoes stationary. The p-values were obtained using an independent Student's t-test.

| Position (mm) | Sum Load (g) | | | | Different? P = |
| | No Pins and No Shoes | | With Pins and Shoes Random | | |
	Average	95% Error	Average	95% Error	
0.00	0.00	0.49	0.02	0.56	0.21921
0.25	0.88	0.56	0.67	0.43	1.29E-04
0.50	1.70	0.45	1.26	0.46	2.83E-07
0.75	2.48	0.48	1.82	0.49	2.47E-09
1.00	3.19	0.45	2.37	0.44	1.68E-16
1.25	3.85	0.47	2.85	0.43	1.07E-04
1.50	4.53	0.49	3.42	0.54	3.08E-13
1.75	5.14	0.47	3.87	0.44	1.02E-12
2.00	5.73	0.47	4.30	0.45	9.79E-14
2.25	6.27	0.44	4.69	0.42	1.55E-14
2.50	6.78	0.32	5.09	0.34	6.10E-15
2.75	7.27	0.32	5.45	0.34	1.06E-15
3.00	7.76	0.32	5.83	0.34	4.04E-16
3.25	8.21	0.34	6.21	0.36	8.51E-17
3.50	8.70	0.37	6.52	0.32	2.19E-17
3.75	9.10	0.31	6.87	0.34	2.71E-17
4.00	9.43	0.50	7.13	0.51	2.64E-17

Table A2.3: Comparison - magnetic load with no pins and no shoes vs. magnetic load with pins and shoes randomly rearranged. The p-values were obtained using an independent Student's t-test.

| Position (mm) | Sum Load (g) | | | | Different? P = |
| | With Pins and Shoes Stationary | | With Pins and Shoes Random | | |
	Average	95% Error	Average	95% Error	
0.00	0.00	0.49	0.02	0.56	0.21982
0.25	0.88	0.56	0.67	0.43	0.29854
0.50	1.70	0.45	1.26	0.46	0.70499
0.75	2.48	0.48	1.82	0.49	0.98435
1.00	3.19	0.45	2.37	0.44	0.62145
1.25	3.85	0.47	2.85	0.43	0.31279
1.50	4.53	0.49	3.42	0.54	0.69615
1.75	5.14	0.47	3.87	0.44	0.56342
2.00	5.73	0.47	4.30	0.45	0.58561
2.25	6.27	0.44	4.69	0.42	0.23948
2.50	6.78	0.32	5.09	0.34	0.29462
2.75	7.27	0.32	5.45	0.34	0.15735
3.00	7.76	0.32	5.83	0.34	0.23022
3.25	8.21	0.34	6.21	0.36	0.25067
3.50	8.70	0.37	6.52	0.32	0.11519
3.75	9.10	0.31	6.87	0.34	0.21430
4.00	9.43	0.50	7.13	0.51	0.23719

Table A2.4: Comparison - magnetic load with pins and shoes stationary vs. magnetic load with pins and shoes randomly rearranged. The p-values were obtained using an independent Student's t-test.

Position (mm)	Variation in Load (g)			
	No Pins and No Shoes		With Pins and Shoes Stationary	
	Std	Range	Std	Range
0.00	0.09	0.26	0.16	0.48
0.25	0.12	0.35	0.15	0.45
0.50	0.12	0.38	0.14	0.45
0.75	0.15	0.47	0.14	0.49
1.00	0.12	0.35	0.18	0.56
1.25	0.12	0.34	0.15	0.44
1.50	0.12	0.37	0.23	0.71
1.75	0.18	0.54	0.17	0.52
2.00	0.17	0.48	0.16	0.54
2.25	0.16	0.53	0.17	0.55
2.50	0.15	0.43	0.17	0.61
2.75	0.17	0.51	0.17	0.60
3.00	0.16	0.50	0.21	0.72
3.25	0.14	0.44	0.20	0.66
3.50	0.14	0.42	0.18	0.61
3.75	0.13	0.46	0.26	0.82
4.00	0.14	0.45	0.23	0.68
Mean	0.14	0.43	0.18	0.58
			Different? P =	Different? P =
			3.42E-04	4.24E-05

Table A2.5: Comparison - variation in magnetic load with no pins and shoes vs. variation in magnetic load with pins and shoes stationary. The p-values were obtained using an independent Student's t-test.

Position (mm)	Variation in Load (g)			
	No Pins and No Shoes		With Pins and Shoes Random	
	Std	Range	Std	Range
0.00	0.09	0.26	0.14	0.44
0.25	0.12	0.35	0.13	0.44
0.50	0.12	0.38	0.14	0.42
0.75	0.15	0.47	0.12	0.33
1.00	0.12	0.35	0.11	0.27
1.25	0.12	0.34	0.14	0.39
1.50	0.12	0.37	0.13	0.34
1.75	0.18	0.54	0.14	0.40
2.00	0.17	0.48	0.14	0.45
2.25	0.16	0.53	0.14	0.36
2.50	0.15	0.43	0.15	0.38
2.75	0.17	0.51	0.13	0.37
3.00	0.16	0.50	0.14	0.39
3.25	0.14	0.44	0.14	0.43
3.50	0.14	0.42	0.15	0.42
3.75	0.13	0.46	0.16	0.47
4.00	0.14	0.45	0.17	0.49
Mean	0.14	0.43	0.14	0.40
			Different? P =	Different? P =
			0.93025	0.21898

Table A2.6: Comparison - variation in magnetic load with no pins and shoes vs. variation in magnetic load with pins and shoes randomly rearranged. The p-values were obtained using an independent Student's t-test.

	Sum Load (g)			
	With Pins and Shoes Stationary		With Pins and Shoes Random	
Position (mm)	Std	Range	Std	Range
0.00	0.16	0.48	0.14	0.44
0.25	0.15	0.45	0.13	0.44
0.50	0.14	0.45	0.14	0.42
0.75	0.14	0.49	0.12	0.33
1.00	0.18	0.56	0.11	0.27
1.25	0.15	0.44	0.14	0.39
1.50	0.23	0.71	0.13	0.34
1.75	0.17	0.52	0.14	0.40
2.00	0.16	0.54	0.14	0.45
2.25	0.17	0.55	0.14	0.36
2.50	0.17	0.61	0.15	0.38
2.75	0.17	0.60	0.13	0.37
3.00	0.21	0.72	0.14	0.39
3.25	0.20	0.66	0.14	0.43
3.50	0.18	0.61	0.15	0.42
3.75	0.26	0.82	0.16	0.47
4.00	0.23	0.68	0.17	0.49
Mean	0.18	0.58	0.14	0.40
			Different? P =	Different? P =
			6.71E-05	7.14E-07

Table A2.7: Comparison - variation in magnetic load with pins and shoes stationary vs. variation in magnetic load with pins and shoes randomly rearranged. The p-values were obtained using an independent Student's t-test.

VITA

Derek D. Nankivil was born in Titusville, FL, on March 4, 1983. He was raised in Cape Canaveral, FL, where he received his elementary education at Cape View Elementary. He obtained his intermediary education at Theodore Roosevelt Junior High School in Cocoa Beach, FL, and at Space Coast Middle School in Cocoa, FL. He received his secondary education at Cocoa High School in Cocoa, FL, and at Duncan U. Fletcher High School, Neptune Beach, FL, where he graduated in May 2001 with honors. In August 2001 he entered Embry-Riddle Aeronautical University, Daytona Beach, FL later to accept a research experience for undergraduates at Princeton University, Princeton, NJ. He transferred to the University of Central Florida, Orlando, FL, where he completed a Bachelor of Science in Aerospace Engineering in May 2005. After a stint in industry with Raytheon Corporation, Andover, MA, in August 2006 he enrolled in graduate studies at the University of Miami, Coral Gables, FL, where he graduated with a Master of Science in Biomedical Engineering in December 2008.

Permanent Address: 201 Tallwood Rd., Jacksonville Beach, FL 32250